

POLITECNICO DI TORINO

Master's Degree in Automotive Engineering



Master's Degree Thesis

Control strategy optimization of Toyota Mirai based fuel cell hybrid electric vehicles

Supervisors

Prof Andrea TONOLI

Prof Sanjarbek RUZIMOV

Candidate

Umidjon USMANOV

June 2022

Acknowledgements

Words cannot describe my great gratitude to my supervisors Sanjarbek Ruzimov and Andrea Tonoli and committee chair for unwavering patience and assistance. I couldn't have made it this far without their help, who kindly shared their knowledge and expertise.

My classmates and cohort members, particularly my office colleagues, deserve special thanks for their editing assistance and moral support. Thanks also to the university librarians, research assistants, and study participants who influenced and motivated me.

Finally, I'd be negligent if I didn't acknowledge my family, particularly my parents and wife. Throughout this process, their faith in me has maintained my spirits and motivation strong.

Summary

Ecological problems concerning air pollution and climate change force people to use alternative energy sources for the transportation sector. Therefore, strict limitations are set for automotive manufacturers concerning the exhaust gases, which become stringent year by year. Implementation of hydrogen instead of fossil fuels for the propulsion of vehicles is the solution to have zero noxious and greenhouse gas emissions, which provides relatively high energy density combined with the water as the only exhaust gas. This paper represents the detailed description and derivation of a Toyota Mirai (1st generation) based fuel cell hybrid vehicle model and its components for the purpose of analysis of the hydrogen consumption, change of the state of charge of battery and the variation of other parameters. In the first part, the introduction to fuel cell technology and its application in transportation sector is provided. Then, fuel cell hybrid electric vehicle mathematical model, which consist of several subsystems is derived and described. These subsystems are drive cycle, vehicle longitudinal dynamics, transmission system, electric machine, energy management system, battery, boost converter and fuel cell system model. The analysis on each subsystem is performed and the governing transfer functions are derived taking into account both traction and regeneration modes. In the second part, the model is simulated in Matlab® Simulink environment and validated using the experimental data obtained from open source ANL (Argonne National Laboratory) database. Finally, the principle of equivalent consumption minimization strategy is explained and implemented in Toyota Mirai control strategy for the purpose of investigation hydrogen consumption change depending on different control strategies. Overall 3 control strategies were used: Experimental control strategy (fuzzy logic controller), Toyota Mirai manually reconstructed control strategy for the simulation purpose (rule based controller) and equivalent consumption minimization strategy implemented control logic. Finally, all these controller are tested in Toyota Mirai (1st generation) vehicle and the values of hydrogen consumption are summarized in proper tables for comparison purposes.

Table of Contents

List of Tables	v
List of Figures	vi
Acronyms	ix
1 Introduction	1
2 Overview on fuel cells	4
2.1 Operating principle of fuel cells	4
2.2 Fuel cell losses	6
2.3 Fuel cell degradation	8
2.4 Fuel cell technologies	10
2.4.1 Alkaline fuel cell	10
2.4.2 Phosphoric acid fuel cell	10
2.4.3 Molten carbonate fuel cell	11
2.4.4 Solid oxide fuel cell	11
2.4.5 Direct methanol fuel cell	12
2.4.6 Proton exchange membrane fuel cell	12
2.5 Fuel cell stack, system and auxiliaries	14
2.5.1 Air supply system	16
2.5.2 Hydrogen supply system	17
2.5.3 Cooling system	18
2.5.4 Humidification system	19
3 Fuel cell technology in automotive industry	20
3.1 Fuel cell electric vehicles	23
3.2 Fuel cell hybrid electric vehicle	23
3.3 Control strategies of hybrid vehicles	24
3.3.1 Rule-based strategies	28
3.3.2 Optimization based strategies	32

3.4	Fuel cell on-vehicle realization	40
4	Fuel cell hybrid electric vehicle modeling and simulation	43
4.1	Vehicle simulation approaches	43
4.1.1	Forward simulation approach	43
4.1.2	Backward simulation approach	44
4.2	FCHEV mathematical model	45
4.2.1	Drive cycle model	47
4.2.2	Vehicle longitudinal dynamics model	47
4.2.3	Transmission system model	49
4.2.4	Electric machine model	50
4.2.5	Fuel cell system model	51
4.2.6	Battery model	55
4.2.7	Boost converter model	59
4.2.8	Energy management system model	59
4.3	Simulation results	64
4.3.1	Results on WLTC driving cycle	65
4.3.2	Results on NEDC driving cycle	67
4.3.3	Results on UDDS driving cycle	69
4.3.4	Results on JC08 driving cycle	71
4.3.5	Results on US06 driving cycle	73
4.3.6	Results on HWY driving cycle	75
4.4	Results discussion and analysis	78
5	Control strategy optimization of Toyota Mirai based FCHEV	81
5.1	Equivalent consumption minimization strategy (ECMS)	81
5.2	Mathematical representation of ECMS	82
5.3	Simulation setup	84
5.4	ECMS simulation results	85
5.4.1	Results on WLTC driving cycle	87
5.4.2	Results on NEDC driving cycle	88
5.4.3	Results on UDDS driving cycle	89
5.4.4	Results on JC08 driving cycle	90
5.4.5	Results on US06 driving cycle	91
5.4.6	Results on HWY driving cycle	92
5.5	ECMS simulation results analysis and discussion	94
6	Conclusion	97
A	Simulation model and its subsystems	99
	Bibliography	112

List of Tables

2.1	Fuel cell losses	8
2.2	Classification of fuel cell technologies	13
3.1	Commercial FCHEV dynamic characteristics	42
4.1	Parameters of Toyota Mirai (1st generation) FCHEV used in calculation	60
4.2	Simulation results for hydrogen consumption	77
4.3	Simulation results for battery SOC	78
5.1	Parameters for ECMS control strategy	84
5.2	Simulation results for hydrogen consumption with ECMS controller	93
5.3	Simulation results for battery SOC with ECMS controller	94

List of Figures

1.1	Earth average temperature	2
1.2	Share of CO_2 emissions	2
2.1	PEM fuel cell unit	5
2.2	FC polarization curve [2]	6
2.3	Sources of voltage losses [3]	7
2.4	Fuel cell stack [13]	14
2.5	FC stack and system efficiency [14]	15
2.6	Fuel cell system	16
2.7	Toyota FCEV air compressor [15]	17
2.8	Toyota FCEV hydrogen circulation pump [15]	18
2.9	Fuel cell cooling system [16]	18
3.1	Classification of fuel cell vehicles	22
3.2	Fuel cell electric vehicle layout	23
3.3	Fuel cell hybrid electric vehicle layout	24
3.4	Operation modes of hybrid vehicles	26
3.5	Classification of control strategies for hybrid vehicles	27
3.6	Baseline mode-based control strategy logic [26]	29
3.7	Structure of fuzzy logic controller [26]	30
3.8	Structure of artificial neural networks [28]	34
3.9	Flowchart of Genetic algorithm optimization [34]	39
3.10	Architecture of first generation Toyota Mirai [35]	41
4.1	Forward simulation approach topology	44
4.2	Backward simulation approach topology	45
4.3	Toyota Mirai FCHEV configuration	45
4.4	Toyota Mirai FCHEV simulink model	46
4.5	Driving cycles	48
4.6	Electric machine efficiency map	51
4.7	FC stack efficiency	52

4.8	FC system efficiency	53
4.9	Hydrogen flow rate	53
4.10	Polarization curve feedback loop	54
4.11	Polarization curve	54
4.12	Battery equivalent circuit model	55
4.13	Battery open circuit voltage	56
4.14	Battery charging resistance	56
4.15	Battery discharging resistance	57
4.16	Experimental working points on WLTC (3-D view)	61
4.17	Experimental working points on WLTC (2-D view, planar projection)	61
4.18	Reconstructed rule based EMS	62
4.19	Block diagram in MATLAB/Simulink environment	64
4.20	Simulation results over WLTC driving cycle (Fuel cell parameters) .	65
4.21	Simulation results over WLTC driving cycle (Battery parameters) .	66
4.22	Simulation results over NEDC (x2) driving cycle (Fuel cell parameters)	67
4.23	Simulation results over NEDC (x2) driving cycle (Battery parameters)	68
4.24	Simulation results over UDDS driving cycle (Fuel cell parameters) .	69
4.25	Simulation results over UDDS driving cycle (Battery parameters) .	70
4.26	Simulation results over JC08 driving cycle (Fuel cell parameters) . .	71
4.27	Simulation results over JC08 driving cycle (Battery parameters) . .	72
4.28	Simulation results over US06 (x2) driving cycle (Fuel cell parameters)	73
4.29	Simulation results over US06 (x2) driving cycle (Battery parameters)	74
4.30	Simulation results over HWY (x2) driving cycle (Fuel cell parameters)	75
4.31	Simulation results over HWY (x2) driving cycle (Battery parameters)	76
5.1	Block diagram in MATLAB/Simulink environment	85
5.2	Calculation algorithm for ECMS output parameters given the re- quired power and battery SOC	86
5.3	Simulation results over WLTC driving cycle with ECMS controller .	87
5.4	Simulation results over NEDCx2 driving cycle with ECMS controller	88
5.5	Simulation results over UDDS driving cycle with ECMS controller .	89
5.6	Simulation results over JC08 driving cycle with ECMS controller . .	90
5.7	Simulation results over US06x2 driving cycle with ECMS controller	91
5.8	Simulation results over HWYx2 driving cycle with ECMS controller	92
5.9	Fuel cell system efficiency for NEDC driving cycle	95
5.10	Fuel cell system efficiency for UDDS driving cycle	95
5.11	Fuel cell system efficiency for JC08 driving cycle	95
A.1	Block diagram in MATLAB/Simulink environment	99
A.2	Driving cycle subsystem	100
A.3	Vehicle longitudinal dynamics subsystem	101

A.4	Gearbox (Transmission system) subsystem	102
A.5	Electric machine subsystem	103
A.6	Energy management system subsystem	104
A.7	Battery subsystem (Part 1)	105
A.8	Battery subsystem (Part 2)	106
A.9	Battery subsystem (Part 3)	107
A.10	Battery subsystem (Part 4)	108
A.11	Fuel cell boost converter subsystem	109
A.12	Fuel cell subsystem	110
A.13	Hydrogen tank subsystem	111

Acronyms

AI

artificial intelligence

FC

fuel cell

FCS

fuel cell system

FCEV

fuel cell electric vehicle

FCHEV

fuel cell hybrid electric vehicle

BEV

battery electric vehicle

HEV

hybrid electric vehicle

ICE

Internal combustion engine

ANL

Argonne National Laboratory

ECMS

Equivalent consumption minimization strategy

EMS

Energy management strategy

SOC

State of charge

EM

Electric machine

OCV

Open circuit voltage

NiMH

Nickel metal hydride

DC

direct current

PCU

Power control unit

WLTC

Worldwide harmonized light-duty testing cycle

NEDC

New European Driving Cycle

UDDS

Urban dynamometer driving cycle

JC

Japan cycle

HWY

Highway fuel economy test cycle

Chapter 1

Introduction

Climate change, in particular global warming, has become one of the main ecological issues in recent years. According to the report of EPA United States Environmental Protection agency, the transportation sector generates the largest share of greenhouse gas emissions (29 % of 2019 greenhouse gas emissions)[1]. Particularly, passenger vehicle, equipped with Internal combustion engines (ICE) as propulsion unit, emit the largest part of greenhouse gas emissions. Therefore, authorities and environmental agencies introduce strict rules and limitations for automotive manufacturers concerning both noxious and greenhouse gas emissions. On one side the amount of noxious emissions of ICE (unburned hydrocarbons HC , carbon monoxide CO , nitrogen oxides NO_x , particulate matter PM and sulphur oxides SO_x) can be controlled by tuning combustion process or improving engine after-treatment systems. On the other side, however, the amount of greenhouse gas emissions, in particular CO_2 emissions, are directly proportional to the amount of fuel consumption, so the only way of reduction of CO_2 emissions is to have engine efficiency as high as possible, although it is limited by Carnot efficiency. Thus, total deliverance of CO_2 emissions for ICE is not possible. To tackle this issue, standards concerning emissions are developed by authorities. European commission, for instance, has introduced EURO standards for light-duty and heavy duty vehicles, which range from 1 to 6 for light-duty and I to VI for heavy duty vehicles and have set a specific type-approval homologation driving cycles for which the vehicle should be tested. This driving cycles are New European Driving cycle (NEDC) and Worldwide harmonized light-duty testing cycle (WLTC). Nowadays NEDC is no more implemented due to inaccuracy in reproducing real-world driving conditions, yet WLTC combined with RDE (Real driving emissions) is a better reflection of driving pattern in real world. In addition, the standards, concerning CO_2 emissions have become 95 g/km in 2020 for an average car of the company in terms of mass, which is a challenging goal. One possible solution is to hybridize existing in market thermal propulsion unit (ICE) with an additional reversible

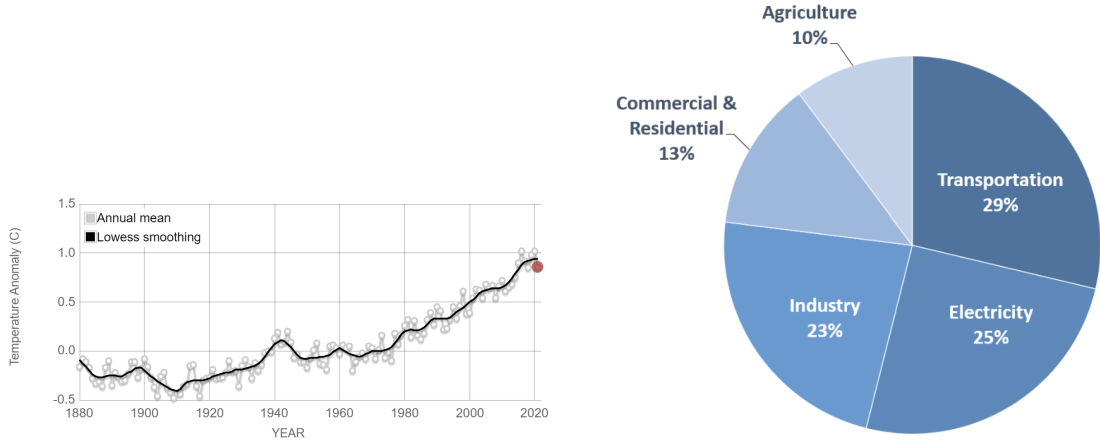


Figure 1.1: Earth average temperature

Figure 1.2: Share of CO_2 emissions

energy source. These vehicles are called hybrid electric vehicles (HEV). Due to the intrinsic properties of reversibility of batteries and supercapacitors, they are used in parallel with ICE being more flexible in terms of power supply and allowing regenerative braking be possible. However, total elimination of CO_2 emissions for HEV is impossible.

Fuel cell technology is a solution to have combustion free power unit, which uses hydrogen and oxygen as reactants to generate electricity with the water as the only products. This solution enables carbon free propulsion with no noxious gas emissions. PEM (Proton exchange membrane or polymeric electrolyte membrane) fuel cells are used in automotive industry due to relatively low working temperature. The intrinsic advantages of fuel cells are high power density, relative to ICE high efficiency, especially at low loads. Vehicles, equipped with FC as the propulsion unit are called fuel cell electric vehicles (FCEV). Usually, an additional power source, battery or supercapacitor is used, because FC have slow response. These vehicles are called fuel cell hybrid electric vehicles (FCHEV). Speaking that FCHEV have zero carbon emissions wouldn't be correct, because hydrogen is not a primary energy source, yet is only energy carrier. The majority of hydrogen nowadays is produced by burning fossil fuels, therefore emission analysis of FCHEV is divided in two parts: tank-to-wheel emissions and well-to-tank emissions analysis. FCHEV have zero tank-to-wheel carbon emissions, however well-to-tank emissions strongly depend on the method of hydrogen production. Due to high current prices of hydrogen and FCHEV and lack of hydrogen refueling stations and infrastructures, fuel cell vehicles are not widely spread today, and are considered as long-term solution.

The control issue of FCHEV arises due to the presence of several power sources. The question of splitting power demand of the vehicle between battery and fuel cell

is important, because overall control logic of the vehicle affects several parameters, that are hydrogen consumption, FC and battery working efficiencies and FC and battery durability. In general, there exist rule-based and optimization-based control strategies. In turn, rule-based strategies are divided into deterministic and fuzzy-logic, while optimization based into online and offline strategies. Rule based strategies operate based on fixed heuristic patterns, that are obtained from a numerous experimental data for the purpose of obtaining maximum optimization of fuel consumption. On the other hand, optimization based strategies are formulated with physical or mathematical relation with the same purpose of minimizing fuel consumption.

In this context, the research, carried out in the development of this thesis focuses in the first part (Chapter 4) on modeling, simulation and validation of FCHEV based on Toyota Mirai (1st generation) vehicle. For this purpose, various subsystems of vehicle are described with mathematical relations and proper block diagram are constructed by means of reverse engineering and backward modeling approaches. Obtained results are compared with experimental data from open-source Argonne national laboratory database. In the second part (Chapter 4), ECMS control strategy is implemented and replaced Toyota Mirai fuzzy-logic control strategy. Finally, results, obtained from different control strategies are summarized to investigate the values and behaviour of certain parameters. Proper modeling techniques, that are developed nowadays by researchers, can serve as a guideline for making material choices in the product development cycle, fuel consumption optimization and aid in the component design process that will help maximize the performance and efficiency of a fuel cell technology. This in turn will result in price reduction of fuel cell vehicles and removes the economic barriers for potential customers and open a new age of zero-emission driving.

Chapter 2

Overview on fuel cells

2.1 Operating principle of fuel cells

Fuel cells are devices that are able to directly, without combustion convert chemical energy of reactants (hydrogen and oxygen) into electricity, heat and water. They operate in reverse principle of electrolysis. Fuel cells can run as far as hydrogen and oxygen are supplied, which makes it different from batteries and supercapacitors, where chemical energy comes from the reactants that are already present. This working principle of FC makes it similar with internal combustion engines (ICE), yet FC doesn't require combustion process. Therefore, FC efficiency doesn't limited by Carnot efficiency, so they can achieve efficiency higher than thermal machines. In addition, unlike ICE, FC doesn't produce carbon emissions, which makes it zero-pollutant technology. Fuel cells can be used in both stationary and mobile applications, particularly they are mainly studied for commercial energy generation, propulsion of transportation technologies and residential applications. The schematic of PEM single fuel cell unit is presented in Figure 2.1.

Single fuel cell unit consists of the following components: bipolar plate, gas diffusion layer, anode and cathode catalyst layer and electrolyte. Hydrogen gas is fed into the voids of anode channel bipolar plate, where part of the hydrogen travels through gas diffusion layer and reach catalytic reaction site. On the other side, oxygen from air is fed into the voids of cathode channel bipolar plate, and traveling through gas diffusion layer reach cathode catalyst layer. From the catalytic action at anode side, hydrogen oxidizes and loses electrons:



The membrane allows the transfer of only hydrogen ions (protons), while blocking the passage of electrons, so they travel through external load, creating current flow under potential difference and thus electrical energy. At cathode side, oxygen

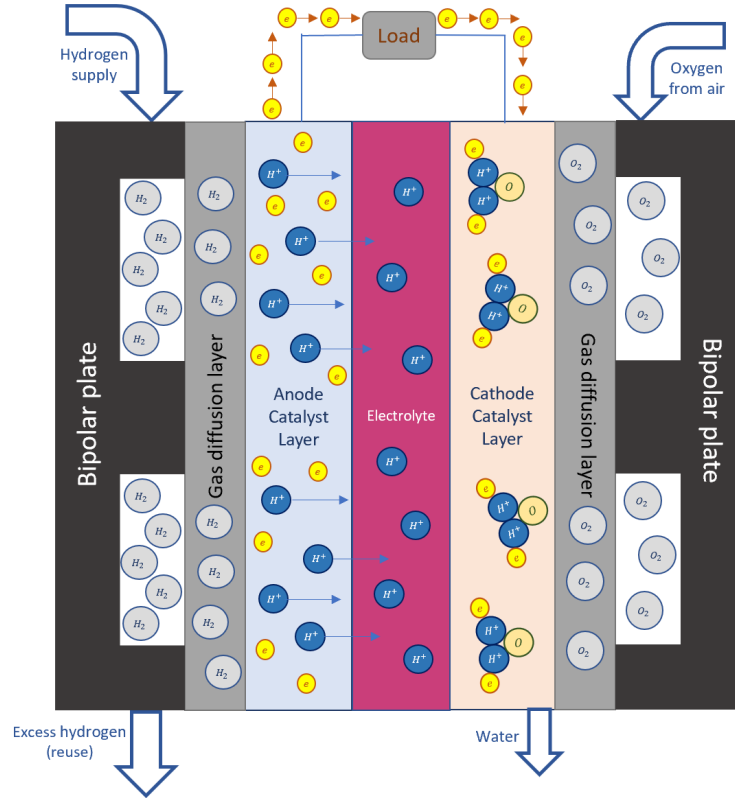


Figure 2.1: PEM fuel cell unit

reacts with hydrogen ions and electrons, producing water, through the following chemical reaction:



The overall reaction is a combination of two half-cell reaction, which occurs separately at two electrodes:



The only products of the overall reaction is water and heat.

The potential difference between two electrodes ranges from 0 and 1,2 depending on the current density. This dependence is graphically illustrated in Figure 2.2 and is called polarization curve. Open circuit voltage (V_{OCV}) is a maximum real voltage and is reached when there is no current. However, maximum theoretical voltage, or Nernst potential can be never reached in practice due to intrinsic internal losses. Polarization curve can be divided into three regions: first and third are highly nonlinear and the second one has an almost linear relationship between current

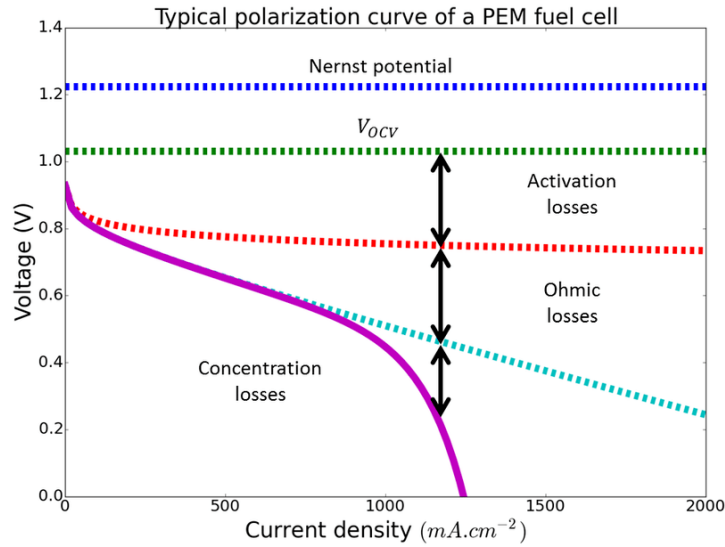


Figure 2.2: FC polarization curve [2]

density and voltage. Usually, FC operate in second region. The energy conversion efficiency of fuel cell can be calculated as a ratio between working voltage and open circuit voltage.

The maximum efficiency of FC is around 70 %, which is almost twice more that of ICE, however smaller than that of batteries or supercapacitors. In addition, since output electrical energy of FC is not converted from heat (as it is for ICE), its efficiency is not limited by Carnot efficiency and can be potentially increased. The operation of FC is not constrained only by pure hydrogen gas, but other hydrogen bounds, such as methane or methanol can be used as reactants. Moreover, FC have zero carbon emissions, so depending on the source of hydrogen production, FC can be treated as green energy producing device. In addition, FC have modular design, so they can be stacked together to achieve required voltage. There is also negligible dependence of efficiency on size of FC and co-generation is possible due to continuous supply of heat.

2.2 Fuel cell losses

There are a number of sources for FC energy losses and can be generalized in 4 categories: activation losses, ohmic losses, concentration or mass transport losses and fuel crossover losses. The share of different losses is graphically illustrated in Figure 2.3 As it is mentioned above, polarization curve is divided into three regions: the abrupt drop in voltage in the first region corresponds to kinetic losses due to

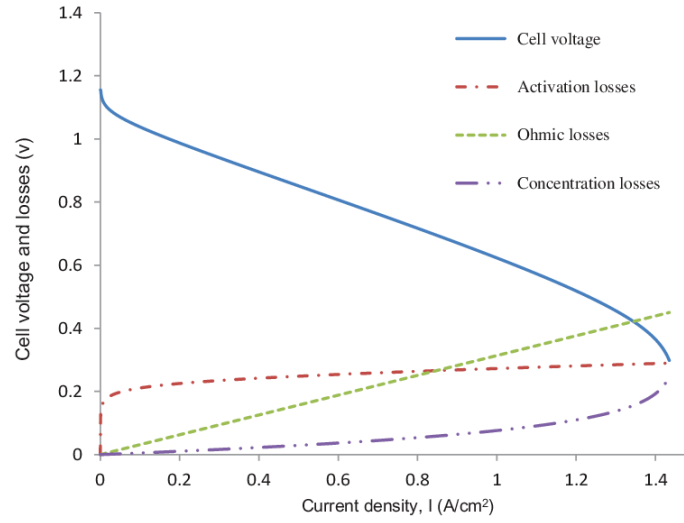


Figure 2.3: Sources of voltage losses [3]

slow kinetics at surface of electrodes. These losses are called **activation losses**, which happen due to potential difference in electrodes, needed for the initiation of reaction. These losses are principal at low current densities and are logarithmically related through the following equation:

$$V_{act} = \frac{RT}{\alpha n F} \ln(i/i_0) \quad (2.4)$$

Where R is the universal gas constant ($R=8,314$ J/molK); F -Faraday constant; T -temperature; α -transfer coefficient; n -number of moles; i -fuel cell current density and i_0 is exchanged fuel cell current density.

In second region, at moderate values current densities, **Ohmic losses** are dominant. These losses happen due to resistance of electrodes for electron flow and resistance of electrolyte membrane to flow of ions. Generally, resistance is present for different elements of FC, but the dominant ones are electrodes and membrane. The resistance of membrane strongly depends on the humidity of FC, so ohmic losses vary with humidity of electrolyte membrane. Ohmic losses are characterized by the following equation:

$$V_{ohm} = I(R_m + R_e) \quad (2.5)$$

Where I is a current; R_m -membrane resistance; R_e -electrode resistance.

In third region, at high values of current density, concentration or mass transport losses become significant. At these values, FC voltage drastically drops to zero. The cause for these losses is the change of concentration of reactants at the surface of electrodes. In addition, the change in concentration of reactants results in the

drop of partial pressures of gases and the extent of change in concentration depends the current, drawn from FC.

$$V_{conc} = -\frac{RT}{nF} \ln\left(1 - \frac{i}{i_l}\right) \quad (2.6)$$

Where i_l is limit current density, where the voltage is null.

Finally, the last category of losses is fuel crossover losses. They are present due to the fact that some amount of hydrogen and electrons can flow through electrolyte membrane. They are negligible with respect to other losses and become important low temperatures.

Losses	Cause	Become important at	Methods for mitigation
<i>Activation losses</i>	Reduced reaction kinetics at electrodes	low current density	improved performance of catalyst and increased cell temperature
<i>Ohmic losses</i>	electrical resistance of electrodes and electrolyte membrane	moderate current densities	use materials with lower resistivity
<i>Concentration or mass transport losses</i>	change of concentration at surface of electrodes	high current density	reduced thickness and increased conductivity of electrodes as well as materials for bipolar plates
<i>Fuel crossover losses</i>	gas and electrons passage through membrane	almost negligible	reduced operating temperature

Table 2.1: Fuel cell losses

2.3 Fuel cell degradation

One of the major current issues of fuel cells is degradation phenomenon. Life-time and durability under various operating condition are the key factors for the commercialization and widespread adoption of polymer-electrolyte fuel cells [4].

FC electrodes and polymeric membrane (membrane-electrode assembly) are the most important FC parts that undergo degradation process. Gas diffusion layer, catalyst layer and polymeric membrane are the components of membrane-electrode assembly (MEA). Catalyst is plated with noble metals (usually with platinum) and is considered as the most expensive part of fuel cell (more than 50 % of total price). However, the degradation of the catalyst layer has a direct impact on the fuel cell's durability. The issue of chemical and morphological instabilities of the catalyst layer is of greater concern at high temperatures when it comes to electrode degradation. The degradation processes of electrodes are the following:

- During operation, the platinum agglomerates and the particle size grows larger [5]. The reaction rate of oxygen reduction steadily reduces as platinum particle size increases over time, and platinum utilization is reduced.
- During long-term operation, platinum is also found to dissolve and re-deposit [6].
- Because of the formation of oxygen atoms at the catalyst, corrosion of the carbon support in the cathode may occur if the cathode is held at relatively high oxidation potentials [7].

The degradation modes of membrane are

- Acid evaporation causes a rise in fuel crossover and a decrease of fuel efficiency [8].
- Potential pinhole development due to membrane thinning [8].

Due to reduced humidity of membrane at high operating temperatures, the proton conductivity property of electrolyte membrane exacerbates. In addition, membrane dehydration results in loss of mechanical stability at high operating temperature [9]. Above a polymer's glass transition temperature, a significant amount of morphological relaxation takes place, which may negatively impact membrane characteristics[10]. Finally, hydroxyl radicals are in charge of the chemical attack on the membrane during fuel cell operation, which starts the degrading process [11].

Loss of phosphoric acid from the membrane and electrodes, in contrast to the aforementioned degradations, is a peculiar feature of high temperature PEMFC degradation. The components of the fuel cell are exposed to a severe environment because of the fuel cell's acidic atmosphere, along with the temperature, humidity, and air quality. One of the main processes of degradation is believed to be phosphoric acid loss, particularly in high current density and high temperature environments [12].

2.4 Fuel cell technologies

Various fuel cells are currently being developed at various levels. According to the mixture of fuel, oxidant, electrolyte, operating temperature, and other factors, fuel cells may generally be divided into different categories. The type of electrolyte utilized determines the most practical categorisation. The choice of electrolyte is crucial since it determines operating temperatures and all other parameters. The major types of fuel cells are alkaline fuel cell (AFC), phosphoric acid fuel cell (PAFC), molten carbonate fuel cell (MCFC), solid oxide fuel cell (SOFC), direct methanol fuel cell (DMFC) and proton exchange membrane or polymeric electrolyte membrane fuel cell (PEMFC).

2.4.1 Alkaline fuel cell

Potassium hydroxide (KOH), an aqueous alkaline solution is used as an electrolyte. In this type of fuel cell, an ion, conducted through the electrolyte is hydroxide ion (OH^-). AFC is one of the most efficient FC, reaching maximum of 70 %. The working temperature varies between 90 and 250 degrees Celsius and depends on the concentration of KOH. Pure oxygen, or purified air, are often used as an oxidant. Thus, generation and storage requirements of pure oxygen make AFC expensive. On the other side, the oxygen reduction reaction (ORR) kinetics at the cathode are significantly simpler than in acidic cells due to intrinsic properties of alkaline chemistry, and therefore making possible to use less expensive catalyst metals. The half-cell reactions are



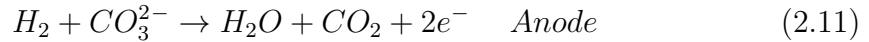
2.4.2 Phosphoric acid fuel cell

Highly concentrated or pure liquid phosphoric acid (H_3PO_4) saturated in silicon carbide (SiC) matrix is used as an electrolyte in PAFC. Platinum is used as a noble metal in catalyst layer. The maximum efficiency, that can be reached is around 70%. The operating temperature range is around 150-200 degrees Celsius and expelled heat can be used fro co-generation. PAFC are more flexible for usable fuels. The half-cell reactions are



2.4.3 Molten carbonate fuel cell

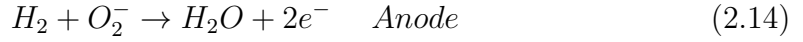
Molten carbonate salt mixture suspended in a porous, chemically inert ceramic matrix of beta-alumina solid electrolyte (BASE) is used as an electrolyte for MCFC. They operate at high temperatures, around 600-700 degrees Celsius. MCFC can reach maximum efficiency around 60% and 85% with co-generation and doesn't require pure hydrogen as a fuel, hydrogen bounded fuels are spontaneously converted to hydrogen by internal reforming. Due to high operating temperature, MCFC are usually implemented in stationary applications and doesn't require precious metals, used in catalyst layer, thus reducing cost. In addition, proper materials should be carefully selected to withstand high thermal loads. On the other side, high working temperature leads to faster component breakdown and corrosion, affecting durability. The current researches on MCFC are mostly concentrated on the development of materials, that withstand harsh corrosive environment without the loss of performance. The half-cell reactions are



2.4.4 Solid oxide fuel cell

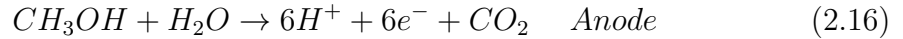
Solid oxide or ceramic electrolyte, like Y_2O_3 or ZrO_2 are used as electrolytes in SOFC. Differently from other types of FC, SOFC electrolyte conducts negative oxygen ions. They operate at extremely high temperature, around 700-1200 degrees Celsius, which creates the issues, concerning prolonged start-up, proper material choice and mechanical (thermal expansion) as well as chemical compatibility. High working temperatures enables the following features of SOFC:

- Relatively low cost. No need of usage expensive precious catalyst metals.
- Fuel flexibility. No need of usage of pure hydrogen, light hydrocarbon fuels (methane, propane or butane) can be internally reformed.
- Improved kinetics of oxygen ion transport due to reduced activation losses. The dominant losses are related to ohmic losses.
- High combined heat and power efficiency



2.4.5 Direct methanol fuel cell

The working principle is similar to PEMFC, however the fuel used here is methanol. The easiness in methanol production, transportation and storage, high energy density and stable liquid phase are the main factors for DMFC selection. The working temperature and efficiency are relatively low, around 60-120 degrees Celsius for the former and 30-40 % for the latter respectively. The main disadvantage of DMFC is methanol cross-over through membrane. This is the main reason for low efficiency. The emissions are carbon dioxide and water.



2.4.6 Proton exchange membrane fuel cell

PEM is also known as polymeric electrolyte membrane fuel cell and operates in reverse principle of electrolysis. Due to relatively low operating temperature (70-120 degrees Celsius), PEM fuel cells are usually used in mobile applications. Hydrogen proton conducting polymeric electrolyte is used as membrane. The maximum efficiency that can be reached is around 60-65 %. The ion conducted through membrane is hydrogen ion (H^+). Platinum is used as catalyst precious metal in carbon supported catalyst layer. The half cell reactions are



Since operating temperature is low, PEM fuel cells are used in fuel cell electric vehicles. Pure hydrogen should be fed due to weak almost negligible internal reforming process and oxygen is taken from air. One of the main issues of PEM fuel cell is water management system. Membrane electrode assembly should be continuously humidified due to excess of air, which results in membrane electrode assembly drying. The summary on fuel cell technologies is provided in Table 2.2.

Type	Electrolyte	Working temp.	Charge carrier	Efficiency	Fuel	Pros	Cons
Alkaline fuel cell	KOH	90-250°C	OH^-	70%	H_2	Low temp.; high eff.; low cost	CO_2 poisoning and durability issues
Phosphoric acid fuel cell	H_3PO_4	150-200°C	H^+	70%	H_2	Low temp.; good transient; high eff.;	CO poisoning; system complexity
Molten carbonate fuel cell	BASE	600-700°C	CO_3^{2-}	60%	H_2, CH_4	Fuel flexibility; fast transient; negl. poisoning	slow start-up; corrosive electrodes
Solid oxide fuel cell	Y_2O_3 or ZrO_2	700-1200°C	O_2^-	55%	H_2, CH_4	Fuel flexibility; fast transient; low cost	brittleness of ceramics; slow start-up;
Direct methanol fuel cell	polymer membrane	60-120°C	H^+	35%	CH_3OH	Metahnol as a fuel	low eff.; methanol crossover;
Proton exchange membrane fuel cell	Polymer membrane	70-120°C	H^+	65%	H_2	air as an oxidant; high power density	drying issues; poisoning issues

Table 2.2: Classification of fuel cell technologies

2.5 Fuel cell stack, system and auxiliaries

The voltage generated by a single fuel cell unit is in the range of 0.9-1 V. In order to increase this value, fuel cell units are connected in series. **Fuel cell stack** is a series connected fuel cell units. The output voltage of FC stack in number of cells times the voltage of single unit.

$$V_{stack} = NV_{unit} \quad (2.20)$$

Where V_{stack} is a voltage of FC stack; N-number of cells and V_{unit} is voltage of FC single unit (1-1.2 V)

The schematics of fuel cell stack is illustrated in Figure 2.4.

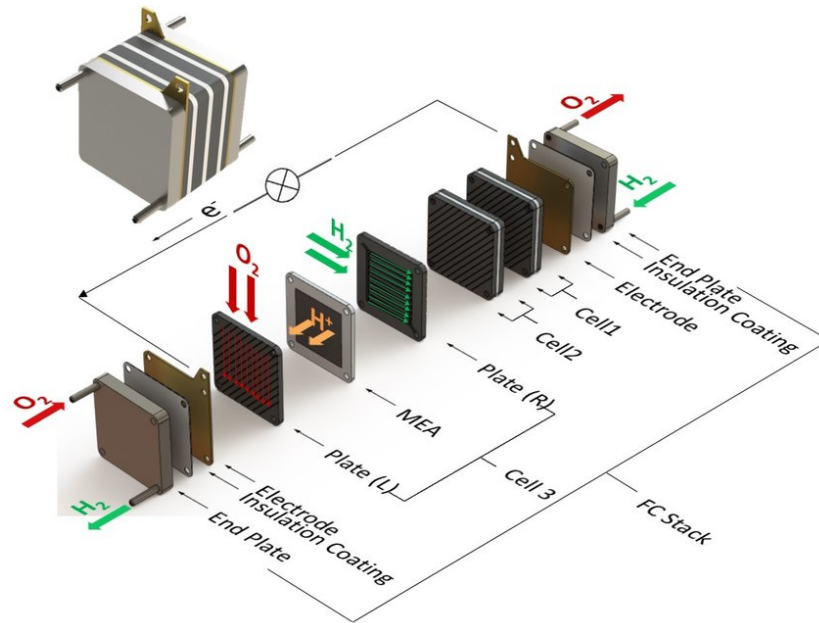


Figure 2.4: Fuel cell stack [13]

A FC stack efficiency can be calculated through the following relation

$$\eta_{stack} = \frac{P_{stack}}{\dot{m}_{H_2} LHV} \quad (2.21)$$

Where P_{stack} - FC stack output power; \dot{m}_{H_2} - hydrogen mass flow rate; LHV - hydrogen lower heating value. It is an amount of heat, released by a combusting specific quantity of fuel at specific initial temperature and pressure (usually standard conditions) and returning the products temperature to a level, where the latent heat of vaporization of water cannot be recovered. This value for hydrogen gas is around 120 MJ/kg.

The type of fuel cell, the size of the cell, the operating temperature, and the pressure of the gases fed into the cell are the variables that affect how much power a fuel cell can generate. However an isolated FC stack cannot generate power. For the continuous operation and power generation of FC stack, it requires auxiliary systems. They are air supply system, fuel supply system, cooling system, humidification system. The combination of FC stack and all its auxiliary systems is called **fuel cell system**. Since all fuel cell auxiliary systems are powered by stack, the effective FC system output power is less than stack power. The largest power consumer is air compressor. FC system efficiency is defined as

$$\eta_{sys} = \frac{P_{sys}}{\dot{m}_{H_2}LHV} \quad (2.22)$$

$$P_{sys} = P_{stack} - P_{aux} \quad (2.23)$$

Where η_{sys} -FC system efficiency; P_{sys} -FC system output power; P_{aux} -FC auxiliary system power. The FC stack and system efficiency and its dependence on power is represented in Figure 2.5

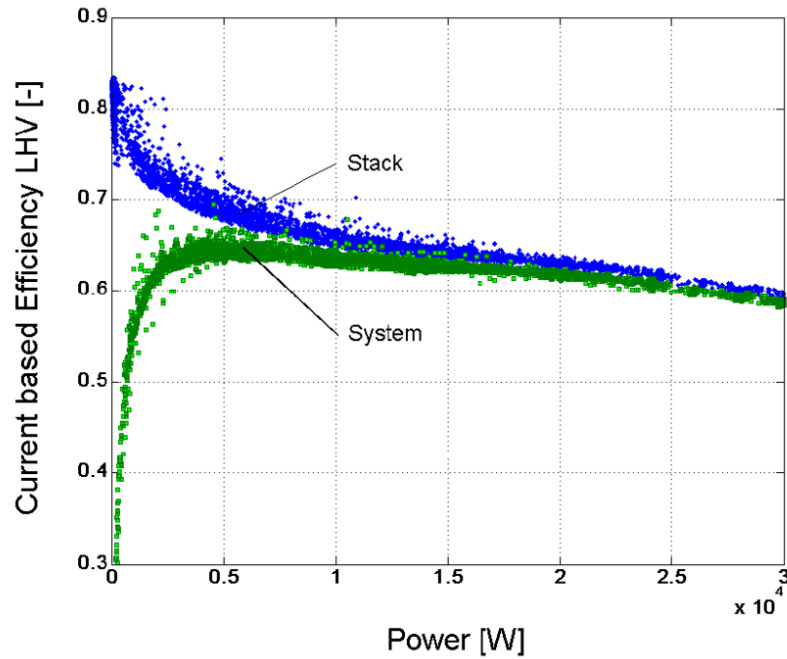


Figure 2.5: FC stack and system efficiency [14]

The general schematics of FC system is illustrated in Figure 2.6.

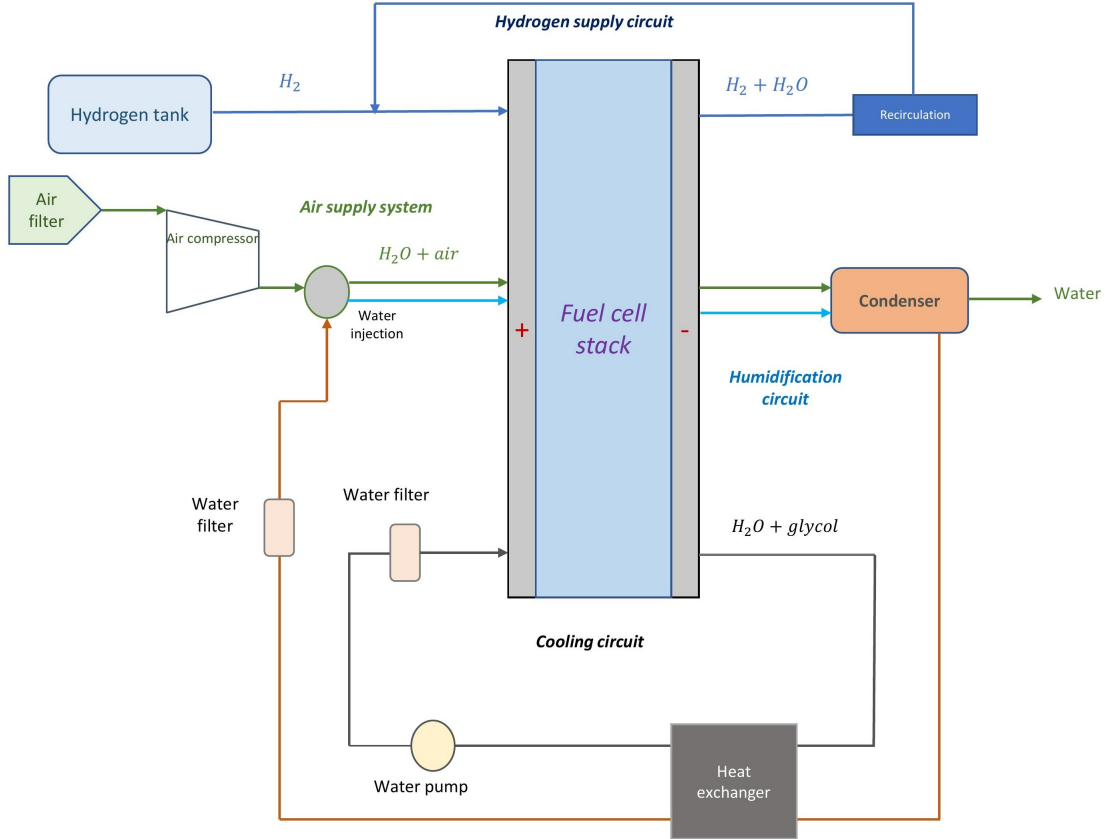


Figure 2.6: Fuel cell system

2.5.1 Air supply system

In order for the reduction process in cathode to take place, an oxidant should be supplied. In case of PEM fuel cells, an oxygen from air serves as an oxidant. Air compressor is required to feed the air to the voids of bipolar plate in cathode side. Air compressor raises the inlet air pressure to 2-4 times than ambient atmospheric pressure. Therefore, an air compressor is necessary for efficiently drawing and compressing air over a wide range of airflow rates. Positive displacement and centrifugal compressor can be used, the difference between them is in the method airflow rate regulation. Figure 2.7 illustrates a FC air compressor, installed in modern Toyota fuel cell electric vehicles (FCEV).

$$\dot{m}_{air} = \frac{\dot{\mu}_{fuel}}{2 * 0.21} M_{air} \quad (2.24)$$

$$\mu_{fuel} = \frac{P_{fc}}{\eta_{fc} LHV_{mol}} \quad (2.25)$$

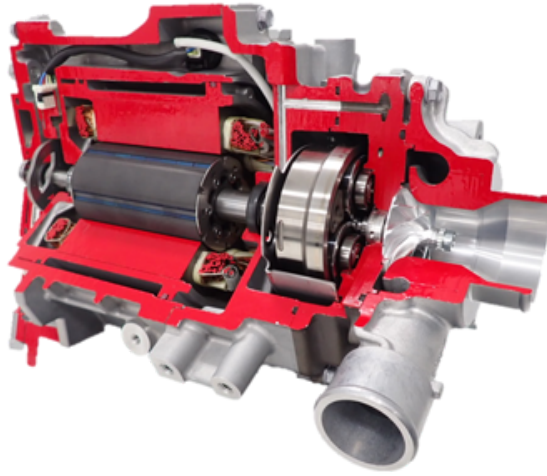


Figure 2.7: Toyota FCEV air compressor [15]

Where m_{air} - air mass flow rate; μ_{fuel} -fuel flow rate (molar); M_{air} -air molecular weight; η_{fc} -fuel cell system efficiency LHV_{mol} -hydrogen lower heating value (molar), equal to 242 kJ/kmol.

Number 0.21 in the denominator of equation 2.24 indicates the oxygen content in air, while 2 indicates that the molar ratio of hydrogen to oxygen for a complete reaction is 2 to 1.

2.5.2 Hydrogen supply system

Practically, hydrogen can be stored on-board in either two ways: gaseous compressed and liquid cryogenic hydrogen. Gaseous hydrogen is stored at ambient temperatures and high pressure (around 600 bar). Usually two or more tanks are used. On the other side, hydrogen liquefies at less than $-253^{\circ}C$. Therefore, hydrogen storage tank should be perfectly insulated to minimize heat transfer. In this case, hydrogen is stored at ambient pressure but extremely low temperature. In automotive industry, hydrogen storage in gaseous form is implemented. The issues of this technology comes from the material, which should withstand the pressure in the order of 600-700 bars. For this purpose, polymer liners with reinforced resistant external shell is used. Concerning hydrogen supply system, a recirculating pump is required to run the excess hydrogen, that did not react during power generation and the generated water again to supply circuit. Figure 2.8 illustrates a FC hydrogen circulation pump, installed in modern Toyota fuel cell electric vehicles (FCEV).

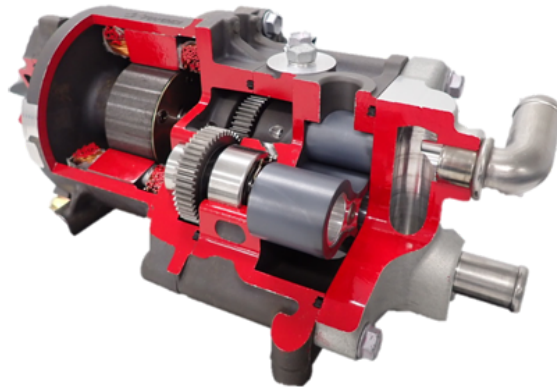


Figure 2.8: Toyota FCEV hydrogen circulation pump [15]

2.5.3 Cooling system

Since the effective efficiency of FC stack is currently no more than 70 %, generated heat should be dissipated by heat management system. The mixture of water and glycol is run through the cooling circuit by means of water pump. In addition, cooling water can be potentially used for humidification purposes. Then, cooling liquid dissipates the heat to external environment through radiator.

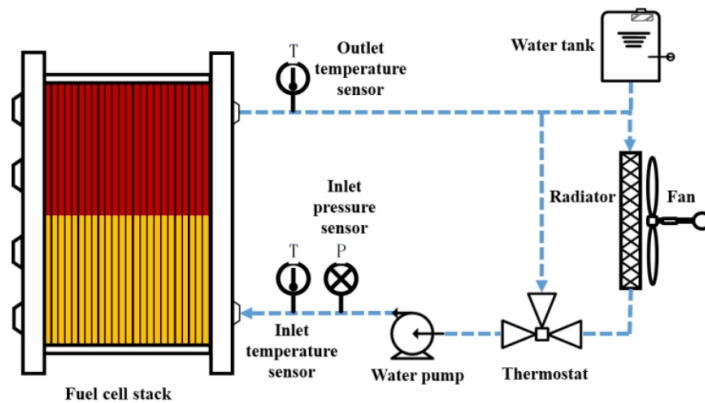


Figure 2.9: Fuel cell cooling system [16]

2.5.4 Humidification system

FC membrane should be continuously humidified to avoid the drying and thus membrane failure. Therefore hydrogen and incoming air should be humidified to prevent the drying of anode and cathode side. In addition, excess of air, that do not react, may remove water, which is produced as a result of chemical reaction. If the rate, at which it is removed is higher than the rate at which is produced, it may result in MEA failure, therefore the important design criteria of humidification system is

$$Q_{prod} > Q_{rem} \quad (2.26)$$

Where Q_{prod} is the water flow rate creation due to chemical reaction and Q_{rem} is the water flow rate, withdrawn by air.

In automotive industry, in order to avoid the dependence on external water for humidification, the condensed water, the product of reaction, is implemented. Therefore, separate components are required for condensation and circulation purposes. There are several humidification techniques: Injection of water (vapor) into the hydrogen/air stream; use the water product to mix it with inlet air; passing inlet air through water. The former one is straightforward solution, but requires some heat to vaporize the water and humidify the air, which is taken from stack excess heat. The next one is the most popular and usually used in mobile applications. The latter one provides large contact area, but has control issues. Therefore it is used in testing or laboratory applications.

Chapter 3

Fuel cell technology in automotive industry

Nowadays, for more than a century, internal combustion engines have been used for vehicle propelling for a number of advantages they possess. These are high power mass and volume density, fast transient response, simple and reliable layout, good durability and relatively low price. However, the presence of noxious emissions and low thermal efficiency force automotive manufacturers to use alternative fuels or totally different propulsion system. Due to the ecological problems concerning the global warming and climate change, governmental authorities set strict limitations on exhaust emission gases for OEMs. Moreover, ICE have almost reached its maturity level up to now and since it is a thermal machine, its efficiency is limited by Carnot efficiency. Battery electric vehicles (BEV) are the possible solution. Electrical energy, stored in chemical form inside the battery packs is converted into mechanical energy via electric motor/generator. Simplicity of this solution, high energy conversion efficiency, reversibility of electric machines, low operation costs, total absence of tank-to-wheels emissions and low noise emissions make this solution promising in automotive market. However, high price of batteries and long charging time are the factors, that create inconveniences for customers and limit the prevalence of BEV in the world.

Another, more promising solution is to combine thermal and electric propulsion systems by taking the advantages of both and make it work in parallel. These kind of vehicles are called Hybrid Electric Vehicles (HEV). Usually, batteries or supercapacitors are used as an additional power/energy source. The main advantages of electric powertrain is high efficiency (80-95 %) and reversibility of power conversion. These factors allow several modes of operation be possible. For example, ICE usage can be avoided when it works in low efficiency regions (low speed/ low torque and high speed/low torque zones), and EM can be used instead,

braking energy can be recovered and stored in batteries to supply later again, ICE and EM can be operated simultaneously during power starving. The presence of these operation modes is intended to achieve reduced fuel consumption, enhanced performance, reduced engine emissions and the possibility of engine downsizing. The first example of HEV, which became widely available is Toyota Prius. It was presented in 1997 in Japan and became the first mass-produced hybrid electric vehicle. Since HEVs have two or more power sources, the question of power control becomes essential. The power required by a vehicle should be distributed between ICE and electric machine in a way that system overall efficiency and fuel consumption is optimized. Therefore, the proper design of energy management system (EMS) to control the power flow is important. Depending on the type of powertrain, HEVs are classified as parallel hybrids, series hybrids, power split hybrids and plug-in hybrids. In parallel hybrids, hybridization is realized at powertrain level with a mechanical direct or indirect link [17]. In series hybrids, hybridization is realized at energy source level with one electric link. This system has one powertrain with the electric machine as a torque actuator [17]. In power split hybrids, parallel and series layouts are combined. As a result, the system becomes more flexible and efficient. In plug-in hybrids, batteries with higher capacity are implemented so that they can be recharged by an external electric power source. Depending on the degree of hybridization, HEVs can be classified as minimal hybrid, mild hybrid and full hybrid. In the case of minimal and mild hybrids, a vehicle cannot be driven separately by an EM due to the lack of electric power. For full hybrids, a vehicle can be propelled by ICE only, EM only or a combination of both.

Another solution is fuel cell electric or fuel cell hybrid electric vehicles (FCEV or FCHEV). An effective integration of FC stack and its auxiliary systems allows to generate electrical energy by the reaction of hydrogen and oxygen. The implementation of fuel cell technology to run a vehicle poses several advantages. These are zero tank-to-wheel carbon emissions, zero tank-to-wheel noxious emissions, high FC power density and high FC energy conversion efficiency (higher than ICE, but lower than EM). The challenges, concerning FC technology implementation in the transportation sector are the cost of hydrogen and the vehicle itself, logistics issues of hydrogen gas, and fuel cell durability and reliability.

The way the FC produces electricity is a reverse principle of electrolysis, so the products are heat and water. No carbon or noxious emissions are present. Therefore, FC vehicles can be considered as zero-emission only from a tank-to-wheel point of view. From a well-to-wheel point of view, the degree of purity of this solution strictly depends on the source of hydrogen production. Steam reforming and electrolysis are the two main methods of hydrogen production. Reforming is a process by which hydrogen can be extracted from hydrocarbons through chemical reactions. Hydrogen is extracted from hydrocarbon fuels like gasoline, methane, or methanol using high-temperature steam. Although this method uses fossil fuels

to make hydrogen and emits pollutants, it is the most popular since it is the most economical. The mechanism by which more than 95 percent of the hydrogen available nowadays in the world is produced is steam reforming. Electrolysis is the most environmentally friendly method of producing hydrogen, but it is also the most expensive. Electrolysis-based hydrogen generation can be up to ten times more expensive than steam reforming-based hydrogen synthesis. In addition, nowadays, according to the report of US Energy Efficiency and Renewable Energy office, most hydrogen is being produced from fossil fuels, specifically natural gas, and only small portion is produced from renewable energy sources [18].

FC vehicles are almost 2-3 times more efficient than conventional gasoline ICE vehicles and 1.5-2 times than diesel ICE vehicles. The maximum efficiency of PEM fuel cells that can be reached is 65 %, while for gasoline and diesel ICE is 35 % and 40 % respectively. Moreover, the maximum achievable efficiency of thermal machines is limited by Carnot efficiency, this value is 55-60 % for diesel and 50 % for gasoline ICE. For the case of FC, improving the performance, implementing less-resistant robust materials for MEA and reducing the losses, listed in chapter 2, the efficiency can be reached up to 90 %.

Another issue concerning FC vehicles is hydrogen storage. In case of PEMFC, proper materials should be used for hydrogen tank to withstand the pressure in the order of 600-700 bar. In case of MCFC, SOFC or DMFC hydrocarbon fuel could be stored in a tank, which would subsequently be processed in an on-board reformer to produce hydrogen. Depending on the layout, FC vehicles can be categorized as fuel cell electric vehicles (FCEV) and fuel cell hybrid electric vehicles (FCHEV). Depending on fuel cell sizing, FCHEV can be further divided into range extender, load follower and full power (Figure 3.1)

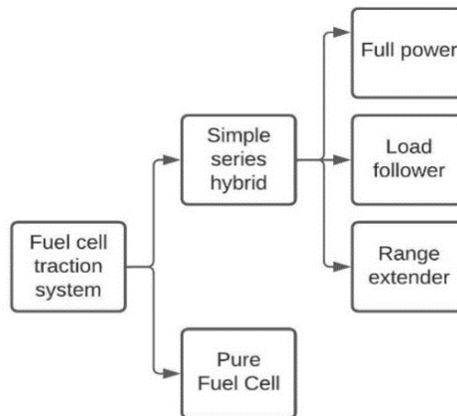


Figure 3.1: Classification of fuel cell vehicles

3.1 Fuel cell electric vehicles

In this layout, fuel cell system serves as the only power source to run the vehicle. Therefore, FC system should be designed to provide maximum transient power request. All the power required by vehicle is supplied by FC. The schematics of this structure is represented in Figure 3.2

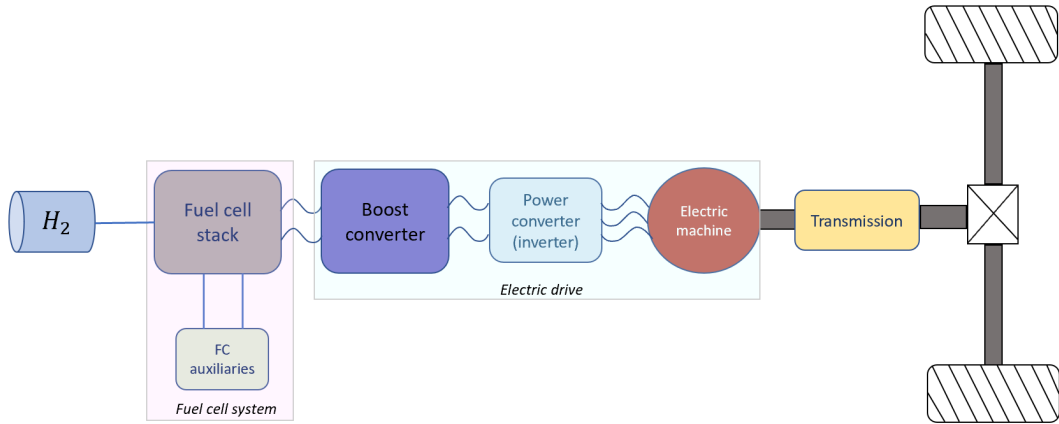


Figure 3.2: Fuel cell electric vehicle layout

Since FC is not a reversible system, regenerative braking mode of operation is not possible in this layout. FC system should correspond to instantaneous vehicle dynamics and face the issues of system warm-up.

3.2 Fuel cell hybrid electric vehicle

The propulsion system is realized as series hybrid layout, so the hybridization is done at energy source level with one electric link [19]. The schematics of this layout is represented in Figure 3.3

In this layout, either battery or supercapacitor is used as an additional power/energy source. The primary distinction between a battery cell and a supercapacitor's functional capabilities is that batteries have a higher energy density than supercapacitors do (i.e., they can store more energy per unit mass), but supercapacitors have a higher power density (they can store and release large power). As a result, supercapacitors are considered to be the best for providing large amounts of power, but batteries continue to be the best at holding vast amounts of energy for extended periods of time. Since there are two power sources on the board, the question of energy management strategy becomes important. FC can be sized either to provide either maximum continuous, maximum transient or average power of a cycle.

The advantages of hybrid fuel cell layout of pure fuel cell traction system are:

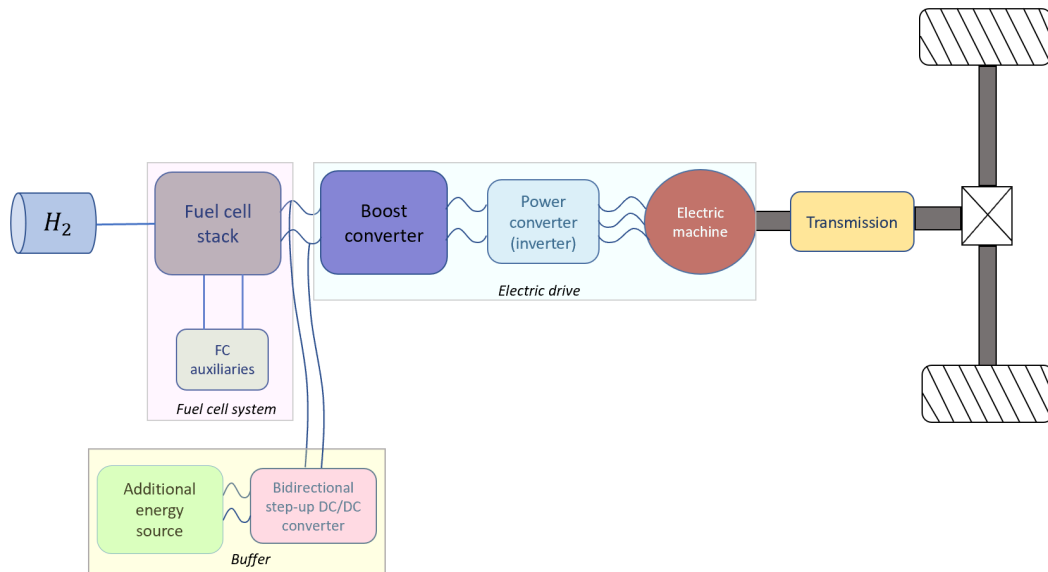


Figure 3.3: Fuel cell hybrid electric vehicle layout

- Regenerative braking is possible
- By managing power flow, it is possible to optimize fuel consumption and system efficiency.
- Less dynamic stress on FC during power phases
- Enhanced transient response of a vehicle
- Faster warm-up of a vehicle

3.3 Control strategies of hybrid vehicles

FCHEV is examined in terms of the various energy sources that must be controlled properly in order to guarantee that the energy supplied to the electric motor is adequate in accordance with the demand or load power. This is due to the fact that, depending on the circumstances, either battery, fuel cell, or both energy sources could be used to generate electricity. Other times, both battery and fuel cell are used to supply the energy, and at some points or both battery and supercapacitor are charged [20]. The general rules of EMS development are established on several general principles, comprising the optimization in both FC and battery optimization. They are

- Both FC and batteries are set to operate at most efficient regions for the majority of time
- Decrease of fluctuating operating points to minimize FC dynamics
- Optimization of ON/OFF periods to fully utilize dual power sources
- Operate the battery in charge sustaining mode to prolong the battery life and to allow EM to work efficiently
- EM's operating point is optimized based on the preferred zone of the torque-speed diagram
- Based on the driver's actions, regenerative braking is intensified to optimum energy regeneration [21]

The realization of these principles in vehicle is done through the following actions, which are the bases for EMS logic:

- At low speeds, when the efficiency of FC is low, battery runs the vehicle
- During acceleration or climbing (power starving modes), both fuel cell and battery provides the power
- When SOC of battery is low, FC provides power both for the traction and charging the batteries
- During the deceleration phases, braking energy is used to charge the batteries.

Overall there are 5 modes of operation of hybrid vehicles: charging while driving; energy regeneration during braking; battery charging; power starving and battery drive (Figure 3.4)

The purpose of EMS for hybrid powertrains is to distribute the required power among various energy sources to maintain battery state-of-charge, maximize drivetrain efficiency, reduce fuel consumption and emissions, or other relevant goals [22]. In this analysis, EMSs are divided into two major categories: **rule-based strategies** and **optimization based strategies**. Rule-based strategies can be further divided into deterministic and fuzzy-logic rule-based strategies, while optimization based strategies are divided into instantaneous (real-time) optimization, global optimization and model predictive control (Figure 3.5). Additionally, all EMSs are categorised into two groups (offline and online) based on the usage of real-time implementation because the goal of building any EMS is to utilize it in practical applications or to serve as a benchmark to assess the efficacy of other techniques [22].

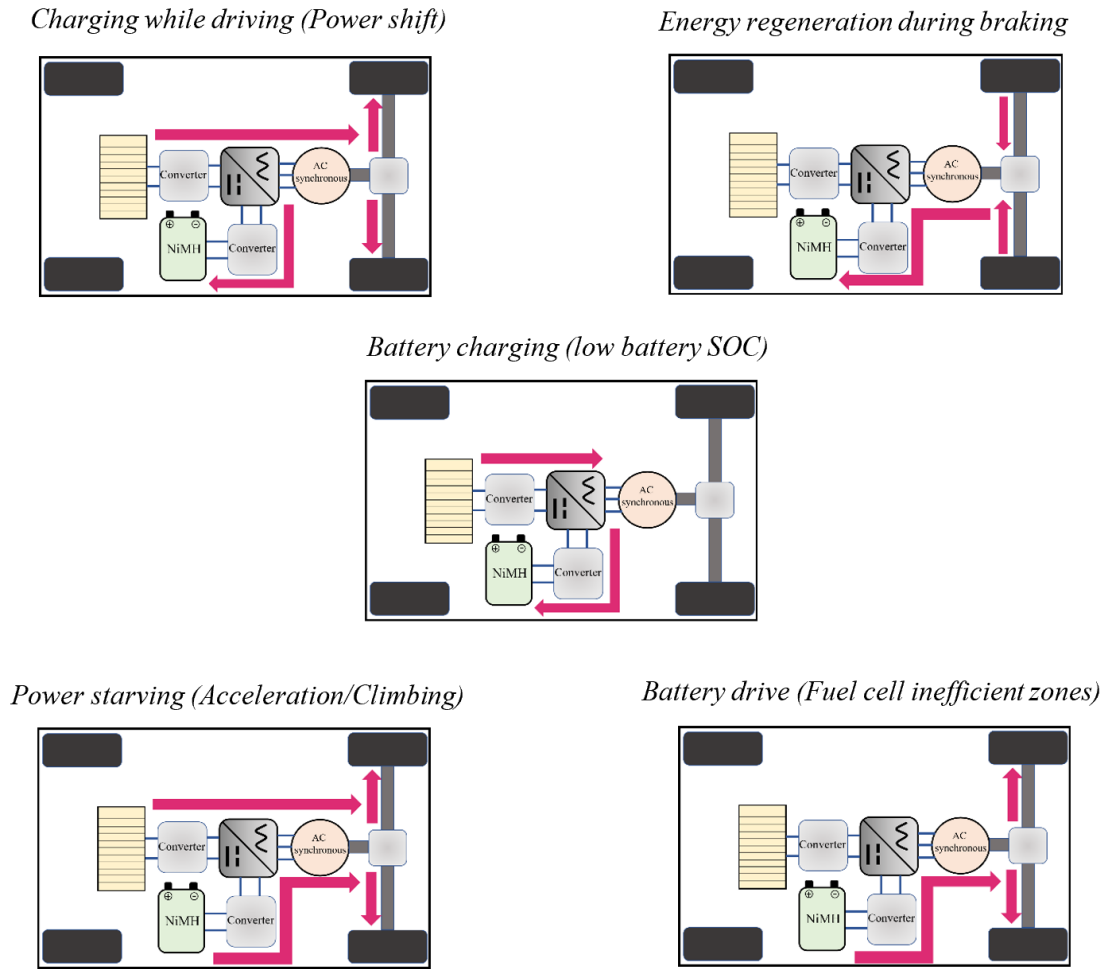


Figure 3.4: Operation modes of hybrid vehicles

Designing effective control strategies is a difficult task. The control strategy's first goal is to maximize vehicle performance while minimizing fuel consumption in order to meet the driver's power requirement. If a controller functions reasonably well with a different set of assumptions, it is considered to be robustly designed for that set of parameters. Robust controllers are intended to work properly with uncertain parameter or disturbance sets in order to deal with uncertainty. An optimization problem's local solution is the best solution (either maximal or minimal) among a set of nearby solutions. A global optimal solution is the best option available among all feasible solutions to an optimization issue, as opposed to a local optima [23].

Until a genuine model is built and substantial simulations or experimental work is done, the real performance of the EMS will only be theoretical. An EMS, however,

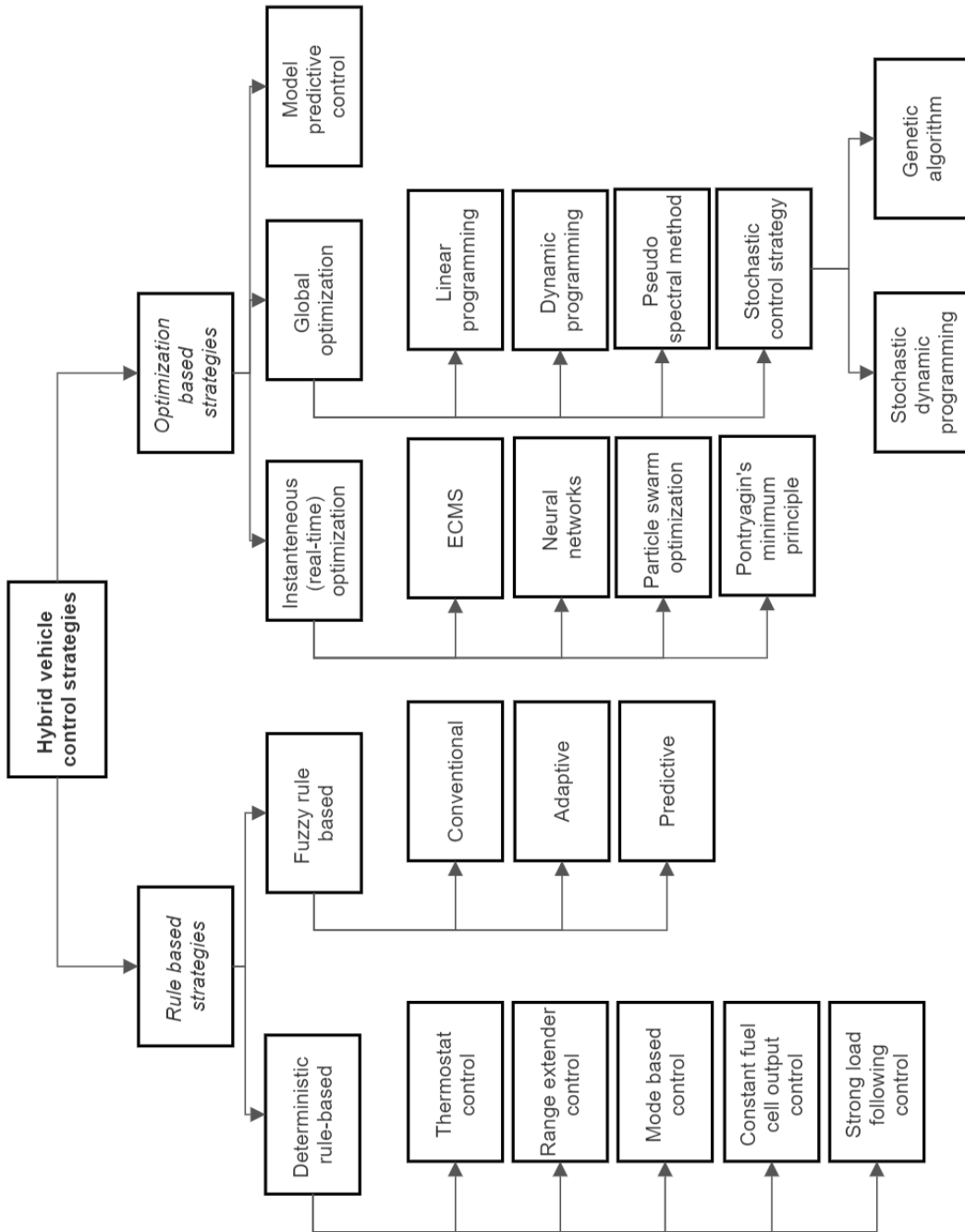


Figure 3.5: Classification of control strategies for hybrid vehicles

is seen to have a high potential to offer the needed degree of performance. This analysis is based on research on several forms of HEV, the use of its EMS, and knowledge of both their benefits and drawbacks. The main issue arises from the lack of knowledge on factors that can only be measured in the future, such as journey length, vehicle speed, driving style, road conditions, weather, etc. When the aforementioned details of a future journey are known in advance, an energy management controller can only choose the best power flow plan [24].

3.3.1 Rule-based strategies

Rule-based (RB) control is a type of vehicle control that relies on human expertise (engineering knowledge), heuristics, intuition, and even mathematical models [25]. It also uses pre-determined driving cycles and load leveling strategies. They base their decision about the distribution of power at each instant on a set of predetermined rules. These strategies can be implemented with real-time supervisory control to manage the power flow in a hybrid drive train [23]. RB controllers are static controllers, so the operating point of components are generally selected using proper tables or charts to best fulfill the needs of driver in an efficient way. The decisions are related to instantaneous inputs only. Deterministic rule-based methods and fuzzy rule-based methods are two categories of rule-based control strategy.

Deterministic rule-based strategies

Designing deterministic rules involves using look-up tables rather than real-time data in deterministic rule-based strategies. Fuel economy or emission data, FC operating maps, power flow inside the drive train, and driving experience are all used in the rules development. Look-up tables are used to implement the regulations and divide the power demand between the electric traction motor and FC [23]. Deterministic rule-based strategies can be further divided into thermostat control, range extender control, mode based control, constant fuel cell output control and strong load following control [19].

For *thermostat control strategy*, FC is used to generate electricity and charge the batteries. Battery SOC is always remained between maximum and minimum levels by turning FC on and off. This control mechanism causes the sources to often turn on and off (charge and discharge), which is problematic for battery systems, for instance. The SOC of the sources determines when they turn on and off [25]. When the battery's charge level exceeds the minimal threshold, the fuel cell, which supplies energy for both propulsion and battery charging, begins to function. The vehicle is first started by using the battery and is kept in this operational condition until this threshold is reached. Battery's state of charge rises throughout the cycle from when the fuel cell is turned on [19]. Although the strategy is simple, the

method is unable to meet all operating modes' power demand.

For *range extender control strategy*, the battery is primarily responsible for the vehicle's propulsion, but FC can generate extra power to keep the battery charged and extend its range. Usually, power delivered by FC is kept constant and battery operates in charge sustaining mode [19]. By taking to the reference BEV, the purpose of hybridization is to increase the travel range by reducing the volume and weight of battery packs. A fuel cell system, which is designed to supply average power demand, is added to the existing electric powertrain. DC/DC mono-directional step-up converter should be used on fuel-cell side, because the FC power is lower than the battery one.

For *mode based control strategy*, the goal is to operate the vehicle in a variety of modes depending on the battery's state of charge and the power requirements of the fuel converter. The battery runs at a fixed set-point proportional to its current SOC while the fuel cell is operated in a variety of modes with an On/Off switch and is used to respond to changes in the power demand. The battery operates in charge-sustaining (CS) mode. The analysis of this control method was done by Luciani et al., 2022 on FCHEV [26]. In that analysis the fuel cell system is assigned as the main power source, and its output power is limited in order to fit the driving power requirements of the vehicle. With the exception of possible initial cold starts, low driving power demands, and when the battery pack is at a high state of charge, the fuel cell system is on for the majority of the driving time. The prior status is checked, deviations are kept to a minimum, and the battery is taken into account to function in CS mode and to produce smooth fuel cell power output changes. Figure 3.6 illustrates the logic behind the baseline mode-based control method.

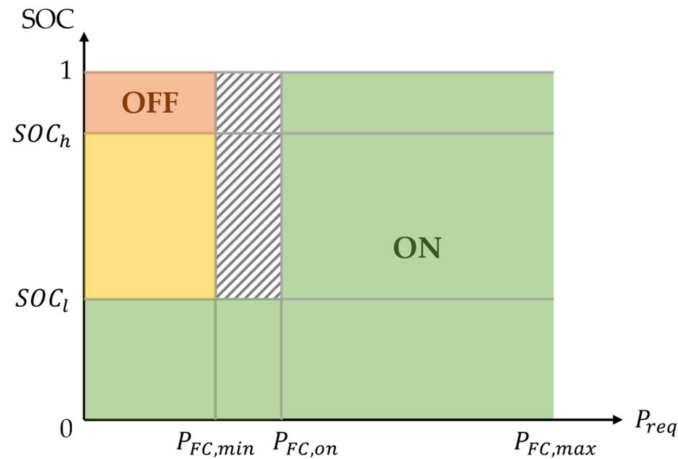


Figure 3.6: Baseline mode-based control strategy logic [26]

FC is always on in the green area and always off in the red area. It maintains its on/off state based on its previous status in the transitional orange region. The traction motor serves as a generator during braking to store kinetic energy contained in the translating mass of the vehicle. In this way, braking torque is provided to the wheels and is used to recharge the battery.

Constant fuel cell output control strategy approach aims to maintain the fuel cell at nearly constant power output (which must meet the average demand) and utilize the battery to meet instantaneous power requirements [19].

Strong load following control strategy. Battery is primarily utilized to create extra power as needed and to offset the losses of the auxiliaries, with the fuel cell handling the majority of the vehicle’s propulsion [19]. Battery runs in CS mode. FC system has to provide maximum transient or maximum continuous power request. In this strategy, fuel cell doesn’t operate in high efficiency regions. Since battery power is lower than FC one, bidirectional converter should be applied on battery side

Fuzzy rule-based strategies

Fuzzy logic is able to manage both linguistic knowledge and numerical data at the same time. Language labels or word sets like slow, quick, low, medium, and high are represented by fuzzy sets. Fuzzy control is straightforward, simple to implement, and robust. Fuzzy set theory is a branch of multi-valued logic that was developed to address the problem of reasoning that is approximate rather than precise. The degree to which a proposition is true depends on fuzzy logic. It can directly translate the designer’s experience into control rules [23]. Expert knowledge can be codified as a rule base and applied to decision-making. The fundamental benefit of fuzzy logic is that it can be adjusted and altered as needed, increasing the level of control. It is also a nonlinear structure that is particularly helpful in a sophisticated power train, a complex system.

The general structure of a fuzzy logic controller is shown in Figure 3.7

The process of transforming data into fuzzy subsets is called fuzzification. The subsets include specific input ranges and membership functions that specify how confidently an input is a member of a particular range. The fuzzy rule base and the

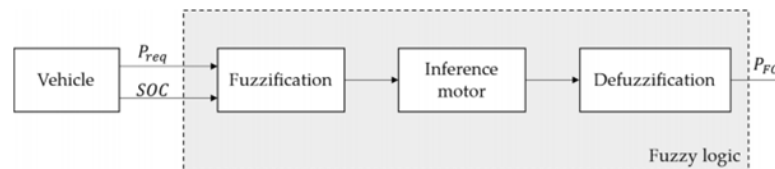


Figure 3.7: Structure of fuzzy logic controller [26]

outputs from this block are then given to the inference engine to generate control actions. The output of the inference motor is processed by the defuzzification module using membership functions, which translate the output into physical terms.

In case of FCHEV, required power and SOC of the battery serve as input variables and fuel cell power is an output variable. The battery power can be calculated as a difference between required and fuel cell power. In addition, in a fuzzy logic-based energy management strategy, maintaining battery charge and improving fuel cell system efficiency depend on the quantity and shape of the membership functions for each of the fuzzy variables.

Fuzzy rule-based strategies can be further divided into conventional, adaptive and predictive strategies.

For *conventional fuzzy control strategy*, drive train operation is managed by two operating modes: optimum fuel utilization and fuzzy efficiency modes. The choice of input, output, and rule-based control method determines efficiency. The needed power as well as the battery SOC are inputs to the fuzzy logic controller. The FC power is set based on these inputs and the mode that has been chosen. The difference between the power needed for the entire load and the power needed from FC is the power needed by the batteries [23]. In case of optimum fuel utilization mode, fuel consumption, determined by fuel economy map is restricted while supplying sufficient power and maintaining SOC of batteries. In case of fuzzy efficiency mode, FC operates at optimum operating zones (OOZ), regions where FC operates with the highest efficiency. Power difference is provided by the batteries.

Adaptive fuzzy control strategy is more suitable for HEV, where emission reduction of ICE is a major concern. In this strategy, both fuel consumption optimization and emission minimization is performed at the same time. However, since these objectives are inversely proportional, the optimal solution can be found through the weighted-sum approach optimization. Therefore, proper values for the weights have to be selected for fuel economy and emissions. Each parameter receives an adaptively assigned relative weight based on the significance of that parameter in various driving conditions. By altering the relative weight values, this control approach can be used to control any one of the objectives. Additionally, a significant reduction in vehicle emissions is made with barely any compromise to fuel consumption.

Predictive fuzzy control strategy best fits if the driving cycle is predefined. In this case, the input parameters for the system is known, thus the global optimization can be performed. For the online control, global positioning system (GPS) can be implemented to define the driving conditions of the vehicle. Depending on these data, controller will define the operating points of fuel cell system and batteries. In addition, based on the available data of driving route, controller may set overload for FC system to charge the batteries. The controller is informed by the GPS signal to charge or discharge the batteries for future reuse.

In conclusion, a fuzzy logic controller is essentially a natural extension of the numerous rules-based controllers used (via lookup tables) in many modern cars. While resistant against the measurement of noises and disturbances and insensitive to model uncertainties, fuzzy logic-based solutions need for a faster microcontroller with more memory.

3.3.2 Optimization based strategies

Optimization based control strategies are based on the minimization of cost function by means of analytical or numerical operations [25]. The cost function takes into account several parameters. These might be fuel consumption, efficiency and emission data. The solution of the problem is optimum either globally or locally (only for a given set of input variables). Global optimum solution can be calculated when the driving pattern is known apriori, which is impossible in real application. Therefore, it cannot be applied in real controllers, yet the online optimization can be done based on the instantaneous minimization of cost function. Instantaneous (real-time) optimization strategies, the optimum solution is done based on the current input data and minimization of instantaneous cost function. Global optimization techniques requires the data for full driving conditions, pattern and time history of other parameters. Instantaneous (real-time) optimization are equivalent consumption minimization strategy (ECMS), neural networks, particle swarm optimization and Pontryagin's minimum principle. Global optimization techniques are linear programming, dynamic programming, pseudo-spectral method and stochastic control strategy, which can be also divided into stochastic dynamic programming and genetic algorithm. The last category of optimization techniques is model predictive strategy.

Equivalent consumption minimization strategy

This technique was first proposed by Paganelli et al. [27] and aims at minimization of cost function, which is equivalent fuel consumption. The idea is that electrical energy can be equivalently converted to fuel consumption. The total fuel consumption, which is the cost function is the sum of direct FC hydrogen consumption and equivalent battery fuel consumption. The calculation of equivalent fuel consumption of batteries is performed by making an assumption that SOC variation in the future is compensated by FC system.

$$\dot{m}_{equ} = \dot{m}_{fc}(P_{fc}(t)) + S_{SOC}\dot{m}_{bat}(P_{bat}(t)) \quad (3.1)$$

Where \dot{m}_{equ} is equivalent (total) fuel consumption rate; \dot{m}_{fc} -fuel cell fuel consumption rate (is a function of FC power); S_{SOC} -penalty function due to battery

SOC stabilization; \dot{m}_{bat} -equivalent battery fuel consumption (is a function of battery power)

Average efficiencies of power units, fuel consumption rate and mean power are required to calculate the equivalent fuel consumption of batteries. The equivalent fuel consumption is calculated using ECMS based on the online measurements of the quantities on board and the current system condition. In order to obtain an optimal solution, no prior knowledge of driving behavior is necessary, and can be applied online. It reduces a global optimization problem into an instantaneous minimization problem and provides the optimum solution at each time instant. Mathematically, ECMS can achieve an optimal solution, yet it cannot maintain battery charge-sustaining mode of operation. Therefore, a penalty function for the equivalent battery fuel consumption should be introduced. In case of low battery SOC, the 'price' for battery power will be high, and thus, the choice of controller will be on fuel cell side. On the other side, in case of high battery SOC, the 'price' for battery power will be low, an controller will choose battery to supply the power. As a result, SOC can be maintained between the threshold values and charge-sustaining mode of operation be realized.

Neural networks

Artificial neural network (ANN) is a computational technique, that can simulate in a biological brain and aimed to perform specific task without actually knowing the physical model of a system. ANN generates output data by learning the previous experience. When processing samples that each have a known "input" and "output", neural networks are trained by creating probability-weighted associations between the two that are then stored within the net's data structure. For ANN training, one must select from a set of permitted models and related techniques. Then, from a given example, one often compares the processed output of the network and the desired output. The network then modifies its weighted associations using this error value and a learning strategy. The neural network will produce output that is increasingly comparable to the goal output as modifications are made over time. These modifications can be made a sufficient number of times before the training can be stopped under certain conditions.

There are three or more interconnected layers in an ANN. Neurons in the input layer make up the first layer. These neurons transmit information to hidden layers, which then transmit the final output information to the final output layer (Figure 3.8).

The units that make up the inner layers, which are all hidden, adaptively transform the information that is passed from layer to layer. Each layer functions as both an input and an output layer, enabling the ANN to comprehend more intricate objects. The neural layer is the collective name for these inner layers. By

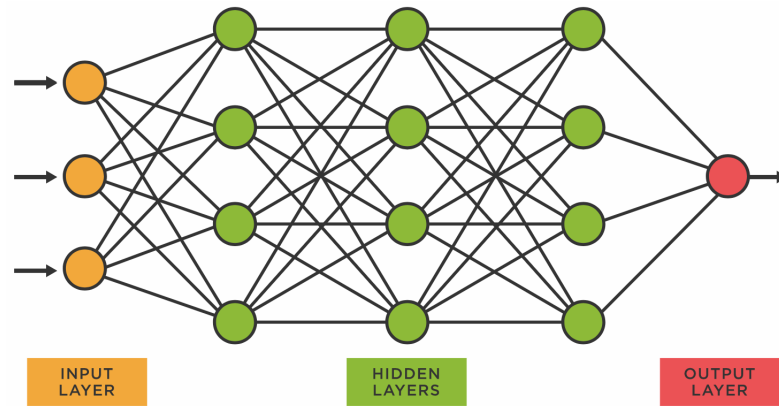


Figure 3.8: Structure of artificial neural networks [28]

weighing the collected data in accordance with the ANN's internal logic, the units in the neural layer attempt to learn about the information. These rules enable units to produce a transformed outcome, which is subsequently sent as an output to the following layer.

One of the most well-known advantages of an ANN is that it can really learn from viewing data sets. An ANN offers a number of other benefits as well. In this approach, ANN serves as a tool for approximating random functions. When defining computing functions or distributions, these tools can be used to estimate the most optimal and economical ways to arrive to solutions.

Particle swarm optimization

Particle swarm optimization (PSO) is a heuristic computational technique, which optimizes objective function by iteratively improving the predicted solution. Particles (also called population or candidate solution) are moved around the search space guided by mathematical relations over the particle's position and velocity. In PSO, particles navigate a search space using both their own best known positions and the positions of the entire swarm. The swarm particles' movements will be directed by the improved placements after they have been found. As a result of these procedures, the swarm is expected to move to the best solution. However, repetition of the process does not ensure a satisfactory outcome. PSO is a meta-heuristic strategy because it can search very wide spaces of candidate solutions and makes little to no assumptions about the problem being optimized. Although, PSO do not ensure the best outcome. More specifically, PSO does not employ the gradient of the problem being improved, which means that, unlike traditional optimization techniques, PSO does not demand that the optimization problem be differentiable [23].

Pontryagin's minimum principle

This principle was first developed by Russian mathematician Lev Semonovich Pontryagin in 1956. It is a generalization of Euler-Lagrange equations, that takes into account constraints on the control input. It provides a control for a dynamical system to be taken from one state to another when the constraints for a state or input control is present. It claims that in order to solve the two-point boundary value problem known as the "Hamiltonian system," which is a two-point optimum control problem, both the optimal state trajectory and any optimal control are required.

Control Hamiltonian function H can be constructed by appending the state equation to the integrand L using the Lagrange multipliers, $\lambda(t)$ follows [29]:

$$H(u(t), z(t), \lambda(t), t) = L(u(t), z(t), t) + \lambda^T(t)f(u(t), z(t), t) \quad (3.2)$$

Where $z(t)$ is the optimal control, and $u(t)$ is the corresponding optimal state. Then, there exists a continuous function λ , called *adjoint function*, which is the solution of the adjoint equation

$$\dot{\lambda}(t) = -H_u(u(t), z(t), \lambda(t), t) \quad (3.3)$$

Where H_u is differential of the Hamiltonian function. The adjoint function is a Lagrange multiplier that informs the optimization problem of the state equation constraint. Hamiltonian function is minimized by $z(t)$, corresponding optimal state $u(t)$ and adjoint $\lambda(t)$ according to the Pontryagin's minimum principle.

$$H_u(u(t), z(t), \lambda(t), t) = H_u(u(t), z^*(t), \lambda(t), t) \quad (3.4)$$

This inequality is satisfied for all admissible trajectory control variables $z^*(t)$, while adjoint function is satisfied. Admissible trajectories are the set of variables that are bounded by neighborhood of minimal solution that satisfies all the constraints.

We can now establish the necessary and sufficient requirements for optimality based on the aforementioned factors. Condition Eq. 3.4 indicates that the Hamiltonian is minimum at the optimal control $z(t)$ for a feasible trajectory that fulfills the minimum principle, such that

$$H_z(u(t), z(t), \lambda(t), t) = 0 \quad (3.5)$$

The equation 3.5 is a *first order necessary condition* for optimal solution and corresponds to a special case of the Euler-Lagrange equation.

In conclusion, the optimal control problem is converted into a multipoint boundary value problem by the Pontryagin Minimum Principle. In other words, control arises from the optimality condition $H_z = 0$ and is represented as

$$z(t) = G(u(t), \lambda(t), t) \quad (3.6)$$

Optimal control variable and corresponding state and adjoint can be computed by solving an ODE system,

$$\dot{u}(t) = f(u(t), G(u(t), \lambda(t), t)) \quad (3.7)$$

$$\dot{\lambda}(t) = -H_u(u(t), G(u(t), \lambda(t), t)) \quad (3.8)$$

with appropriate initial and end time condition.

Linear programming

Linear programming (LP) is special case of mathematical optimization which aims in achieving the best solution in a mathematical model, where the requirements are represented by linear relationships. The constraints are described by linear equality and linear inequality relationships and objective function is represented by linear relationships. In order to locate the feasible region and optimize the solution to have the highest or lowest value of the function, linear programming problems are a significant class of optimization problems. LP problems can be solved by different methods, like graphical method, simplex method or by using other tools.

Some assumptions must be taken into account while using LP optimization technique

- Constraints are expressed in quantitative terms
- Linear relationship between the constraints and objective function
- Linear function (objective function) has to be optimized

The components of LP technique are

- Objective function
- Constraints
- Decision variables
- Data

The formulation of LP method is as follows

$$f(x_1, x_2) = c_1x_1 + c_2x_2 \quad (3.9)$$

The constraints are

$$\bar{A}\bar{X} \leq \bar{B} \quad (3.10)$$

where $\bar{X} = (x_1, x_2)$

In reality, fuel economy optimization is a convex nonlinear optimization problem and finally approximated by linear programming method. In series HEVs, linear programming is primarily utilized to improve fuel efficiency. The result of LP optimization method is a global optimal solution.

Dynamic programming

Dynamic programming (DP) is an optimization technique that transforms a complex problem into a series of simpler ones. A broad framework for studying a wide variety of problem types is provided by dynamic programming. This framework allows for the use of a range of optimization strategies to address specific issues with a more general formulation. It has the benefit of being applicable to problems with constraints and without constraints as well as linear and nonlinear systems. It should be emphasized that the overall problem depends on the optimal solution to its subproblems. The appropriate division of optimization problems into several levels, each of which is solved one level at a time is a crucial component of DP [30]. Each level is solved using standard optimization problem approaches, and the features of the next level problem in the series are defined by the result. Typically, the levels in the overall problem's perspective correspond to several time periods.

However, the main disadvantage of this technique is the "curse of dimensionality," which increases the computational difficulty and restricts the use of the method to complex systems. The DP algorithm cannot be used in real time because it requires prior knowledge of the driving cycle. Its outputs, however, can be utilized to design and fine-tune real controllers.

Pseudo-spectral method

Pseudo-spectral optimization technique is a combination of theoretical and computational methods for solving optimization problems. The concept of pseudospectral optimum control encompasses a fairly broad range of concepts [31]. These include, among others, the Bellman pseudospectral approach, the flat pseudospectral method, the Legendre pseudospectral method, the Chebyshev pseudospectral method, the Gauss pseudospectral method, the Ross-Fahroo pseudospectral method, and many others [32]. The integration in the cost function, the differential equation of the control system, and the state-control constraints must all be approximated in order to solve an optimal control issue [33]. All three approximate objectives should respond well to the ideal approximation method. It's possible that a technique

that works well for one of them say, an effective ODE solver might not work well for the other two. Because PS methods are effective at approximating all three mathematical objects, they are the best choice for addressing these requirements. In a pseudospectral technique, a set of carefully chosen quadrature nodes are used to approximate the continuous functions. The related orthogonal polynomial basis employed for the approximation determines the quadrature nodes. Legendre and Chebyshev polynomials are frequently utilized in PS optimal control.

Stochastic control strategy

A framework for modeling optimization issues including uncertainty is the stochastic strategy. An infinite-horizon stochastic dynamic optimization problem is formulated using this method. The driver's power request is modeled as a stochastic Markov process. The probability distribution for the future power needs is produced by the Markov driver model, which then forecasts what they will be. The choices made in the past are not necessary for this prediction. Stochastic dynamic programming is then used to determine the best control approach. The derived control law is directly implementable and takes the form of a stationary full-state feedback. It is discovered that a suboptimal rule-based control approach learned from deterministic DP findings performs worse than the derived SDP control technique. The stochastic technique, as opposed to deterministic optimization over a specific DC, optimizes the control policy over a family of various driving cycles [23]. Stochastic control strategy is further divided into stochastic dynamic programming and genetic algorithms.

In case of *Stochastic dynamic programming*, the random variables are used to describe the optimization problem. Stochastic dynamic programming is the optimization method, where state or decision functions are formulated in terms of probability function. The solution of this technique requires high computational effort.

In case of *Genetic algorithm* (GA), a heuristic search algorithm is used to optimize the the search problems. Darwin's theory of evolution lies behind the principle of GA. An initial set of solutions from a given population should be provided as a starting point. Depending on their ability to create new populations, the answers from one population are used. The process is continued until the desired condition is met since the best solutions have a better probability of growing than the worst ones. GA is a reliable and workable method with a large search space that quickly optimizes the parameters using straightforward methods. They have been shown to be successful in resolving challenging engineering optimization issues with nonlinear, multimodal, nonconvex objective functions.

Solution for GA technique is a global optima. Contrary to the traditional gradient-based approach, the GA technique doesn't call for any firm assumptions or additional data regarding the objective parameters. Using GA, the problem-solving

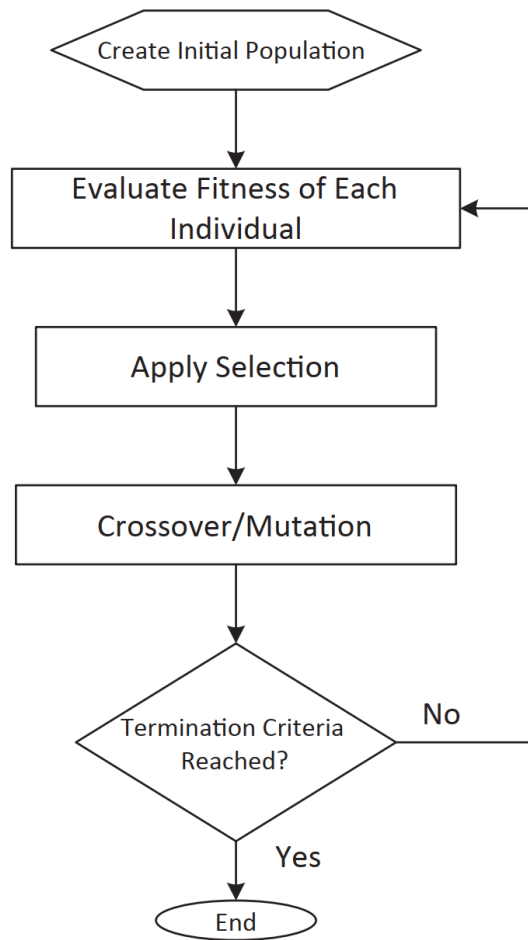


Figure 3.9: Flowchart of Genetic algorithm optimization [34]

space can be efficiently explored. However, this approach takes a lot of effort and does not give the designer a wider perspective [23]. The general logic of GA is illustrated in Figure 3.9

Model predictive control

Model predictive control (MPC) uses a model to predict the future outputs based on previous and current values. The models, that are used in MPC describe the behaviour of complex and simple dynamic systems. MPC models forecast the change in the modeled system's dependent variables that will result from changes in the independent variables. Future changes in the dependent variables are calculated using MPC using the current plant data, the present dynamic state of the process, the MPC models, and the process variable targets and limits.

These adjustments are calculated to respect limitations on both the independent and dependent variables and keep the dependent variables around their desired values. When a subsequent modification is required, the MPC normally repeats the calculation after sending out the first change for each independent variable to be applied. Several strategies can be utilized when linear models are insufficiently accurate to capture the true process nonlinearities. To lessen nonlinearity, the process variables may occasionally be changed prior to and/or following the linear MPC model. Nonlinear MPC, which employs a nonlinear model directly in the control application, may control the process. The main advantage of MPC is that it enables timeslot optimization while taking future timeslots into consideration. This is accomplished by repeatedly optimizing a finite time horizon while only using the current time slot for implementation.

3.4 Fuel cell on-vehicle realization

In 2013 first commercially produced fuel cell electric vehicle was produced by Hyundai Motors. The model was Hyundai ix35 FCEV, which was available from 2014 to 2018. The next vehicle that was mass-produced and sold commercially was Toyota Mirai. It was introduced in November 2014 in Los Angeles Auto show. Honda motors has also introduced its fuel cell vehicle, namely Honda Clarity Fuel Cell, which was produced from 2016 to 2021. The current available FC vehicles are Toyota Mirai, Hyundai Nexa.

Toyota Mirai is a mid-size hydrogen fuel cell vehicle sedan, which was one of the first examples of FCHEV. Mirai is the most fuel-efficient and the one with longest travel range FC vehicle, with a hydrogen consumption of 3.6L/100km on a EPA combined city/highway driving cycle according to United States Environmental Protection Agency. The *first generation* of Toyota Mirai can travel a total range of 502 km with a full tank, while accelerating from 0 to 100 km/h in 9.6 seconds with a refueling time between 3 to 5 minutes. In addition, it is equipped with a 3-D fine mesh flow FC stack with a maximum output power of 114 kW. Enhanced air dispersion and uniform electricity generation on cell surfaces is ensured by fine three-dimensional lattice structure. This layout provides the world-leading power density of 3.1 kW/L. FC stack consist of 370 single-line stacking cells. FC boost converter is used to develop to increase the stack voltage up to 650 volts. Toyota Mirai is equipped with two hydrogen tanks made of carbon fiber-reinforced plastics, which can store 122 liter hydrogen at 70 MPa (5 kg capacity). The total weight of tanks is 87.5 kg. The electric motor/generator of Mirai delivers maximum power of 113 kW and maximum torque of 335 Nm. Sealed nickel-metal hydride (NiMH) rechargeable battery pack with a nominal voltage of 245 V is implemented as an additional power source. The *second generation* of Toyota Mirai was introduced in

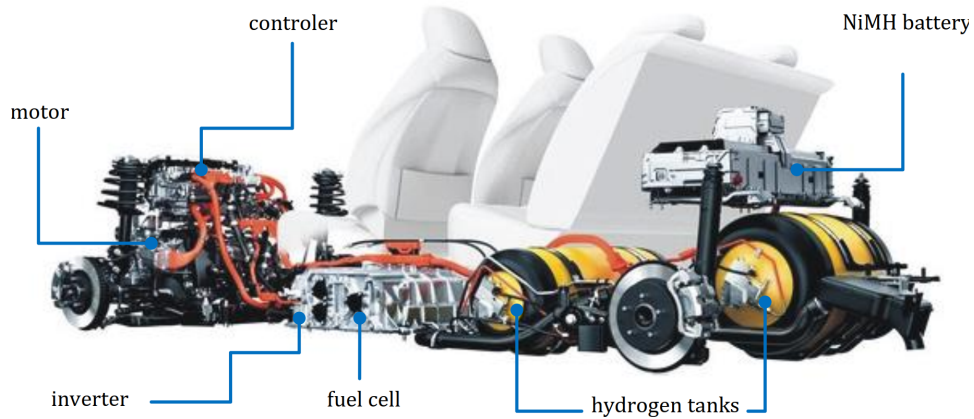


Figure 3.10: Architecture of first generation Toyota Mirai [35]

December 2020. It has an prolonged driving range through the improvements to the fuel cell system and increased capacity on-board hydrogen tanks. The architecture of first generation Toyota Mirai is illustrated in Figure 3.10

Hyundai Nexa is a hydrogen fuel cell powered crossover SUV developed by Hyundai Motors and revealed in March 2018 in South Korea. According to EPA rated range, it has from 570 to 611 km travel distance (depending on the edition, Blue or Limited edition) with a full tank. It is equipped with 3 hydrogen on-board tanks with a total capacity of 156 liters and 6.3 kg hydrogen capacity. The electric motor/generator has maximum power of 120 kW and maximum torque of 400 Nm, which is able to accelerate the vehicle from 0 to 100 km/h in 8,4 seconds.

Honda Clarity Fuel Cell is a mid-size sedan hydrogen fuel cell vehicle was introduced in 2017 by Honda Motors. The previous model Honda FCX Clarity was launched in 2008 in Japan. It has 100 kW vertical flow hydrogen fuel cell stack and uses a separate battery pack as power buffer. The maximum power of EM is 100 kW and 256 Nm maximum torque. The fuel consumption of this vehicle is 116 km per kilogram in combined driving conditions and has 386 km travel range with a full tank, which can store 4.1 kg of hydrogen at 344 bar. Honda Clarity fuel cell vehicle was initially available as a plug-in hybrid electric vehicle, then as a hydrogen fuel cell vehicle and as an electric vehicle and will end production in August 2021 This vehicle has 589 km of travel distance according to EPA rated range and combined fuel economy of 3.5 L/100km. It is equipped with PEMFC stack with a maximum power of 103 kW. AC permanent-magnet synchronous electric motor is installed to convert the power coming from FC into mechanical power with a maximum power of 135 kW and maximum torque of 298 Nm, which can accelerate the vehicle from 0 to 100 km/h in 8.7 seconds. The additional power source is lithium-ion battery pack with a nominal voltage of 346 volts.

FC vehicle	Travel range (EPA)	Curb weight	EM max. power	Top speed	Acceleration time (0-100 km/h)	Fuel economy (combined)
Toyota Mirai (1st generation)	502 km	1850 kg	113 kW	173 km/h	9.6 seconds	0.76 kg/100km
Toyota Mirai (2nd generation)	647 km	1950 kg	136 kW	175 km/h	9 seconds	0.55 kg/100km
Hyundai Nexo Fuel Cell	611 km	1873 kg	120 kW	177 km/h	8.4 seconds	0.84 kg/100km
Honda FCX Clarity	390 km	1600 kg	100 kW	165 km/h	8.2 seconds	0.86 kg/100km
Honda Clarity Fuel cell	589 km	1875 kg	103 kW	165 km/h	8.7 seconds	0.76 L/100km

Table 3.1: Commercial FCHEV dynamic characteristics

Chapter 4

Fuel cell hybrid electric vehicle modeling and simulation

4.1 Vehicle simulation approaches

In general, there are two common approaches for predicting the fuel consumption in vehicles through the simulation process, namely *backward approach* and *forward approach*. In case of backward scheme, the input for the model is preset driving cycle, which is initially assumed and followed, and thus a vehicle speed is not a dynamic parameter. However, in case of forward scheme, a vehicle is controlled by a driver model in order to follow the input driving cycle and therefore a vehicle speed is a dynamic state [36].

4.1.1 Forward simulation approach

In the forward scheme, a driving cycle provides a target speed, but it goes through a driver model. Based on the (difference between the) target and the vehicle speed, the driver controls the longitudinal vehicle interfaces, the accelerator, and the brake pedals. The tractive force is sustained by the traction at the wheels, which is where the energy carrier (fuel, charge, etc.) is pumped into the prime mover and the torque is transmitted forward through the powertrain. The acceleration of the vehicle, which is integrated for speed and location, is calculated by Newton's second law. The calculation loop is closed by feeding the position back into the driving cycle to determine a target speed. The method is known as forward because the effort flows in the powertrain in the opposite direction from the backward approach.

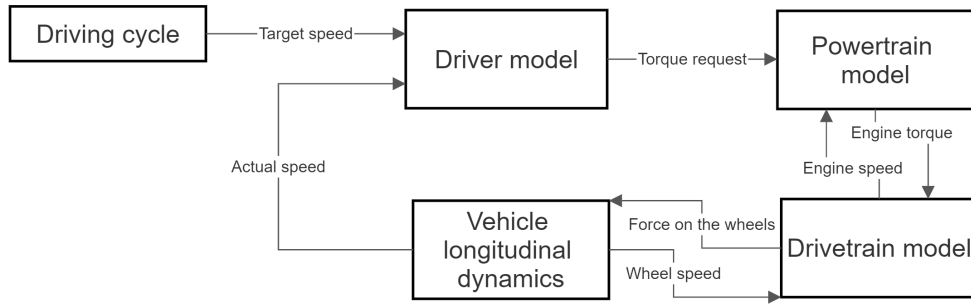


Figure 4.1: Forward simulation approach topology

This method may be more accurate to what actually occurs. The topology of this approach is illustrated in Figure 4.1

There will always be a small margin of error between the actual vehicle speed and the speed target since the speed trace is not "forced" onto the vehicle model in forward approach. The driver model's job is to reduce this margin of error. This is comparable to the role of a test driver conducting an emissions test for vehicle type approval in the real world. The drivability of the vehicle model is revealed through forward approach, which also capture the physical system's boundaries. However, because a typical forward-facing model has multiple state equations, the simulation must be repeated in smaller time steps in order to compute the vehicle speed (and subsequently the drivetrain angular velocity) using multiple state integration. As a result, the simulation periods are longer compared to backward approach [37].

4.1.2 Backward simulation approach

A driving cycle provides a target speed in the backward scheme. Newton's second law is used to calculate the required propulsion force, which is transmitted from the wheels through the drivetrain to the prime mover where the required input power for the propulsion effort is calculated. The data goes through the engine backwards, hence the name "backward" method [36]. The topology of this approach is illustrated in Figure 4.2

Backward approach rely on efficiency maps, which were often built during steady-state real-world testing based on torque and speed data. Because state equations are effectively replaced by lookup tables in this computation as opposed to forward approach, the calculation can be performed across considerably greater time steps. Unfortunately, backward approach perform poorly when it comes to represent dynamic impacts due to the very nature of using steady state maps [37].

Backward simulation approach is used during this research analysis. Fuel hybrid electric vehicle is modeled and simulated by using backward approach.

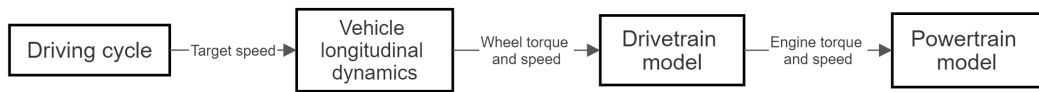


Figure 4.2: Backward simulation approach topology

4.2 FCHEV mathematical model

Typically, a fuel cell stack is used as the primary power source for an FCHEV, and a battery is used as an energy storage system. Toyota Mirai (1st generation) FCHEV is selected as a reference vehicle for the modeling and simulation purposes. The structure of selected FCHEV is shown in Figure 4.3

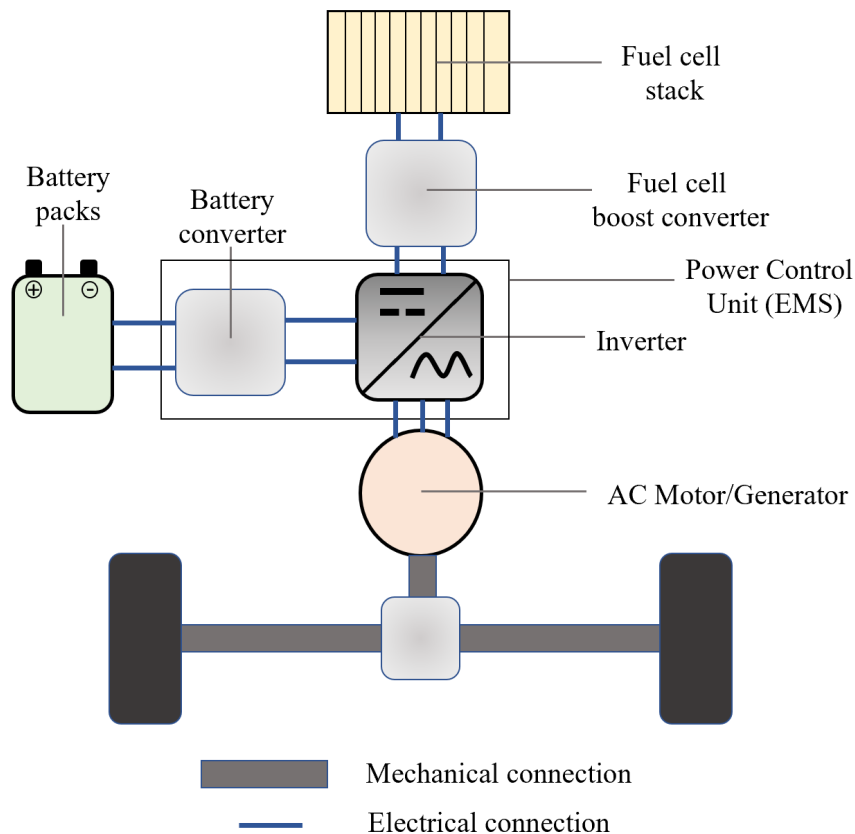


Figure 4.3: Toyota Mirai FCHEV configuration

The vehicle electrical traction system is powered by either fuel cell system, which supplies DC electrical energy through the electrochemical conversion of hydrogen and oxygen into water and heat or by Nickel Metal Hydride battery module. The hydrogen fuel required for the stack operation is provided through an onboard high pressure storage system. FC voltage is increased by monodirectional fuel cell DC/DC boost converter, while the voltage of battery is raised by bidirectional battery DC/DC converter. The electrical energy of both sources is summed up and supplied to AC motor/generator through the inverter, which is able to convert DC electrical power to AC and modulate its frequency and amplitude. Then, mechanical power from the AC machine is provided to the wheels through the single speed transmission.

Simulink block diagram was constructed on the basis of Toyota Mirai FCHEV configuration (Figure 4.3) and is illustrated in Figure 4.4

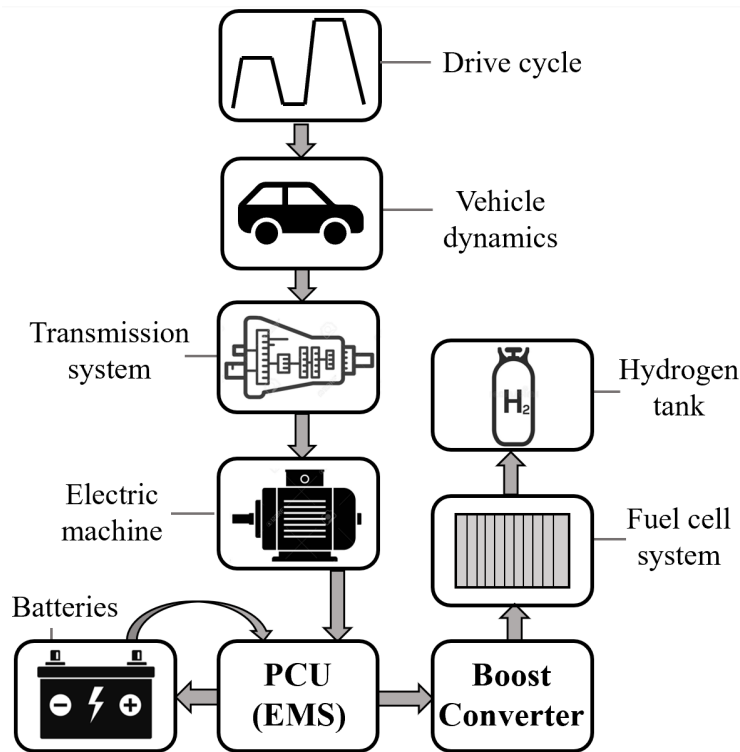


Figure 4.4: Toyota Mirai FCHEV simulink model

According to the principle of backward modeling approach of a vehicle with hybrid drive, the speed profile is set according to the normalized driving cycle. It is assumed that the car perfectly follows the set speed without any deviations. Next, the traction force on the wheels is calculated, which is necessary to set the appropriate vehicle dynamics, the torque and the angular velocity of the input

shaft of the transmission. Depending on the distribution of the required power between FC and battery, the fuel and electrical energy consumption are calculated.

The main advantage of this model is the small computational time and the ability to use with optimization methods that require simulation, expressed using analytical equations. The disadvantages are the inability to use in real time, calculation errors the required torque at high loads exceeding the maximum capabilities of the power sources.

4.2.1 Drive cycle model

This subsystem includes the model of driving cycle, which consists of the velocity versus time history. Figure 4.5 illustrates NEDC, WLTP, UDDS, US06, HWY and JC08 normalized driving cycles.

The acceleration/deceleration of the vehicle can be calculated as the difference between current (v_i) and one previous (v_{i-1}) value of the velocity divided by time step Δt

$$a = \frac{v_i - v_{i-1}}{\Delta t} \quad (4.1)$$

The sign of a defines whether there is a traction or regeneration.

4.2.2 Vehicle longitudinal dynamics model

This subsystem takes as an input parameters velocity and the acceleration, calculated in *Drive cycle* subsystem. Vehicle longitudinal dynamics evaluates the necessary traction force and thus torque and longitudinal resistant force. The output parameters of this subsystem are torque on the wheels, wheel angular velocity and wheel angular acceleration.

The total torque on the wheels T_{wh} is equal to the sum of torque, exerted by total longitudinal force and torque, due to wheels inertial resistance, which is equal to wheel mass moment of inertia J_{wh} time wheel angular acceleration $\dot{\omega}_{wh}$

$$T_{wh} = (F_{aer} + F_{r.r.} + F_{grade} + F_{in}) \cdot r_{wh} + 4 \cdot J_{wh} \cdot \dot{\omega}_{wh} \quad (4.2)$$

Aerodynamic drag F_{aer} is evaluated as

$$F_{aer} = \frac{1}{2} \cdot \rho \cdot v^2 \cdot A_f \cdot C_d \quad (4.3)$$

ρ -air density;

v -vehicle speed;

A_f -vehicle frontal area;

C_d -aerodynamic drag coefficient.

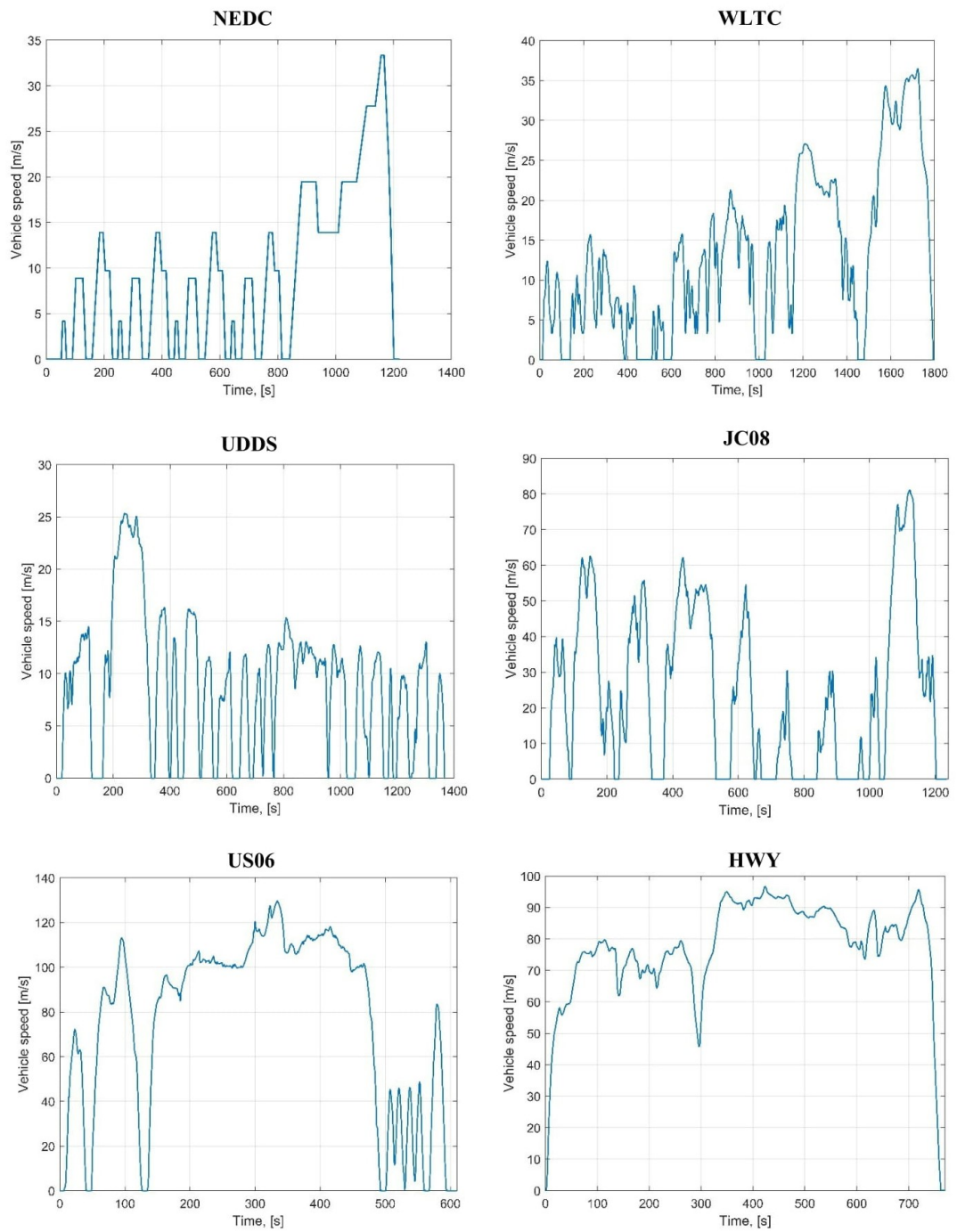


Figure 4.5: Driving cycles

The rolling resistance force depends the total weight of the vehicle and rolling resistance coefficient f_r .

$$F_{r.r.} = f_r \cdot M \cdot g \quad (4.4)$$

The resistance force, due to road grade is equal to

$$F_{grade} = M \cdot g \cdot \sin\alpha \quad (4.5)$$

Where M is vehicle total mass; g -acceleration due to gravity; α -road inclination angle.

Finally, inertial force of the vehicle is equal to the vehicle mass M times the longitudinal acceleration a

$$F_{in} = M \cdot a \quad (4.6)$$

Angular speed ω_{wh} and angular acceleration $\dot{\omega}_{wh}$ of the wheels can be calculated as

$$\omega_{wh} = \frac{v}{r_{wh}} \quad (4.7)$$

$$\dot{\omega}_{wh} = \frac{a}{r_{wh}} \quad (4.8)$$

Where the wheel radius r_{wh} is calculated from the tire code.

The impact of lateral dynamics is ignored and the torque required to overcome the inertia of rotating parts are taken into account separately for each part of the vehicle and included in the model of the corresponding part.

4.2.3 Transmission system model

Transmission system model includes the function of gearbox and final drive, which is intended to increase the torque and reduce the speed of electric machine. Toyota Mirai FCHEV is equipped with single speed transmission system. The input parameters of this subsystem are T_{wh} , ω_{wh} and $\dot{\omega}_{wh}$. The output parameters of this subsystem T_{em} , ω_{em} and $\dot{\omega}_{em}$ correspond to electric machine torque, angular speed and acceleration.

$$T_{em} = \begin{cases} \frac{T_{wh}}{\tau \cdot \eta_{gb}} & \text{if } T_{wh} \geq 0 \text{ (Traction mode)} \\ \frac{T_{wh} \cdot \eta_{gb}}{\tau} & \text{if } T_{wh} < 0 \text{ (Regeneration mode)} \end{cases} \quad (4.9)$$

Equation 4.35 takes into account gearbox efficiency η_{gb} and gearbox reduction ratio τ .

Electric motor angular speed ω_{em} and angular acceleration $\dot{\omega}_{em}$ are defined from the kinematic relationship between motor output shaft and wheel axle.

$$\omega_{em} = \omega_{wh} \cdot \tau \quad (4.10)$$

$$\dot{\omega}_{em} = \dot{\omega}_{wh} \cdot \tau \quad (4.11)$$

4.2.4 Electric machine model

An electric machine (EM) is device which converts electrical energy, supplied by batteries and FC system into mechanical energy. One of the main advantages of this device is the high conversion efficiency and reversibility of power conversion, so mechanical energy can be converted back to electrical energy, enabling regenerative mode of operation. Required power (P_{req}) to electric machine can be calculated from transmission system power request and electric machine efficiency.

$$P_{req} = \begin{cases} \frac{T_{em} + J_{em} \cdot \dot{\omega}_{em}}{\eta_{em}} \cdot \omega_{em} + P_{aux} & \text{if } T_{em} \geq 0 \text{ (Traction mode)} \\ (T_{em} + J_{em} \cdot \dot{\omega}_{em}) \cdot \eta_{em} \cdot \omega_{em} + P_{aux} & \text{if } T_{em} < 0 \text{ (Regeneration mode)} \end{cases} \quad (4.12)$$

P_{req} -power, that should be supplied by batteries and fuel cell system;

J_{em} -electric machine mass moment of inertia;

η_{em} -electric machine efficiency;

P_{aux} -vehicle auxiliary system power;

EM efficiency depends on torque and speed, and is graphically represented in EM efficiency map.

$$\eta_{em} = f(T_{em}, \omega_{em}) \quad (4.13)$$

AC synchronous machine with a maximum power of 113 kW and maximum torque of 335 Nm is used Toyota Mirai (1st generation) FCHEV. Since the efficiency map of this machine is not available in open source database, similar motor with almost the same peak power and torque is considered. YASA P400 R SERIES [38] AC synchronous EM's efficiency map is used and parameters are scaled to fit the peak torque and speed. The scaling of the EM is carried out by normalizing its torque and angular velocity in relation to a point that characterizes the point of maximum power. Scaling is carried out around it, since this point is the main parameter in the EM specification. The final representation of performance curve and efficiency map of EM is illustrated in Figure 4.6

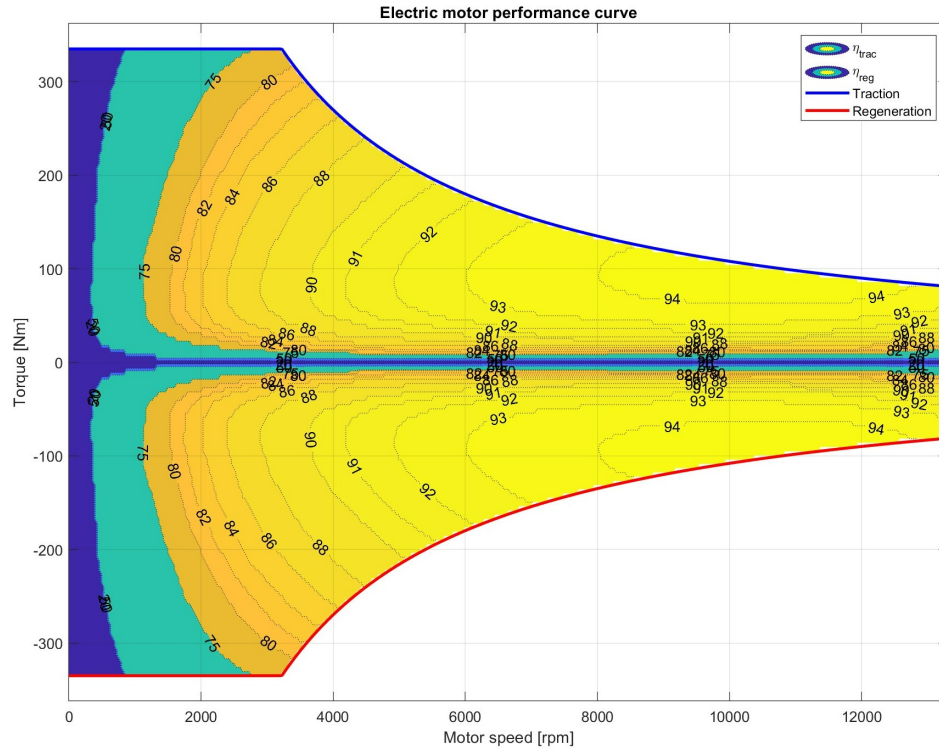


Figure 4.6: Electric machine efficiency map

4.2.5 Fuel cell system model

A fuel cell stack and other auxiliary components, such as hydrogen circuit as well as air, water, coolant, and electrical circuits make up an entire onboard fuel cell system. The complete model takes into account detailed internal dynamic responses but require more computational time. In this work, a simplified model is implemented to obtain a rapid response. Due to the complexity of FC model, this work is mainly concerned with the power split of the bus, but not the detailed conversion process of FC. Thus, a simple efficiency graph model is applied for the simulation.

The anode and cathode inlets on the Toyota Mirai do not have external humidifiers like those on other fuel cell systems. Through internal circulation within the anode, the water produced downstream of the cathode is redirected upwards of it. Air and hydrogen circulate in the system in opposite directions to facilitate water recirculation, which aids in this. Traditional stacks have straight grooves, but they suffer from water buildup, which hinders oxygen flow and results in uneven power generation. Utilizing turbulence, the Toyota Mirai system's intricate 3D mesh air flow field encourages oxygen penetration to the catalyst layer. In the simulations it has not been considered that the Mirai stack is humidifier-less.

In this selected model, reverse engineering method of modeling is used, i.e. experimental data is used to establish the model of FC.

FC stack efficiency, FC system efficiency and hydrogen flow rate curves has been found by Argonne National Lab testing data and then it has been reconstructed sampling point by point.

After the processing the experimental results, the dependence of FC stack and system efficiency and hydrogen flow rate on the FC output power has the following form, illustrated in Figures 4.7, 4.8 and 4.9 respectively.

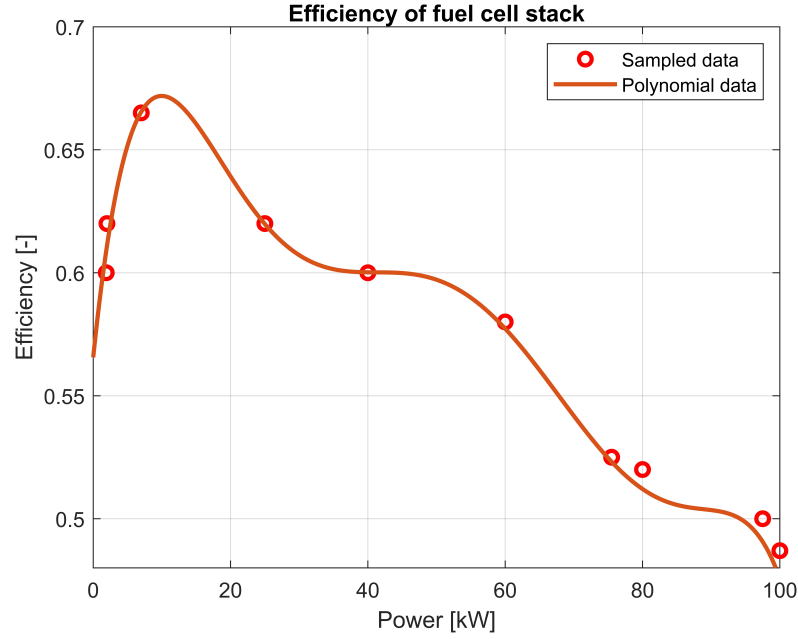


Figure 4.7: FC stack efficiency

Consequently, this dependence can be approximated with the polynomial of sixth degree for FC stack efficiency, fifth degree for FC system efficiency and second degree for hydrogen flow rate.

$$\eta_{stack} = k_1 \cdot P^6 + k_2 \cdot P^5 + k_3 \cdot P^4 + k_4 \cdot P^3 + k_5 \cdot P^2 + k_6 \cdot P + k_7 \quad (4.14)$$

Where $k_1 = -3.322 \cdot 10^{-11}$; $k_2 = 1.08 \cdot 10^{-8}$; $k_3 = -1.343 \cdot 10^{-6}$; $k_4 = 7.986 \cdot 10^{-5}$; $k_5 = -2.3 \cdot 10^{-3}$; $k_6 = 2.69 \cdot 10^{-2}$; $k_7 = 0.56$

$$\eta_{sys} = a_1 \cdot P^5 + a_2 \cdot P^4 + a_3 \cdot P^3 + a_4 \cdot P^2 + a_5 \cdot P + a_6 \quad (4.15)$$

Where $a_1 = 4.94 \cdot 10^{-10}$; $a_2 = -1.357 \cdot 10^{-7}$; $a_3 = 1.335 \cdot 10^{-5}$; $a_4 = 5.658 \cdot 10^{-4}$; $a_5 = 7.05 \cdot 10^{-3}$; $a_6 = 0.6092$.

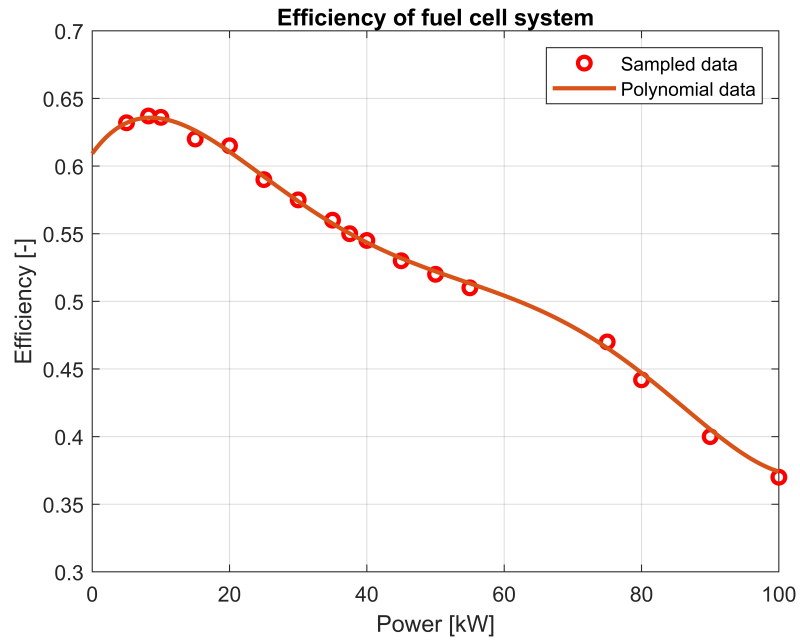


Figure 4.8: FC system efficiency

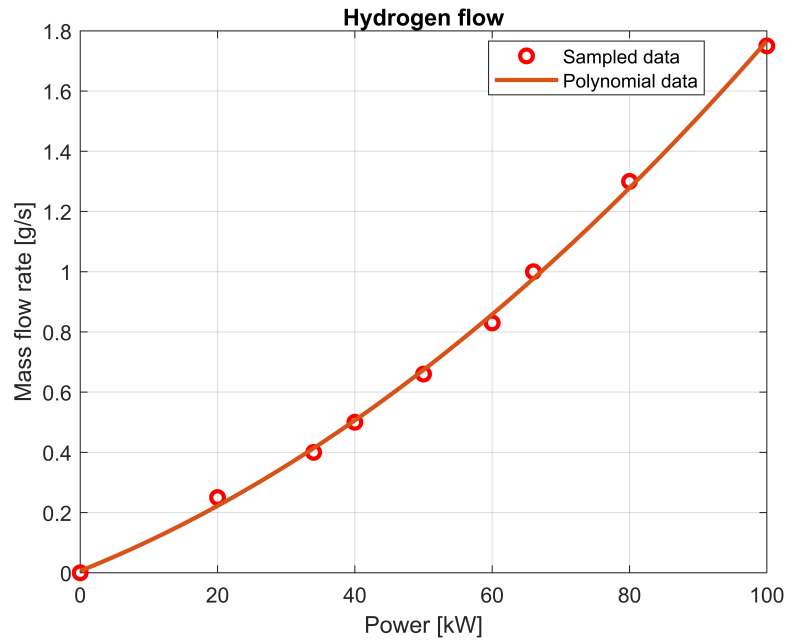


Figure 4.9: Hydrogen flow rate

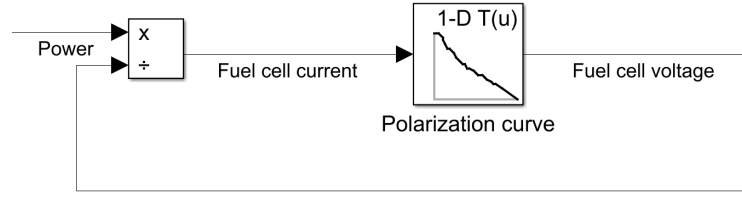


Figure 4.10: Polarization curve feedback loop

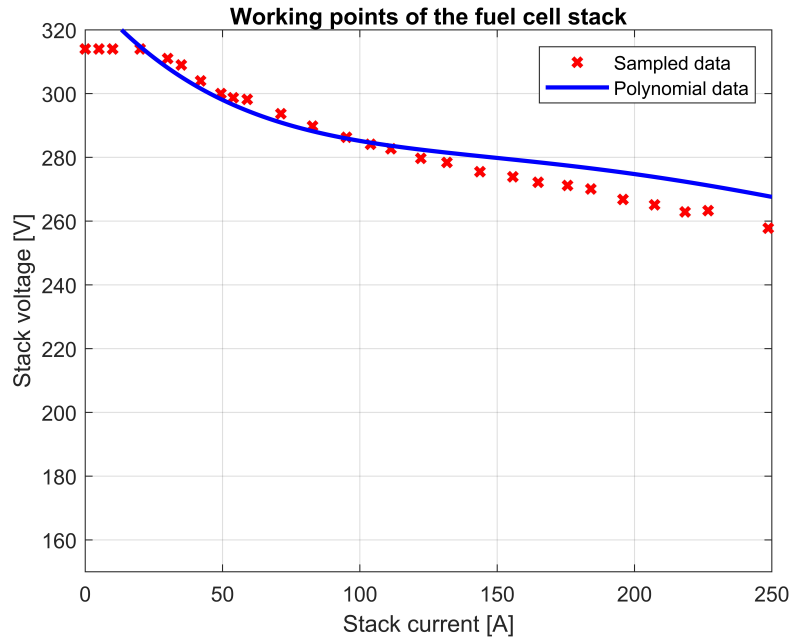


Figure 4.11: Polarization curve

$$\dot{m}_{H_2} = b_1 \cdot P^2 + b_2 \cdot P + b_3 \quad (4.16)$$

Where $b_1 = 8.5 \cdot 10^{-5}$; $b_2 = 9.1 \cdot 10^{-3}$; $b_3 = 0.0064$.

Fuel cell stack current can be found from FC polarization curve look-up table and constructing feedback loop, illustrated in Figure 4.10. Polarization curve has been also reconstructed from ANL data and is illustrated in Figure 4.11.

$$V_{stack} = c_1 \cdot I^5 + c_2 \cdot I^4 + c_3 \cdot I^3 + c_4 \cdot I^2 + c_5 \cdot I + c_6 \quad (4.17)$$

Where $c_1 = -4.587 \cdot 10^{-11}$; $c_2 = 6.67 \cdot 10^{-8}$; $c_3 = -3.553 \cdot 10^{-5}$; $c_4 = 0.0085$; $c_5 = -1.028$; $c_6 = 332.2$.

4.2.6 Battery model

Lithium-ion batteries have been the most popular energy storage system for FCHEV thanks to their high power density and great reliability. Regenerative braking is made possible and the drivability and efficiency of the vehicle are improved by incorporating a battery pack into the propulsion system.

Most batteries are modeled using a Thevenin equivalent circuit model, which includes the internal resistance model (R_{int}) and resistance-capacitance model, from the perspective of energy management. Although the Thevenin equivalent model does not adequately capture the dynamic behavior of the battery, it can accurately describe its energy consumption. The model is simple in form and has an acceptable accuracy range.

In this analysis, a NiMH equivalent circuit model is considered. Due to unavailability of battery parameters, 2004 Toyota Prius data is used, which is the most similar battery data. The shape of the parameters are kept constant, but adapted to the different nominal values, provided by Toyota datasheets for Toyota Mirai. This model includes three components: ideal voltage source, internal charging resistance and internal discharging resistance (Figure 4.12).

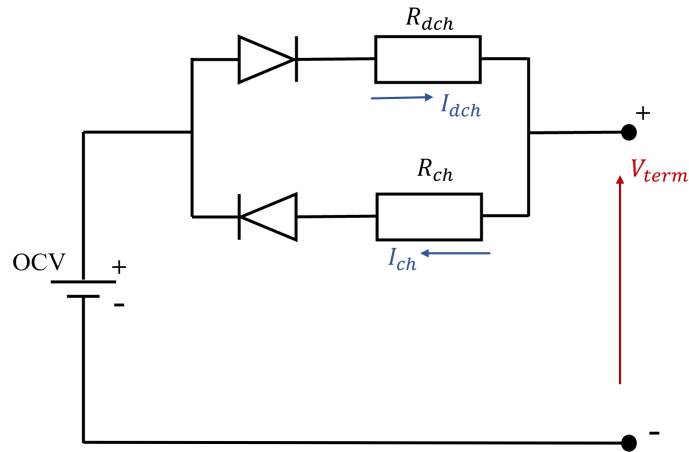


Figure 4.12: Battery equivalent circuit model

Ideal voltage source represents the open circuit voltage (OCV) of the battery and depends on SOC of the battery (Figure 4.13), while V_{term} represents terminal voltage. R_{ch} and R_{dch} represent battery internal charging and discharging resistances, and have strong dependence on battery SOC as well. This dependence is illustrated in Figure 4.14 and 4.15. I_{ch} and I_{dch} are the charging and discharging currents. The open circuit voltage and internal resistances are the functions of SOC and temperature. However, the temperature is assumed constant and the dependence on temperature is ignored in this work.

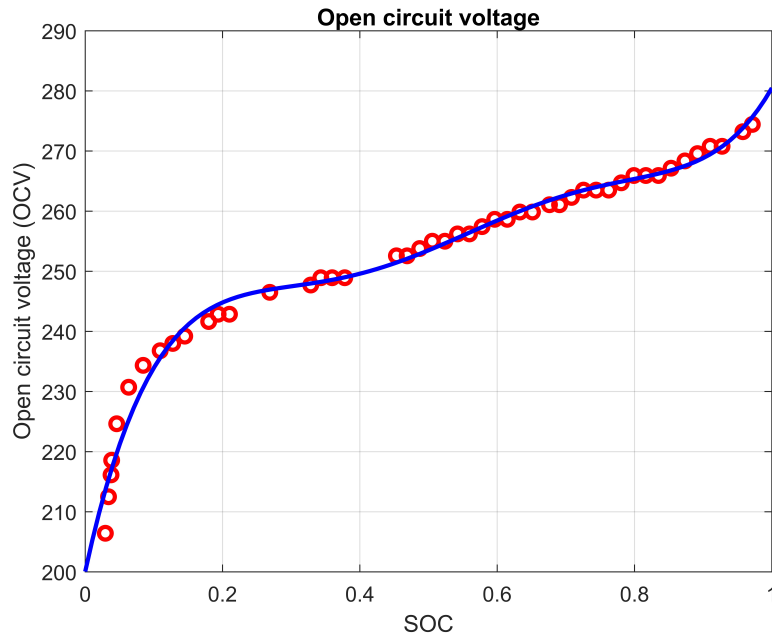


Figure 4.13: Battery open circuit voltage

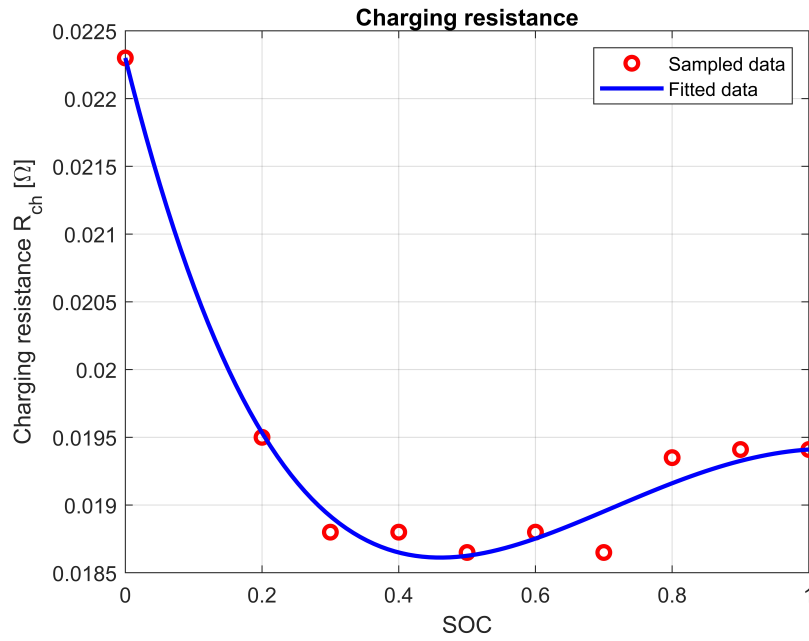


Figure 4.14: Battery charging resistance

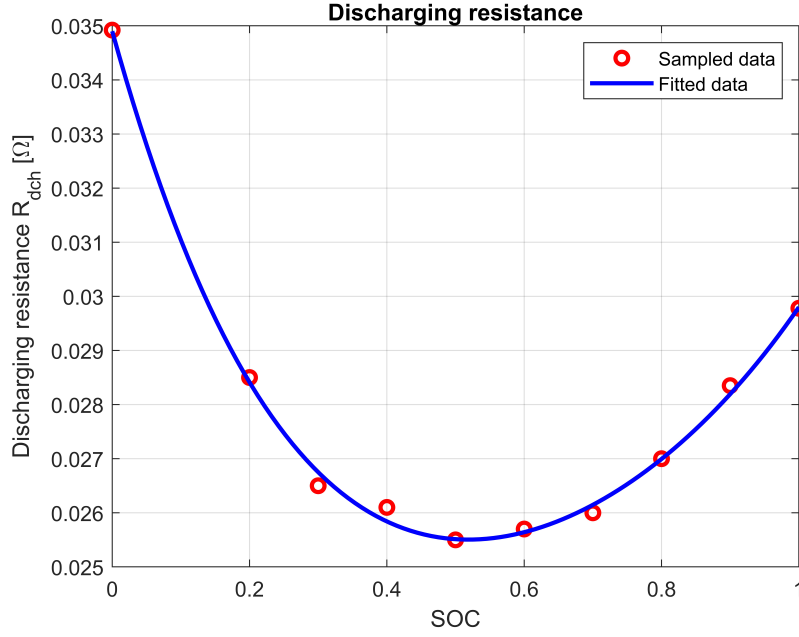


Figure 4.15: Battery discharging resistance

These relations can be approximated with the polynomial of fifth degree of battery OCV, fourth degree for battery charging and discharging resistances.

$$OCV = m_1 \cdot SOC^5 + m_2 \cdot SOC^4 + m_3 \cdot SOC^3 + m_4 \cdot SOC^2 + m_5 \cdot SOC + m_6 \quad (4.18)$$

Where $m_1 = 1722.4$; $m_2 = -4747.5$; $m_3 = 4891.9$; $m_4 = -2312.1$; $m_5 = 525.72$; $m_6 = 200.06$.

$$R_{ch} = n_1 \cdot SOC^4 + n_2 \cdot SOC^3 + n_3 \cdot SOC^2 + n_4 \cdot SOC + n_5 \quad (4.19)$$

Where $n_1 = 0.0056$; $n_2 = -0.0254$; $n_3 = 0.0372$; $n_4 = -0.0203$; $n_5 = 0.0223$.

$$R_{dch} = q_1 \cdot SOC^4 + q_2 \cdot SOC^3 + q_3 \cdot SOC^2 + q_4 \cdot SOC + q_5 \quad (4.20)$$

Where $q_1 = 0.0188$; $q_2 = -0.0547$; $q_3 = 0.0765$; $q_4 = -0.0457$; $q_5 = 0.0349$. The coefficient of correlation (R^2) in all the above equations is within 0.80-0.95, which is interpreted as a correspondence between the equations and experimental data.

Battery charging (Regeneration) mode

In charging mode, from Kirchhoff's voltage rule, battery terminal voltage is the sum of battery open circuit voltage and voltage drop in the resistance.

$$V_{term} = OCV + I_{ch} \cdot R_{ch} \quad (4.21)$$

Equation 4.21 can be written in terms of power by multiplying both sides by charging current.

$$V_{term} \cdot I_{ch} = OCV \cdot I_{ch} + I_{ch} \cdot I_{ch} \cdot R_{ch} \quad (4.22)$$

The term $V_{term} \cdot I_{ch}$ in the equation 4.22 represents the battery charging power P_{ch} , the power at the battery terminals during charging phases.

$$P_{ch} = OCV \cdot I_{ch} + I_{ch}^2 \cdot R_{ch} \quad (4.23)$$

Battery discharging (Traction) mode

In discharging mode, from Kirchhoff's voltage rule, battery open circuit voltage is the sum of battery terminal voltage and voltage drop in the resistance.

$$OCV = V_{term} + I_{dch} \cdot R_{dch} \quad (4.24)$$

Equation 4.24 can be written in terms of power by multiplying both sides by discharging current.

$$OCV \cdot I_{dch} = V_{term} \cdot I_{dch} + I_{dch} \cdot I_{dch} \cdot R_{dch} \quad (4.25)$$

The term $V_{term} \cdot I_{dch}$ in the equation 4.26 represents the battery discharging power P_{dch} , the power at the battery terminals during discharging phases.

$$OCV \cdot I_{dch} = P_{dch} + I_{dch}^2 \cdot R_{dch} \quad (4.26)$$

The values of charging and discharging currents (I_{ch} and I_{dch}) can be calculated by solving the quadratic equations 4.23 and 4.26.

$$I_{dch} = \frac{OCV - \sqrt{OCV^2 - 4 \cdot R_{dch} \cdot P_{dch}}}{2 \cdot R_{dch}} \quad (4.27)$$

$$I_{ch} = \frac{-OCV + \sqrt{OCV^2 + 4 \cdot R_{ch} \cdot P_{ch}}}{2 \cdot R_{ch}} \quad (4.28)$$

Battery state of charge (SOC) can be formulated from charge conservation law and has the following form:

$$SOC = SOC_0 - \frac{\int_0^T I_{dch}^k dt}{Q_{nom,Ah}} + \frac{\int_0^T I_{ch} dt}{Q_{nom,Ah}} \quad (4.29)$$

SOC_0 -initial value of state of charge;

T -final value of time instant for charging or discharging;

$Q_{nom,Ah}$ -nominal value of battery capacity (in Ampere hours);

Coefficient k in Equation 4.29 is Peukert coefficient. It takes into account the change in battery capacity for different values of discharging currents. For NiMH batteries, literature [39] suggests the value of k between 1 and 1.2. In this work, Peukert coefficient is chosen to be equal to 1.1.

4.2.7 Boost converter model

A boost converter (step-up) converter is a DC-to-DC power converter that increases voltage (while reducing current) from supply to the load. In our case since voltage that should be supplied to AC synchronous motor is around 650 V, while the voltage of FC stack is around its nominal value (245V), boost converter is required to be installed to step-up the voltage of fuel cell stack. Simulink model of this subsystem takes into account its efficiency, which is on average 95 %.

4.2.8 Energy management system model

Since there are two energy sources, there is a flexibility in terms of power distribution between fuel cell stack and batteries. This task should be performed by optimizing hydrogen consumption and maintaining battery SOC. Due to the fact that efficiency of fuel cell stack is not constant and strongly depends on power, the main logic of power control unit is to force the fuel cell stack to work at optimum operating line, i.e., to work at high efficiency points so that hydrogen consumption is minimized while battery provides the lacking power. The decision of power splitting also depends on the value of SOC of the battery. Battery pack can only provide power when SOC is higher than certain threshold value.

In order to determine the energy management strategy of Toyota Mirai (1st generation FCHEV), experimental data of Argonne National Laboratory [40] is used. The decision on distribution of power between fuel cell stack and batteries strongly depends on battery SOC and power required by electric machine. Working points of FC and batteries over WLTC driving cycles is represented as a function of required power by electric machine and battery SOC, which are illustrated in Figure 4.16 and as a function of required power only (the planar projection of Figure 4.16), which is illustrated in Figure 4.17.

Parameters	Label	Unit	Values
<i>General vehicle specifications</i>			
Mass	M	kg	1927
Frontal area	A_f	m ²	2.23
Aerodynamic drag coefficient	C_d	Ns ² m ²	0.29
Rolling resistance coefficient	f_r	[-]	0.01
Radius of the wheel	R	m	0.316
Inertia of the wheel	J_{wh}	kgm ²	0.32
Auxiliary power	P_{aux}	W	440
Air density	ρ_{air}	kg/m ³	1.2
<i>Gearbox specifications</i>			
Reduction ratio	τ	[-]	9.09
Gearbox efficiency	η_{gb}	[-]	0.98
<i>Electric machine specifications</i>			
Motor model code	4JM		
Maximum power	$P_{em,max}$	kW	113
Maximum torque	$T_{em,max}$	Nm	335
Inertia of electric motor	J_{em}	kgm ²	0.008
<i>Fuel cell specifications</i>			
Maximum power	$P_{fc,max}$	kW	114
Volume power density	[-]	kW/L	3.1
Fuel cell efficiency at 60 mph	η_{60mph}	[-]	60.6
Number of cells in stack	N_{stack}	[-]	370
Total area	A_{tot}	[cm ²]	370
<i>Hydrogen tank specifications</i>			
Number of tanks	N_{tank}	[-]	2
Nominal working pressure	P_{H_2}	[MPa]	70
Volume	V_{H_2}	[L]	37
Weight of both tanks	m_{tank}	[kg]	87.5
Hydrogen capacity	m_{H_2}	[kg]	5
<i>Battery specifications</i>			
Number of series connections	N_{ser}	[-]	34
Number of parallel connections	N_{par}	[-]	1
Capacity	Q	Ah	6.5
Nominal capacity	Q_{nom}	kWh	1.6
Nominal voltage	V_{nom}	V	245

Table 4.1: Parameters of Toyota Mirai (1st generation) FCHEV used in calculation

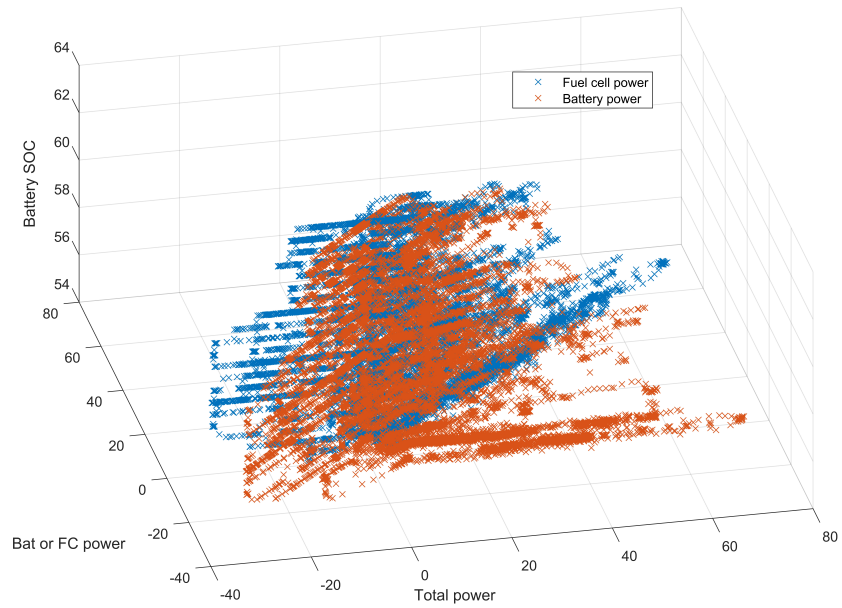


Figure 4.16: Experimental working points on WLTC (3-D view)

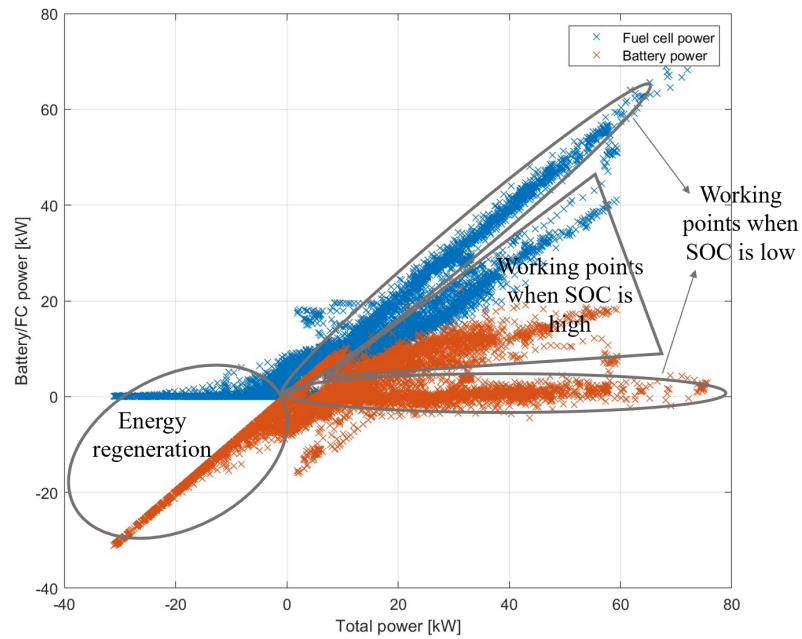


Figure 4.17: Experimental working points on WLTC (2-D view, planar projection)

In Figure 4.17, the low values of SOC means the values, lower than 57 %, while the high values of SOC means the values, higher or equal than 57 %.

Experimental EMS is reconstructed by means of rule based strategy and approximated by means of linear regression process for simulation purposes (Figure 4.18).

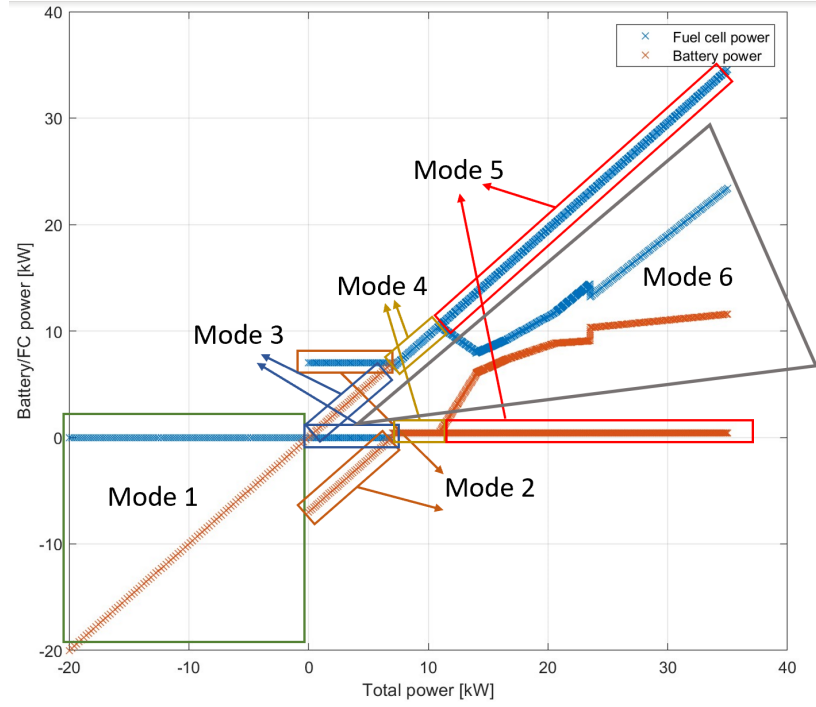


Figure 4.18: Reconstructed rule based EMS

FC and battery working point location depends on required power from EM and battery SOC and can be divided in six different modes.

Mode 1

FCHEV works in mode 1 during energy regeneration phases, when EM supplied negative power. Since FC is irreversible device, the braking energy is stored in batteries.

$$P_{fc} = 0kW; \quad P_{bat} = P_{req} \quad (4.30)$$

Mode 2

FCHEV operates in mode two at low power requests ($0 < P_{req} < 7kW$) and low SOC ($< 57\%$). Since the FC efficiency is extremely small at low power outputs

(lower than $7kW$), it provides constant power output, while the excess charges the batteries.

$$P_{fc} = 7kW; \quad P_{bat} = P_{req} - 7kW \quad (4.31)$$

Mode 3

Mode three is on at low power requests ($0 < P_{req} < 7kW$) and high SOC ($\geq 57\%$). Battery provides all the power request, while the FC is off.

$$P_{fc} = 0kW; \quad P_{bat} = P_{req} \quad (4.32)$$

Mode 4

In mode 4, battery supplies only the auxiliary devices, while the FC provides power for the traction.

$$P_{fc} = P_{req} - P_{aux}; \quad P_{bat} = P_{aux} \quad (4.33)$$

Mode 5

FCHEV operates in mode five at high power requests ($P_{req} > 11kW$) and low SOC ($< 57\%$). All the power request is provided by the FC whereas batteries supply auxiliary power.

$$P_{fc} = P_{req} - P_{aux}; \quad P_{bat} = P_{aux} \quad (4.34)$$

Mode 6

Mode six on at high power request ($P_{req} > 11kW$) at high values of SOC ($\geq 57\%$). Both batteries and FC provide the power is a proportion which is described by complex linear equations.

$$P_{fc} = \begin{cases} -0.79 \cdot P_{req} + 19.11 & 11kW \leq P_{req} < 14kW \\ 0.5 \cdot P_{req} + 0.925 & 14kW \leq P_{req} < 16.5kW \\ 0.6265 \cdot P_{req} - 1.168 & 16.5kW \leq P_{req} < 20.7kW \\ 0.92 \cdot P_{req} - 7.2 & 20.7kW \leq P_{req} < 23.5kW \\ 0.89 \cdot P_{req} - 7.7285 & P_{req} \geq 23.5kW \end{cases} \quad (4.35)$$

$$P_{bat} = P_{req} - P_{fc} \quad (4.36)$$

The coefficient of correlation (R^2) in all the above equations is within 0.80-0.95, which is interpreted as a correspondence between the equations and experimental data.

4.3 Simulation results

This section presents the evaluation of the performance of the obtained techniques. This was done on the basis of simulations over WLTC, NEDC, UDDS, US06, HWY and JC08 driving cycles. The validation of the current model was done by comparing the results of the simulation in MATLAB Simulink environment and comparing it with the ANL experimental data. The parameters used in the control strategy block have been fitted to be as close as possible to the real operation of the car.

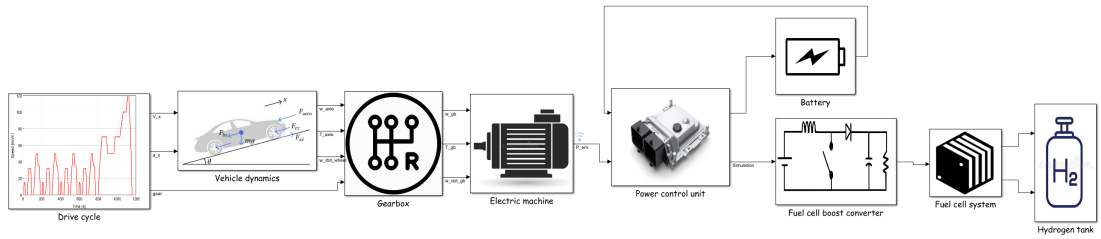


Figure 4.19: Block diagram in MATLAB/Simulink environment

4.3.1 Results on WLTC driving cycle

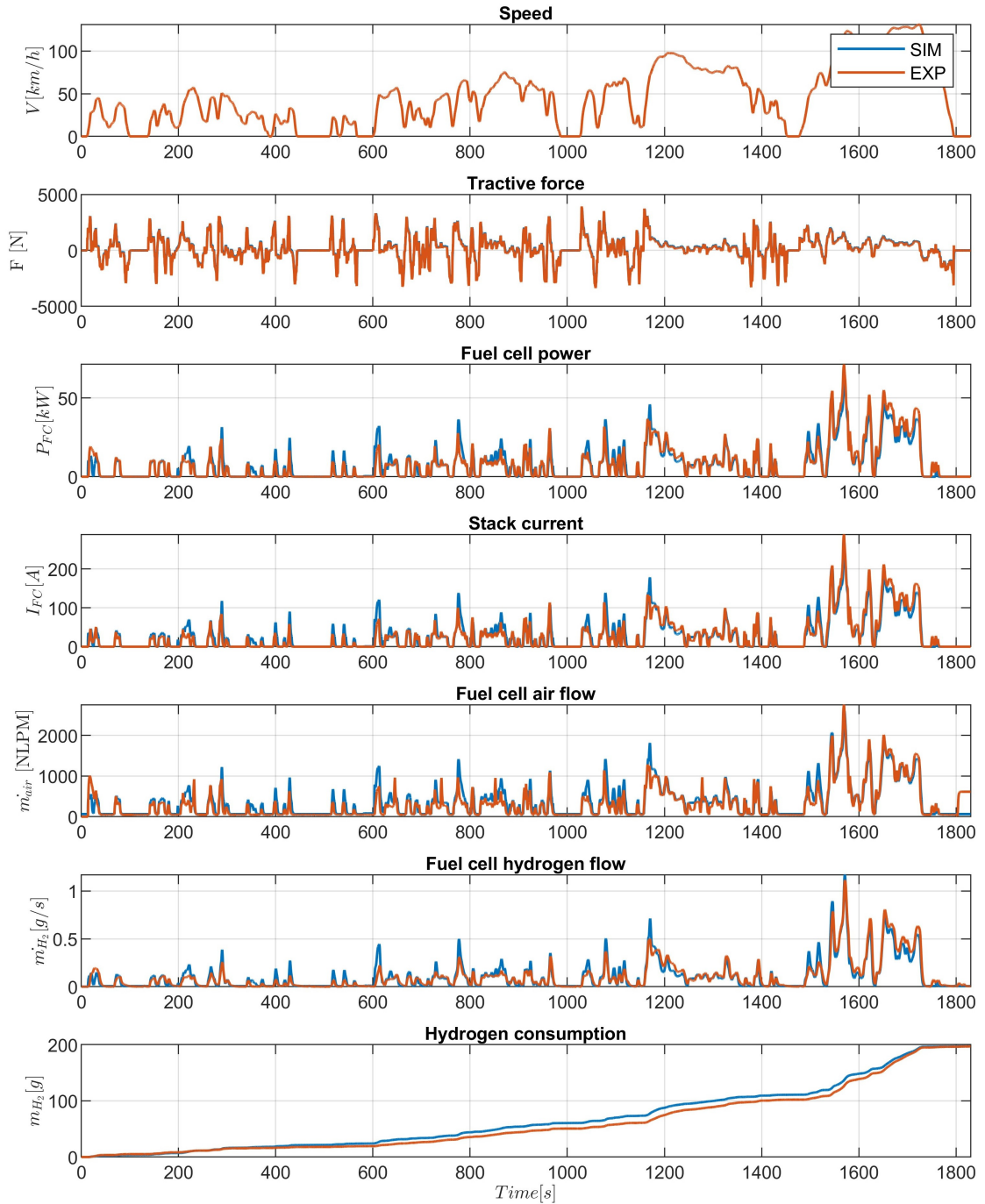


Figure 4.20: Simulation results over WLTC driving cycle (Fuel cell parameters)

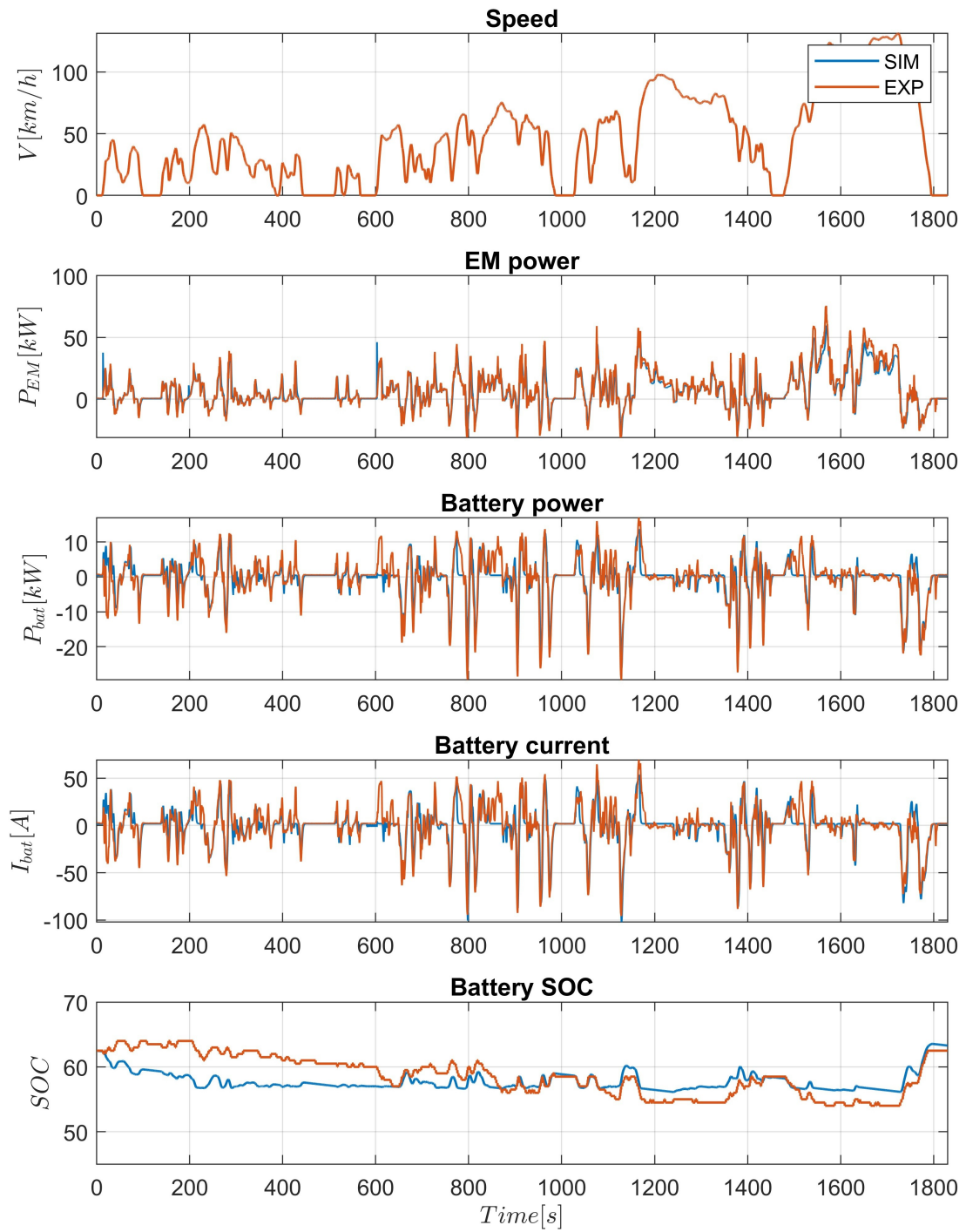


Figure 4.21: Simulation results over WLTC driving cycle (Battery parameters)

4.3.2 Results on NEDC driving cycle

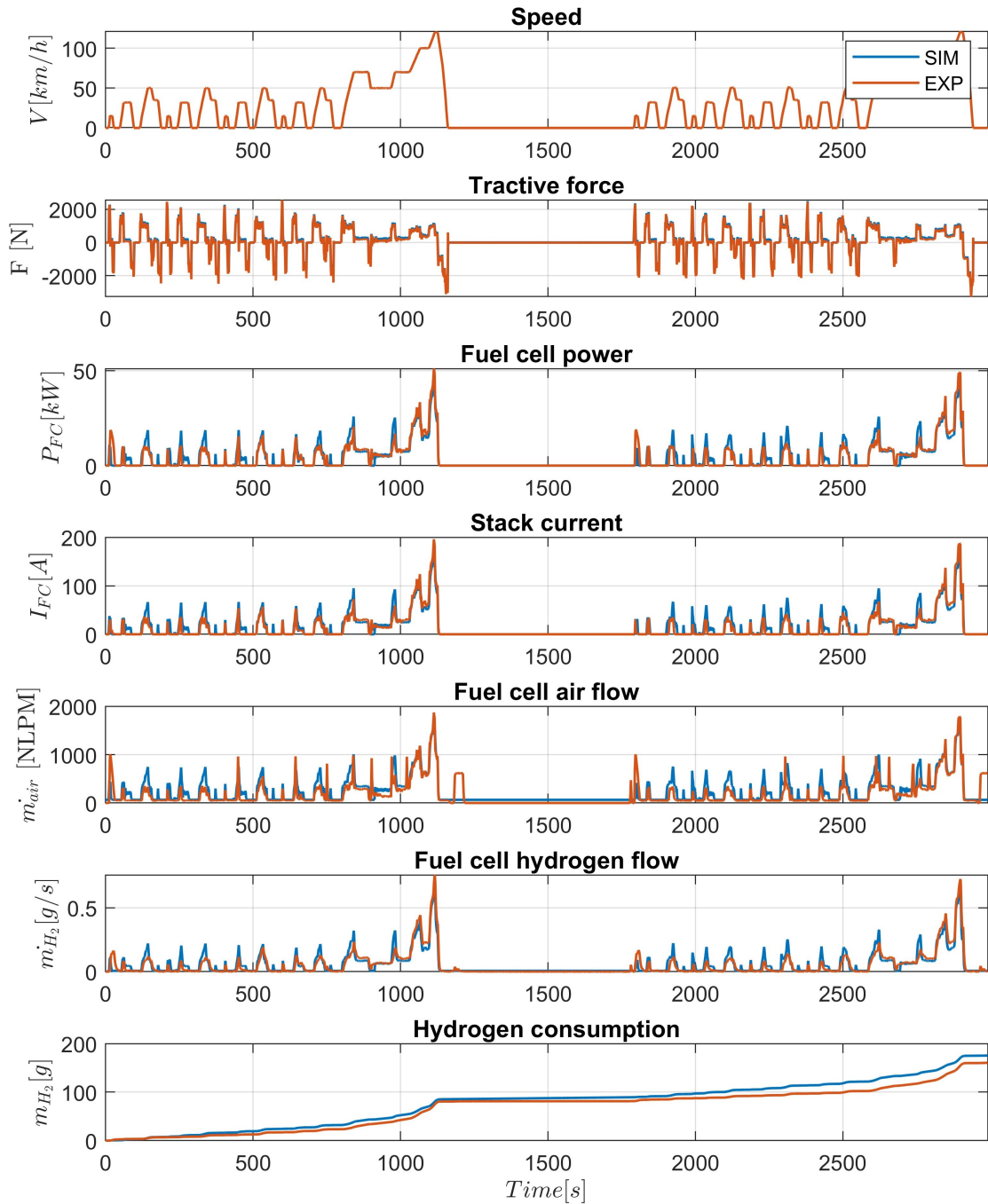


Figure 4.22: Simulation results over NEDC (x2) driving cycle (Fuel cell parameters)

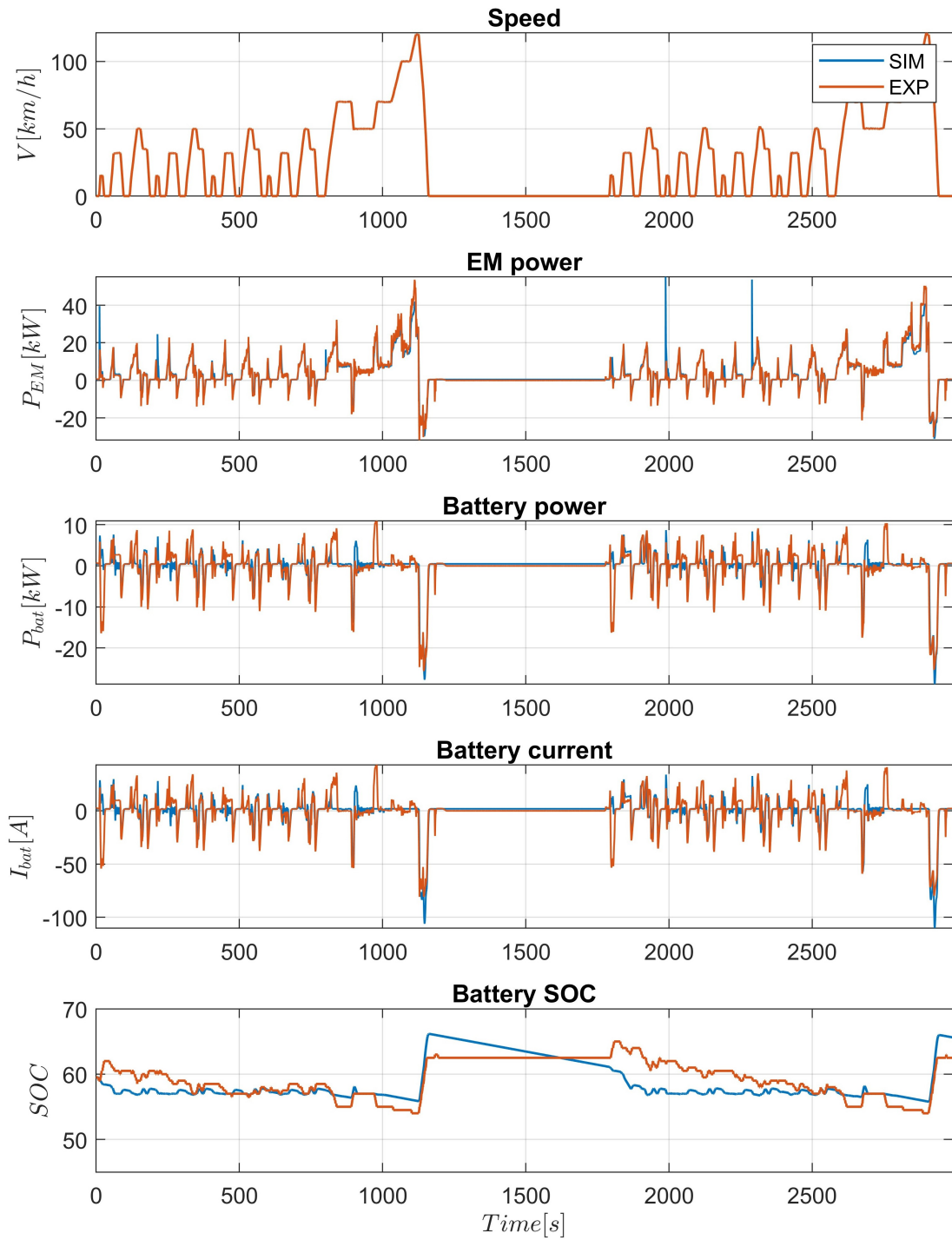


Figure 4.23: Simulation results over NEDC (x2) driving cycle (Battery parameters)

4.3.3 Results on UDDS driving cycle

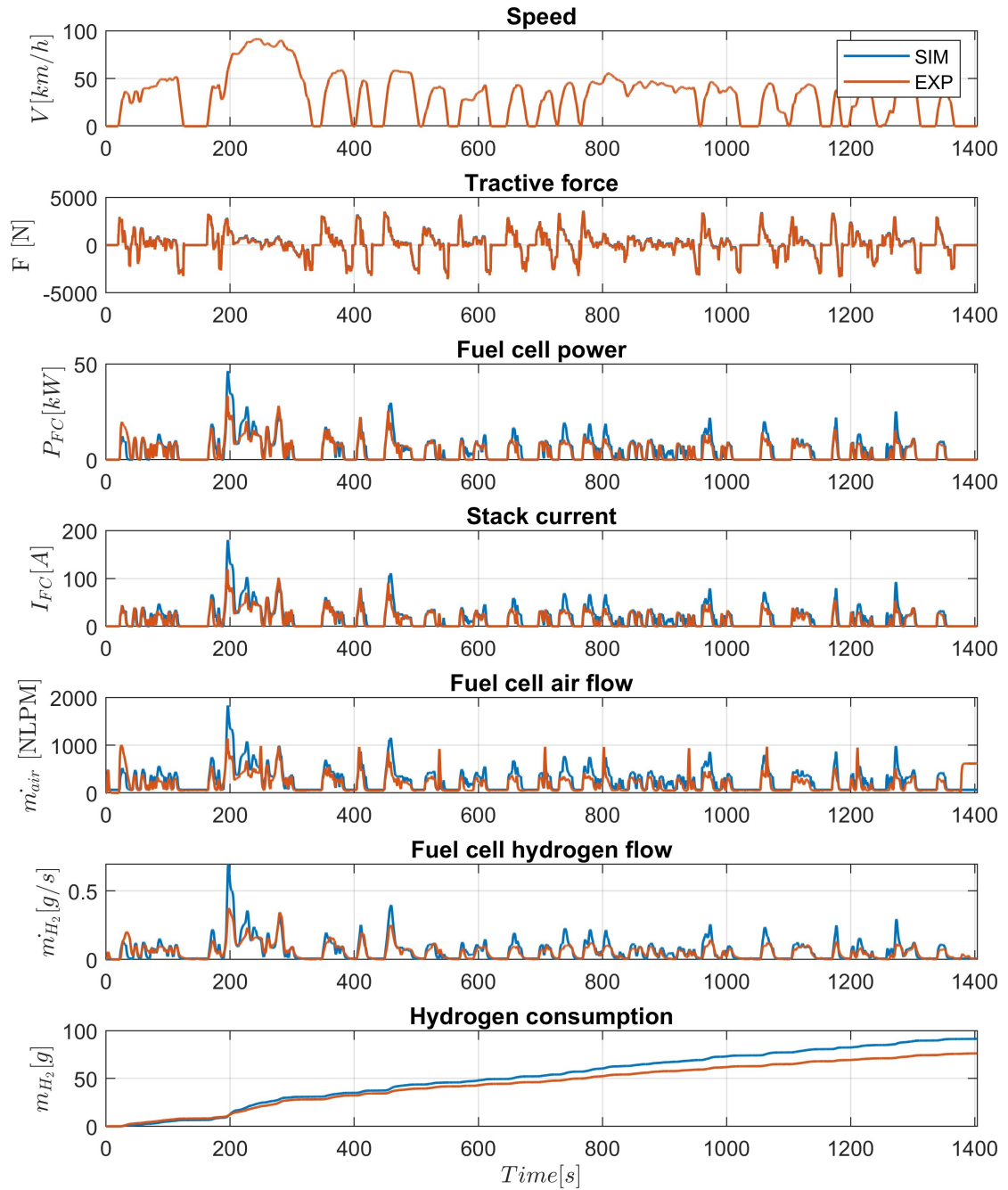


Figure 4.24: Simulation results over UDDS driving cycle (Fuel cell parameters)

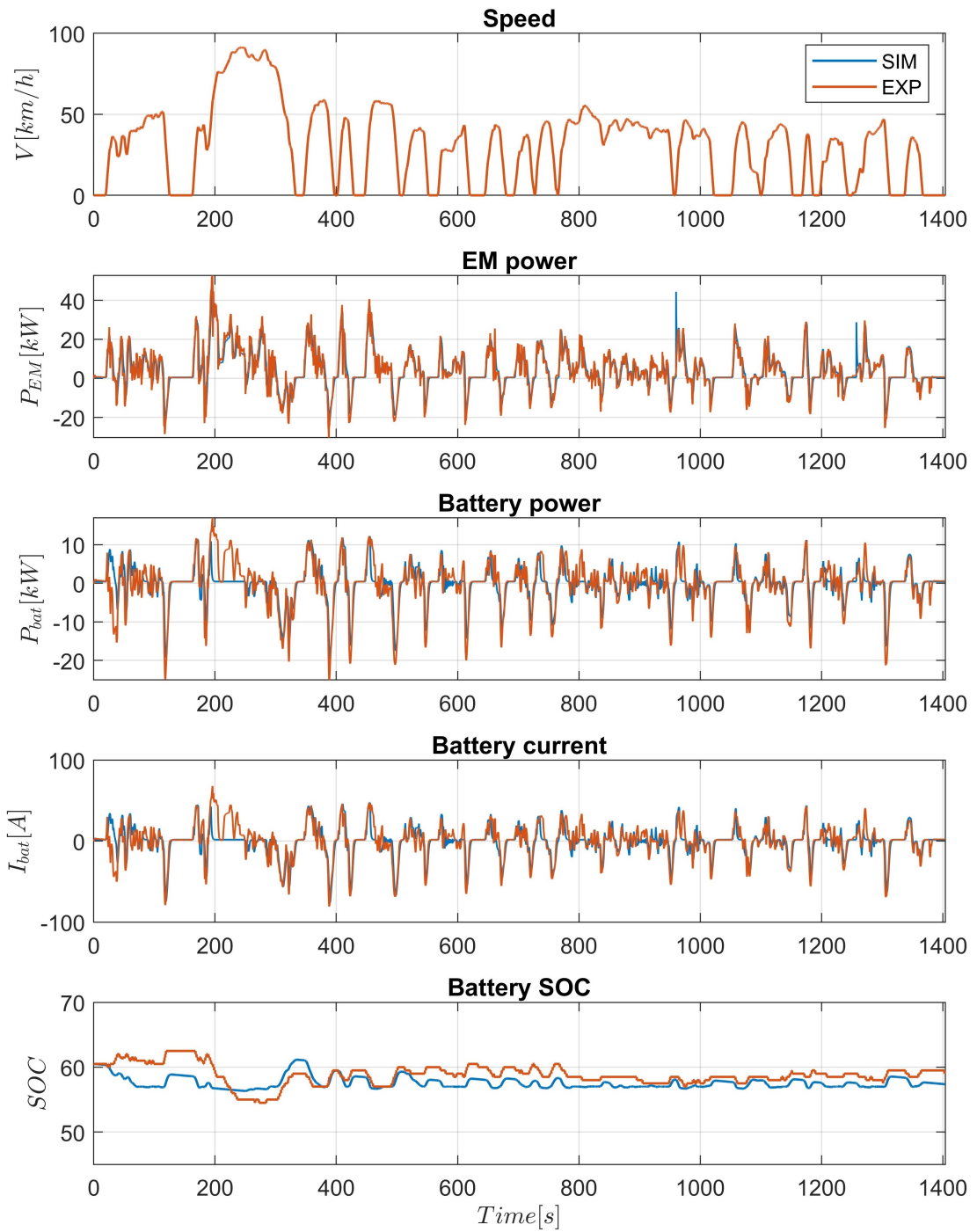


Figure 4.25: Simulation results over UDSS driving cycle (Battery parameters)

4.3.4 Results on JC08 driving cycle

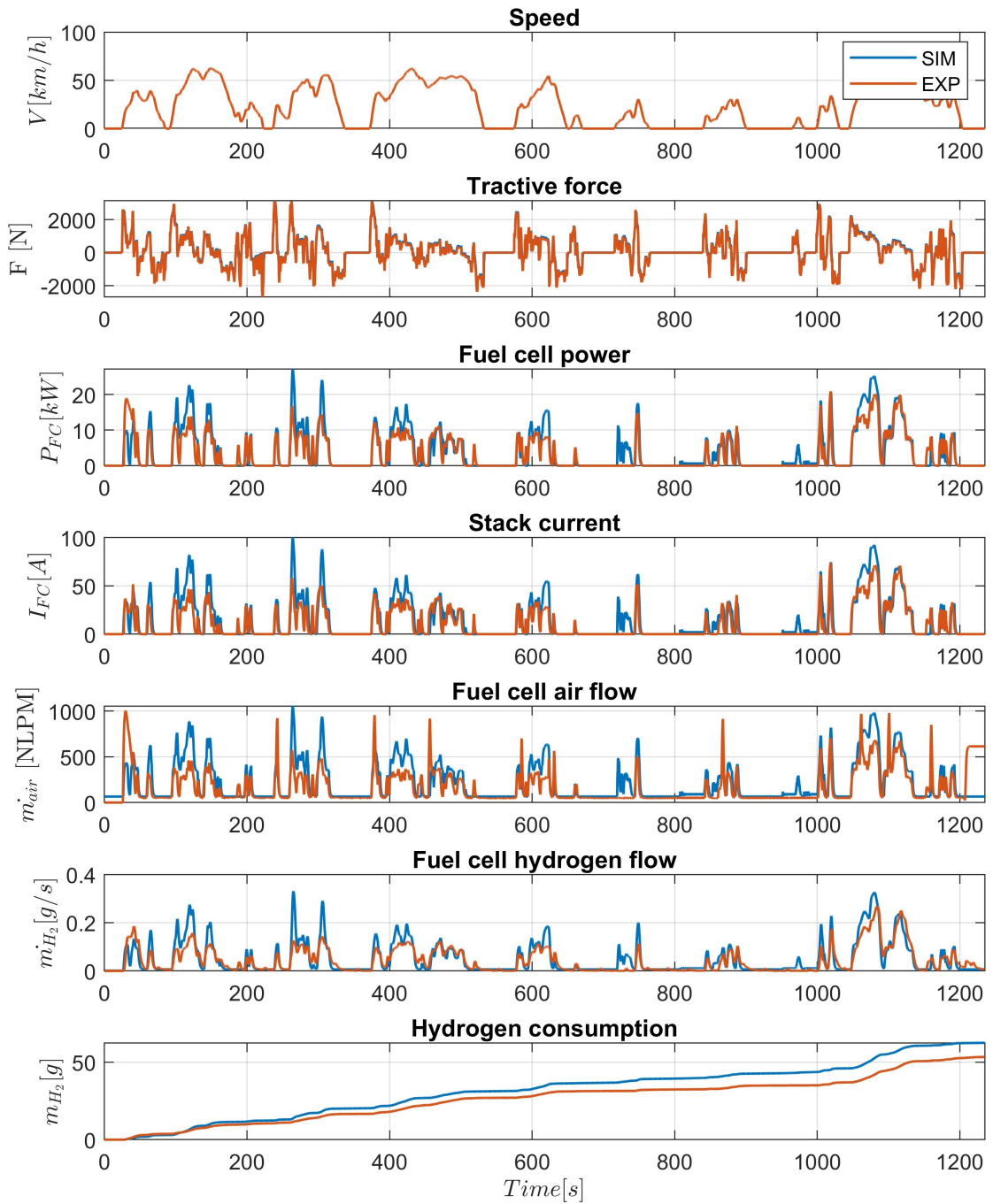


Figure 4.26: Simulation results over JC08 driving cycle (Fuel cell parameters)

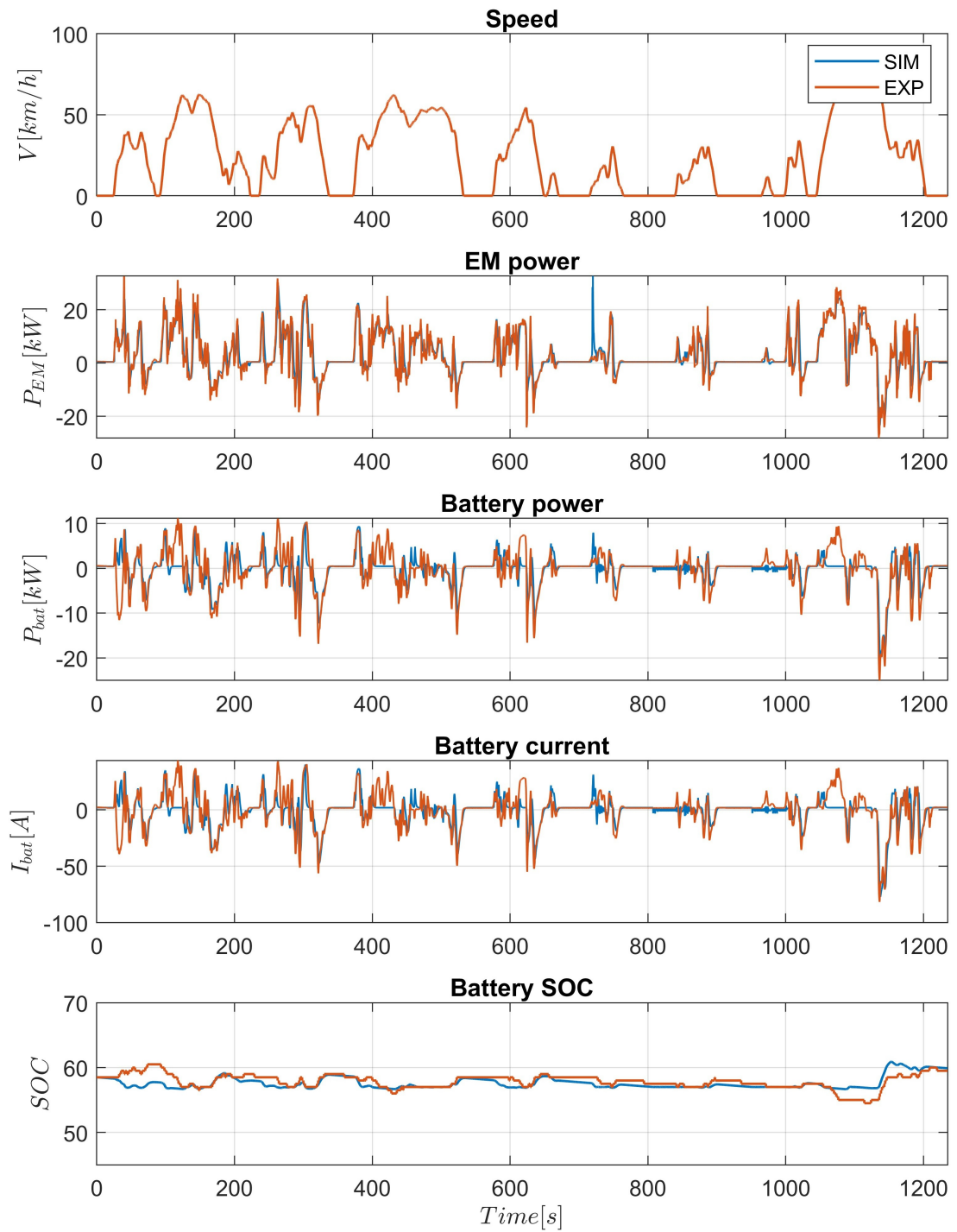


Figure 4.27: Simulation results over JC08 driving cycle (Battery parameters)

4.3.5 Results on US06 driving cycle

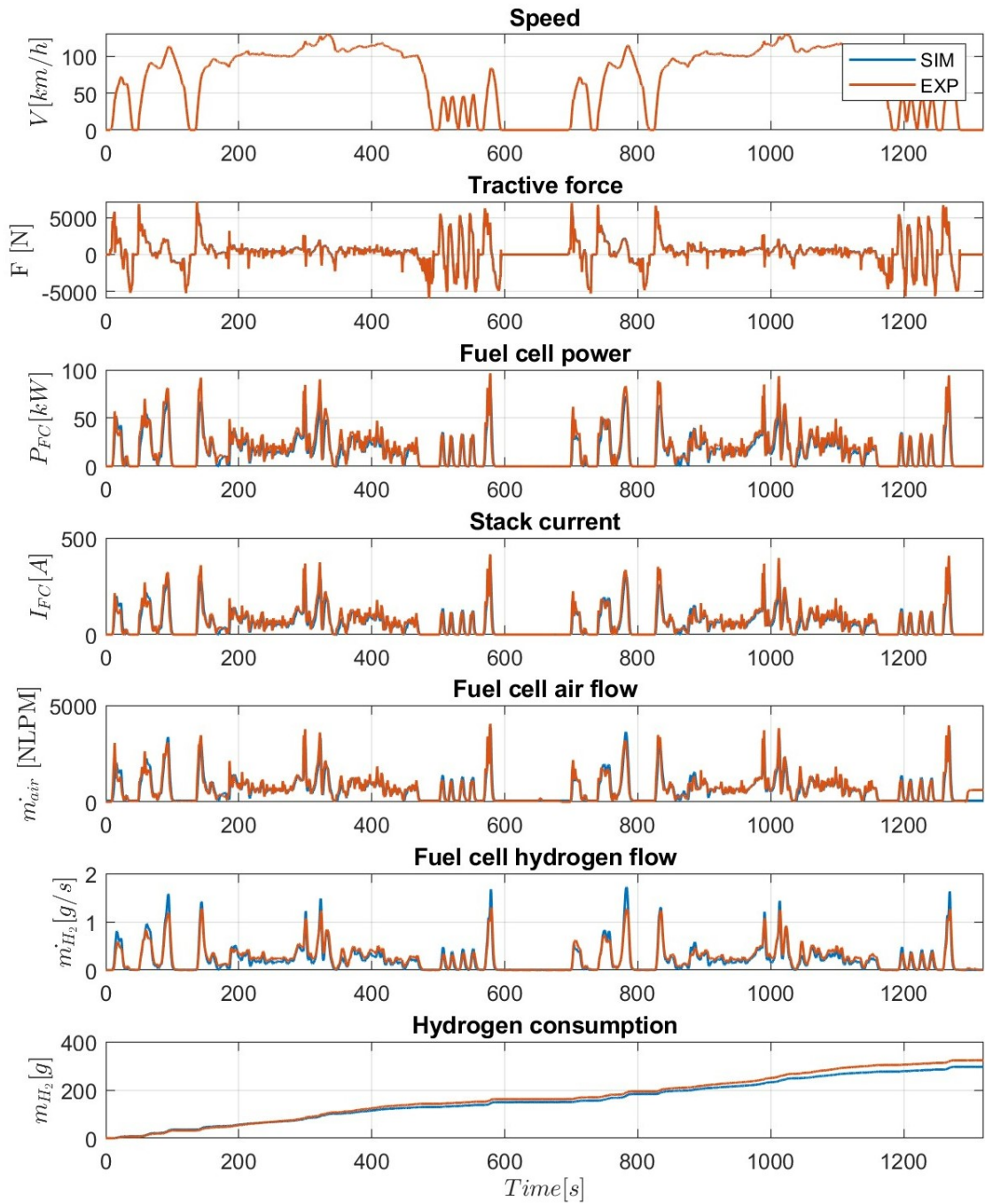


Figure 4.28: Simulation results over US06 (x2) driving cycle (Fuel cell parameters)

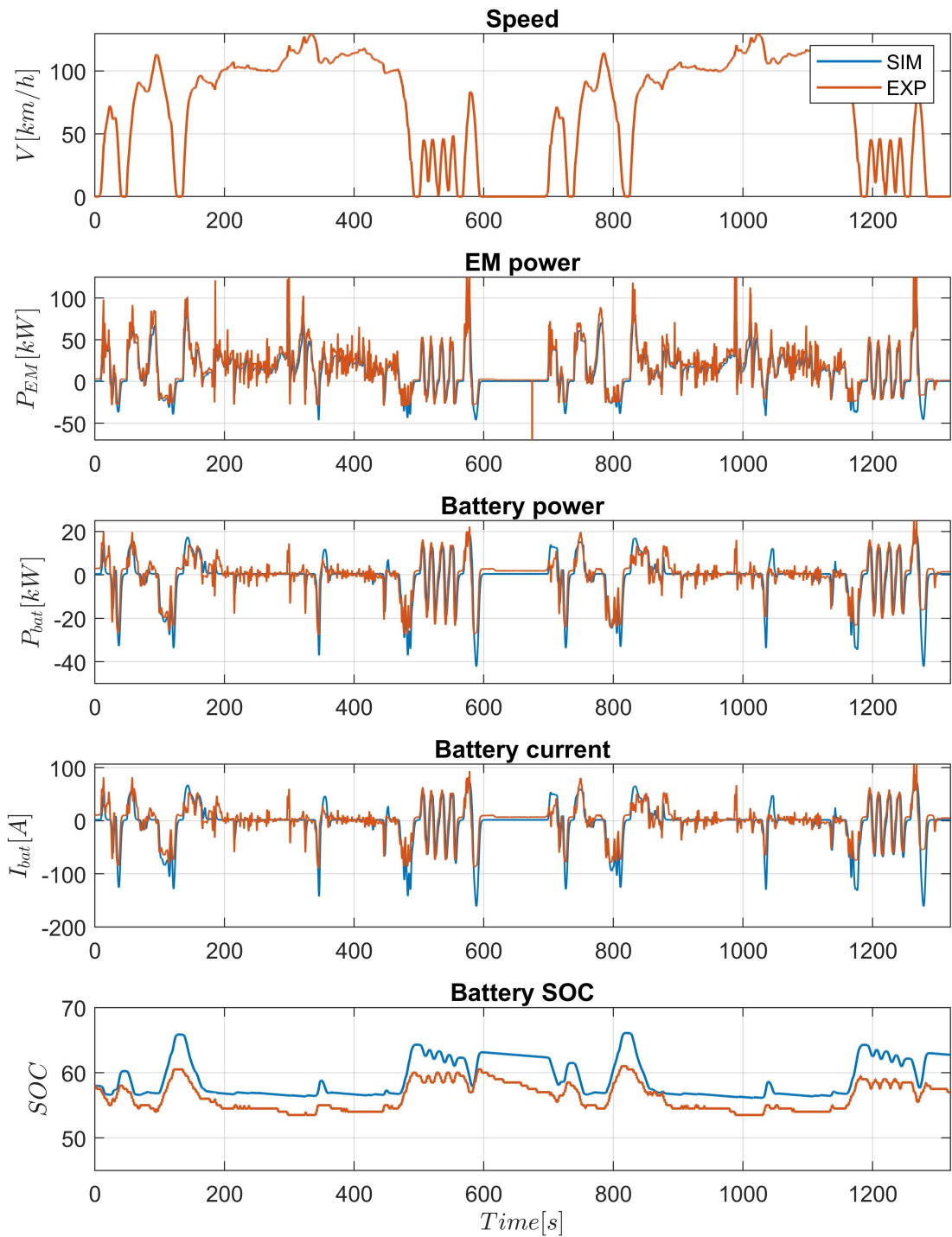


Figure 4.29: Simulation results over US06 (x2) driving cycle (Battery parameters)

4.3.6 Results on HWY driving cycle

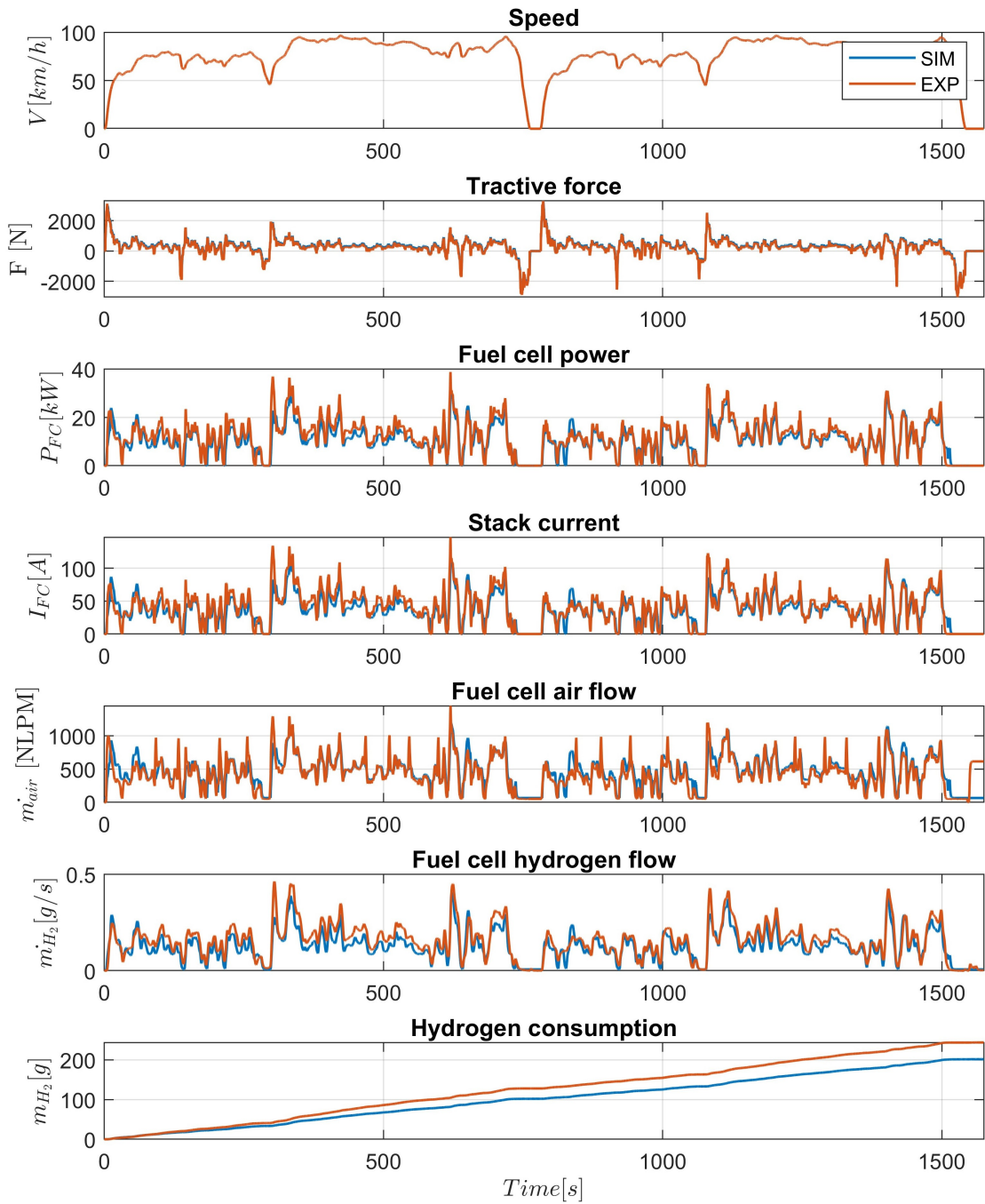


Figure 4.30: Simulation results over HWY (x2) driving cycle (Fuel cell parameters)

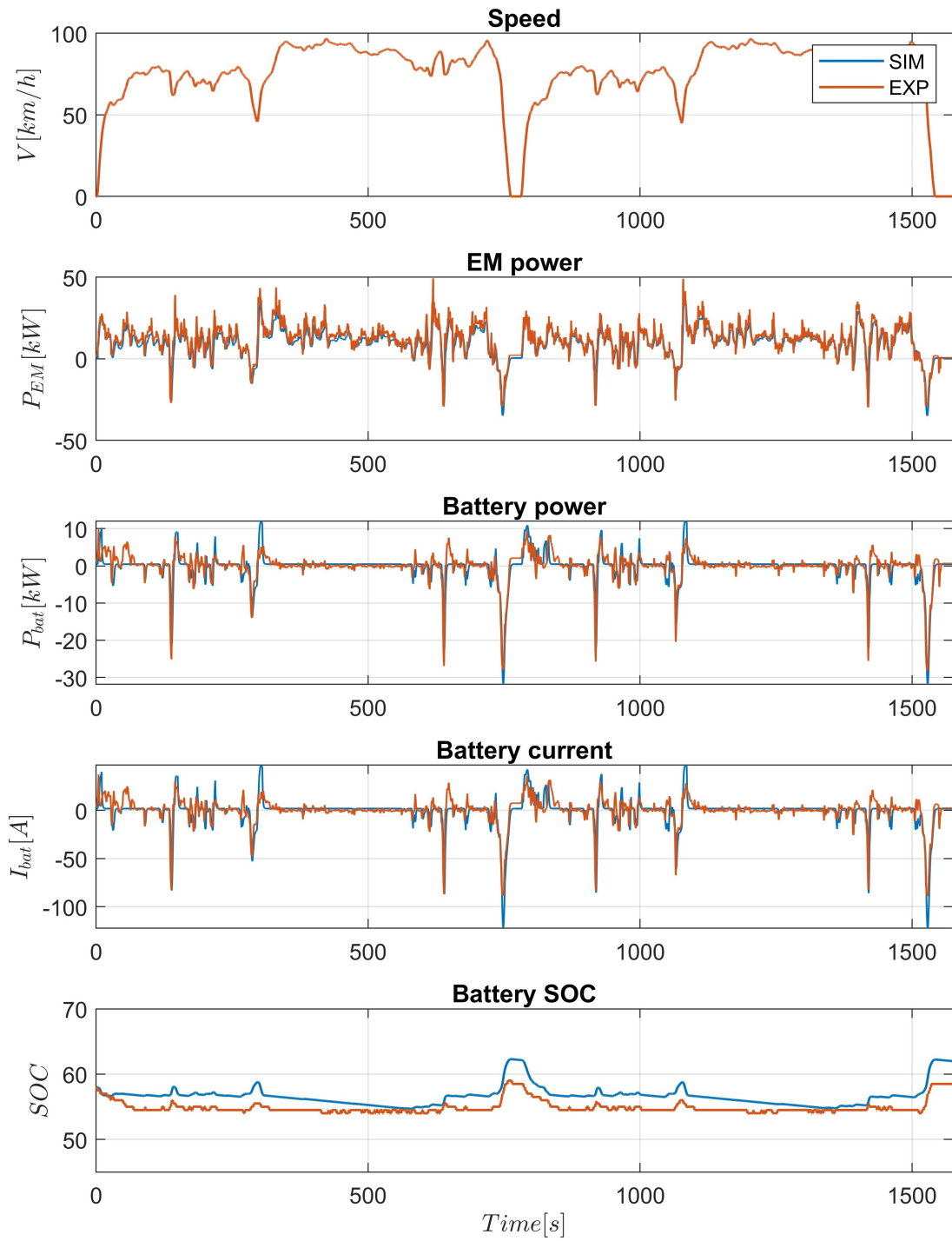


Figure 4.31: Simulation results over HWY (x2) driving cycle (Battery parameters)

Driving cycle	Hydrogen consumption [g]				
	Simulation	SOC compensation	Total	Experimental	Difference
WLTC	197	0.711	197.711	196.8	0.5 %
NEDC	175	2.808	177.808	160.3	10.9 %
UDDS	91.4	-1.467	89.933	76.18	18.1 %
JC08	62.46	-5.571	56.889	53.3	6.7 %
US06	296	5.166	301.166	323	6.8 %
HWY	201.6	3.141	204.741	243.9	16.1 %

Table 4.2: Simulation results for hydrogen consumption

SOC [%]			
Driving cycle	Simulation	Experimental	Difference
WLTC	63.29	62.5	1 %
NEDC	65.62	62.5	5 %
UDDS	57.37	59	3 %
JC08	53.31	59.5	10 %
US06	62.74	57	10 %
HWY	61.99	58.5	6 %

Table 4.3: Simulation results for battery SOC

4.4 Results discussion and analysis

Figures 4.20-4.31 illustrate speed, tractive force, fuel cell power, stack current, fuel cell air flow rate, fuel cell hydrogen flow rate, cumulative hydrogen consumption, electric machine power, battery power, battery current and battery state of charge time history for WLTC, NEDC, UDDS, JC08, US06 and HWY driving cycles. Red line present experimental data profile, while blue line shows simulated. Tables 4.2 and 4.3 summarize the data for hydrogen consumption and final battery SOC.

Table 4.2 provides information about simulated and experimental cumulative hydrogen consumption, expressed in grams. Due to the difference in simulated and experimental final battery SOC, the corresponding compensation in terms of hydrogen is takes into account. Through iterative calculation procedure, it was found that the energy content in 1 percent of battery SOC corresponds to 0.9 grams of hydrogen. The minimum difference in battery SOC was found for WLTC driving cycle, being at 1%, while the maximum difference for JC08 and HWY cycles, standing at 10 %.

It can be seen from Table 4.2, that WLTC driving cycle data presents maximum matching between simulated and experimental data, with the difference, being at just 0.5 %. On the other side, the maximum difference in simulated and experimental data was observed for UDDS and HWY driving cycles, specifically 18.1 % for UDDS and 16.1 % for HWY respectively. The moderate difference has been noticed JC08 and US06 cycles, both standing at slightly less than 7 %. Finally, 10.9 % difference exists for NEDC cycle.

The main differences are the following

- Simulated FC power, current, air and hydrogen flow cannot catch the peaks of experimental data.

- The general shape of battery power and current is slightly different comparing with experimental one.
- Simulated battery current and power cannot fully catch the negative peaks of experimental data.
- In middle and high peaks, fuel cell hydrogen flow is lower than experimental results

The following aspects are the reason for deviation between simulated and experimental data.

- **EMS mismatching.** The rule based EMS (Figure 4.18), used during the simulation is obtained by linear regression procedure of experimental data (Figure 4.16). Therefore it doesn't perfectly match the real EMS of Toyota Mirai, which is presumably fuzzy logic control strategy.
- **Quasi-static simulation.** All the simulated parameters are obtained by following quasi-static approach. So, the time history of these parameters are not continuous, rather they are quasi-static with a step-size of 0.1 seconds
- **Effect of backward modeling.** Backward modeling approach rely on efficiency maps, which were often built during steady-state real world testing. Therefore, it doesn't fully reflect the dynamic impacts.
- **Effect of reverse engineering for fuel cell model.** Due to the complexity of real fuel cell system mathematical model, the simplified model, taking into account efficiency and hydrogen consumption look-up tables are used for fuel cell modeling, which doesn't fully reflect the dynamic behaviour of fuel cell system.
- **Effect of different EM efficiency map.** Due to the lack of data, concerning the efficiency map and performance curve for Toyota Mirai's electric machine, YASA P400 R SERIES AC synchronous EM's efficiency map is used and parameters are scaled to fit the peak torque and speed. Therefore, this map doesn't fully match the real EM's map.
- **Effect of Peukert coefficient.** Peukert coefficient for NiMH batteries ranges between 1 and 1.2, depending on different discharging currents [39]. In this work, the average value, equal to 1.1, which is constant for any discharging currents is applied for Peukert coefficient.
- **Lack of data for some parameters.** The exact values for some parameters, like wheel's or EM's mass moment of inertia or vehicle frontal area weren't known. Therefore, they were roughly estimated.

In conclusion, the general shape of fuel cell and battery parameters are well reproduced and obtained numerical results are similar. Therefore, this mathematical model can be used to simulate FCHEVs to estimate the hydrogen consumption given the driving pattern.

Chapter 5

Control strategy optimization of Toyota Mirai based FCHEV

5.1 Equivalent consumption minimization strategy (ECMS)

Equivalent consumption minimization strategy (ECMS) is based on the conversion of electrical energy in the energy storage sources into an equivalent fuel consumption and minimization of the sum of instantaneous fuel consumption and equivalent fuel consumption [41]. In this strategy, all energy of the vehicle comes directly or indirectly from hydrogen. Charging and discharging of battery or supercapacitor should be equivalent to hydrogen consumption according to set of rules. The energy consumption of the vehicle should be equal to hydrogen in order to reduce the system's instantaneous hydrogen consumption [42]. The calculation of equivalent fuel consumption of batteries is performed by making an assumption that SOC variation in the future is compensated by FC system.

This principle was first introduced by Paganelli et al. [27] and presents an algorithm for the EMS of HEV that chooses the power split between electric motor and engine in order to minimize the fuel consumption. As a result, 17.5 % of fuel reduction was able to be achieved in simulation. Concerning the implementation of ECMS on FCHEV, several works have been done by researchers. Paganelli et al. [43] propose ECMS control strategy for real time application of instantaneous power split between fuel cell and an electrical accumulator in a charge sustaining fuel cell hybrid vehicle and allowing the overall minimization of hydrogen consumption while meeting the driver demand. Han et al. [44] studied the performance of dynamic

programming control strategy are compared with Pontryagin's minimum principle and ECMS. Liu et al. [42] proposed ECMS to solve power allocation problem of FCHEV in order to reduce hydrogen energy consumption and prolong battery life. As a result, the optimal output power of FC was obtained by using ECMS and battery output power was smoothed, achieving the best power distribution between battery and supercapacitor. Bassam et al. [45] simulated different control strategies, including ECMS on hybrid fuel cell/battery passenger vessel. In this work, an optimized proportional-integral (PI) controller based energy management strategy was presented and made a comparative analysis with original PI controller, ECMS and state-based energy management strategies in terms of hydrogen consumption and FC stresses with no additional first cost or hardware changes. Li et al. [46] designed an ECMS strategy for a fuel cell hybrid electric vehicle powered by fuel cell, battery and supercapacitor to operate FC system at its best efficiency zone and battery as a long term energy buffer and supercapacitor supplying peak power. Kamal et al. [47] a comparative analysis of the performance of different energy management strategies, including ECMS was done through the simulation over UDDS driving cycle.

5.2 Mathematical representation of ECMS

The purpose of EMS is the optimal distribution of EM's required power between FC system and battery. The equivalent hydrogen consumption due to the power, provided by the battery is considered by taking into account all the intermediate efficiencies. Finally, total hydrogen consumption is the sum of fuel cell and battery hydrogen consumption.

$$\dot{m}_{eqv} = \dot{m}_{fc}(P_{fc}(t)) + S_{SOC} \cdot \dot{m}_{bat}(P_{bat}(t)) \quad (5.1)$$

\dot{m}_{eqv} -equivalent (total) hydrogen consumption;

\dot{m}_{fc} -(instantaneous)hydrogen consumption due to fuel cell power demand;

S_{SOC} -penalty function, which takes into account SOC variation;

\dot{m}_{bat} -equivalent hydrogen consumption due to battery power demand;

The purpose of S_{SOC} is to use more the battery energy at high values of SOC and less at low values. In literature [48], it is suggested to take S_{SOC} in the following form:

$$S_{SOC} = 1 - \left(\frac{SOC(t) - SOC_t}{(SOC_{max} - SOC_{min}) \cdot 0.5} \right)^{k_s} \quad (5.2)$$

$SOC(t)$ -current value;

SOC_t -desired value;

SOC_{max} -maximum value;
 SOC_{min} -minimum value;
 k_s -power;

The equivalent hydrogen consumption due to battery power demand is different for the cases of discharging (traction) or charging (regeneration) and can be expressed as follows:

$$\dot{m}_{bat} = \begin{cases} \frac{P_{bat}}{\eta_{ch} \cdot \eta_{dch} \cdot \eta_{dc} \cdot \eta_{fc} \cdot LHV} & \text{if } P_{bat} \geq 0 \text{ (Discharging mode)} \\ \frac{P_{bat} \cdot \eta_{ch} \cdot \eta_{dch}}{\eta_{dc} \cdot \eta_{fc} \cdot LHV} & \text{if } P_{bat} < 0 \text{ (Charging mode)} \end{cases} \quad (5.3)$$

P_{bat} -battery power;
 η_{ch} -charging efficiency;
 η_{dch} -discharging efficiency;
 η_{dc} -fuel cell DC boost converter efficiency;
 η_{fc} -fuel cell efficiency, which depends on fuel cell output power;
 LHV -hydrogen lower heating value;

Equation 5.3 can be expressed in terms of hydrogen consumption dependence on fuel cell power (Figure 4.9). This dependence is described by quadratic equation 4.16. So,

$$\dot{m}_{H_2} = f(P_{fc}) \quad (5.4)$$

Therefore, equivalent hydrogen consumption due to battery power is

$$\dot{m}_{bat} = \begin{cases} f\left(\frac{P_{bat}}{\eta_{ch} \cdot \eta_{dch} \cdot \eta_{dc}}\right) & \text{if } P_{bat} \geq 0 \text{ (Discharging mode)} \\ f\left(\frac{P_{bat} \cdot \eta_{ch} \cdot \eta_{dch}}{\eta_{dc}}\right) & \text{if } P_{bat} < 0 \text{ (Charging mode)} \end{cases} \quad (5.5)$$

The objective function J to be minimized is described as follows:

$$J(P_{bat}, P_{fc}) = \min(\dot{m}_{equiv}(t)) \quad (5.6)$$

The constraints that should be taken into account are

$$\begin{cases} P_{bat} + P_{fc} = P_{req} \\ SOC_{max} > SOC > SOC_{min} \\ P_{fc,max} > P_{fc} > P_{fc,min} \\ P_{bat,max} > P_{bat} > P_{bat,min} \end{cases} \quad (5.7)$$

The values of the parameters, used in ECMS control strategy are provided in Table 5.1

Parameters	Label	Unit	Values
Desired state of charge	SOC_t	%	60
Maximum state of charge	SOC_{max}	%	70
Minimum state of charge	SOC_{min}	%	45
Power coefficient	k_s	[-]	3
Battery charging efficiency	η_{ch}	[-]	0.9
Battery discharging efficiency	η_{dch}	[-]	0.9
DC boost converter efficiency	η_{dc}	[-]	0.95
Hydrogen lower heating value	LHV	MJ/kg	120
Fuel cell minimum power	$P_{fc,min}$	kW	0
Fuel cell maximum power	$P_{fc,max}$	kW	113
Battery minimum power	$P_{bat,min}$	kW	-20
Battery maximum power	$P_{bat,max}$	kW	20

Table 5.1: Parameters for ECMS control strategy

Fuel consumption for transient processes are not taken into account during the calculations. They can affect the fuel consumption in the range of 2-4 % depending on the type of vehicle as well as the complexity of driving cycles.

It is possible to include into the Equation 5.1 different correction factors as penalty functions. The main purpose of these coefficients is to change the weight of real or virtual fuel consumption in the objective function. For example, they may represent adjustment for driving cycle complexity [49], temperature or battery life [50].

The calculation algorithm is provided in Figure 5.2

5.3 Simulation setup

The objective function $J(P_{bat}, P_{fc})$ in Equation 5.6 is minimized by using Matlab's built-in function $fmincon$ for the optimization of multi-variable linear and nonlinear problems.

The syntax of this function in Matlab is

$$x = fmincon(fun, x0, A, b, Aeq, beq, lb, ub, nonlcon, options)$$

This function uses "SQP" algorithm - series quadratic programming. The constraints, that should be taken into account during the minimization procedure are

$$\begin{cases} c(x) \leq 0 \\ ceq(x) = 0 \\ A \cdot x \leq b \\ Aeq \cdot x \leq beq \\ lb \leq x \leq ub \end{cases} \quad (5.8)$$

x is a vector of output parameters $[P_{fc}, P_{bat}]$
 lb and ub take into account lower and upper bounds for fuel cell and battery power.

$$lb = [0, P_{bat,min}]$$

$$ub = [P_{fc,max}, P_{bat,max}]$$

A_{eq} and b_{eq} take into account equality constraints. In our case the sum of fuel cell and battery power should be equal to power required by electric motor.

$$A_{eq} = [1 \ 1]$$

$$b_{eq} = [P_{req}]$$

The boundary condition, defined by vector b , matrix A and functions $c(x)$ and $ceq(x)$ can be excluded since in Equation 5.8 there are no boundary conditions corresponding to the conditions, described by them.

5.4 ECMS simulation results

This section presents the evaluation of the performance of ECMS control strategy on Toyota Mirai FCHEV and provides numerical results on the advantages, taken in terms of hydrogen consumption with respect to rule-based and experimental fuzzy-logic control strategy. An additional controller block has been included to the existing Simulink block diagram (Figure 4.4). Simulation was performed over WLTC, NEDC, UDDS, US06, HWY and JC08 driving cycles.

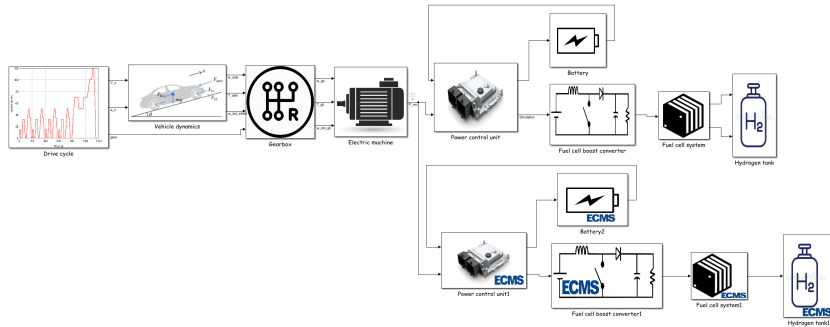


Figure 5.1: Block diagram in MATLAB/Simulink environment

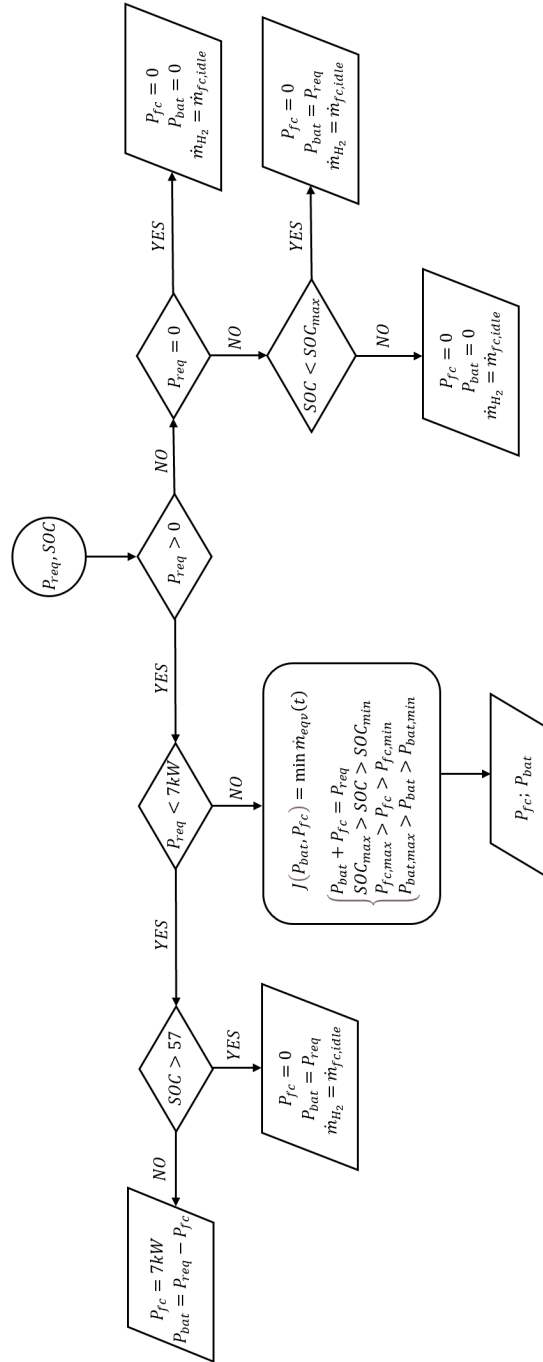


Figure 5.2: Calculation algorithm for ECMS output parameters given the required power and battery SOC

5.4.1 Results on WLTC driving cycle

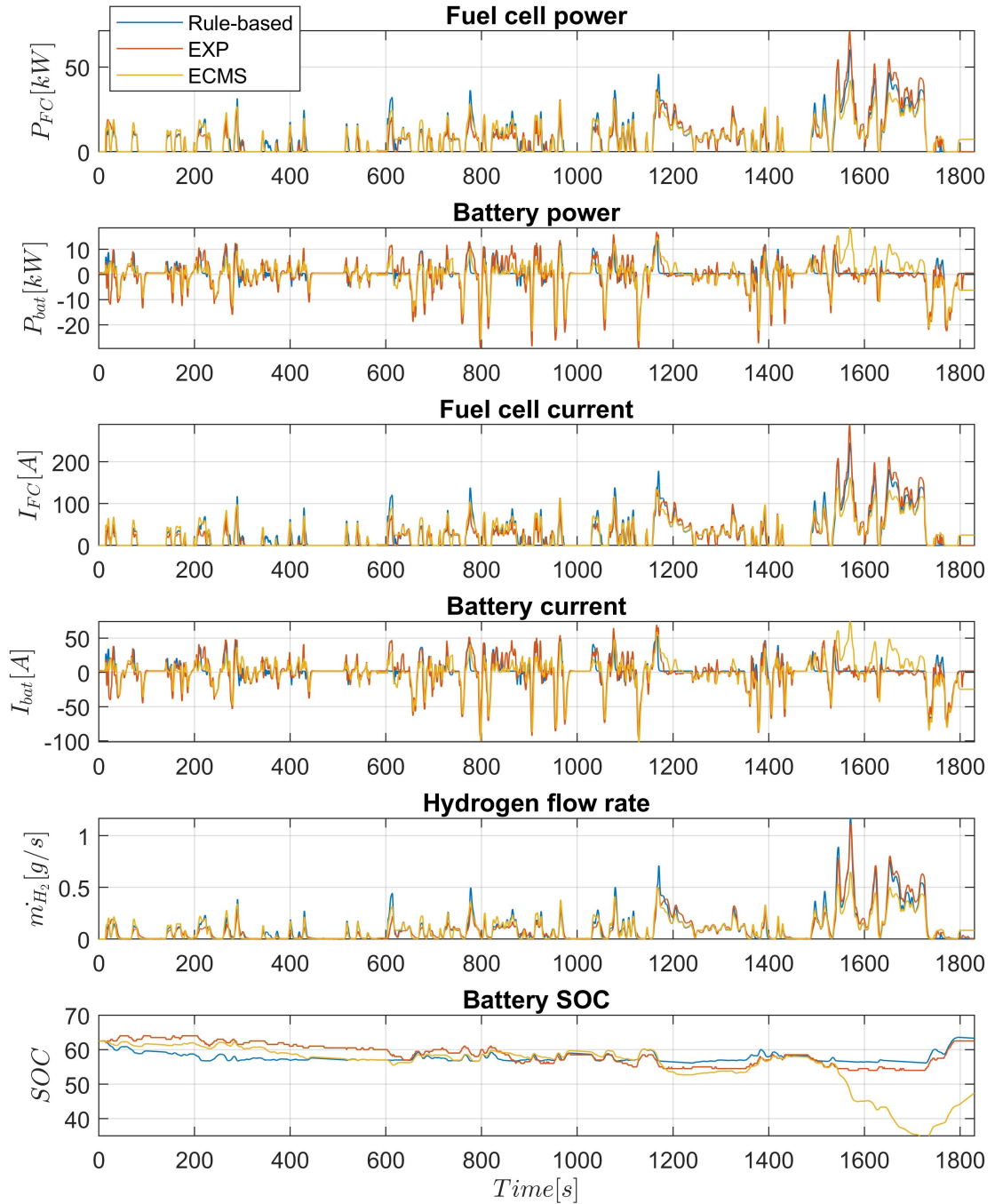


Figure 5.3: Simulation results over WLTC driving cycle with ECMS controller

5.4.2 Results on NEDC driving cycle

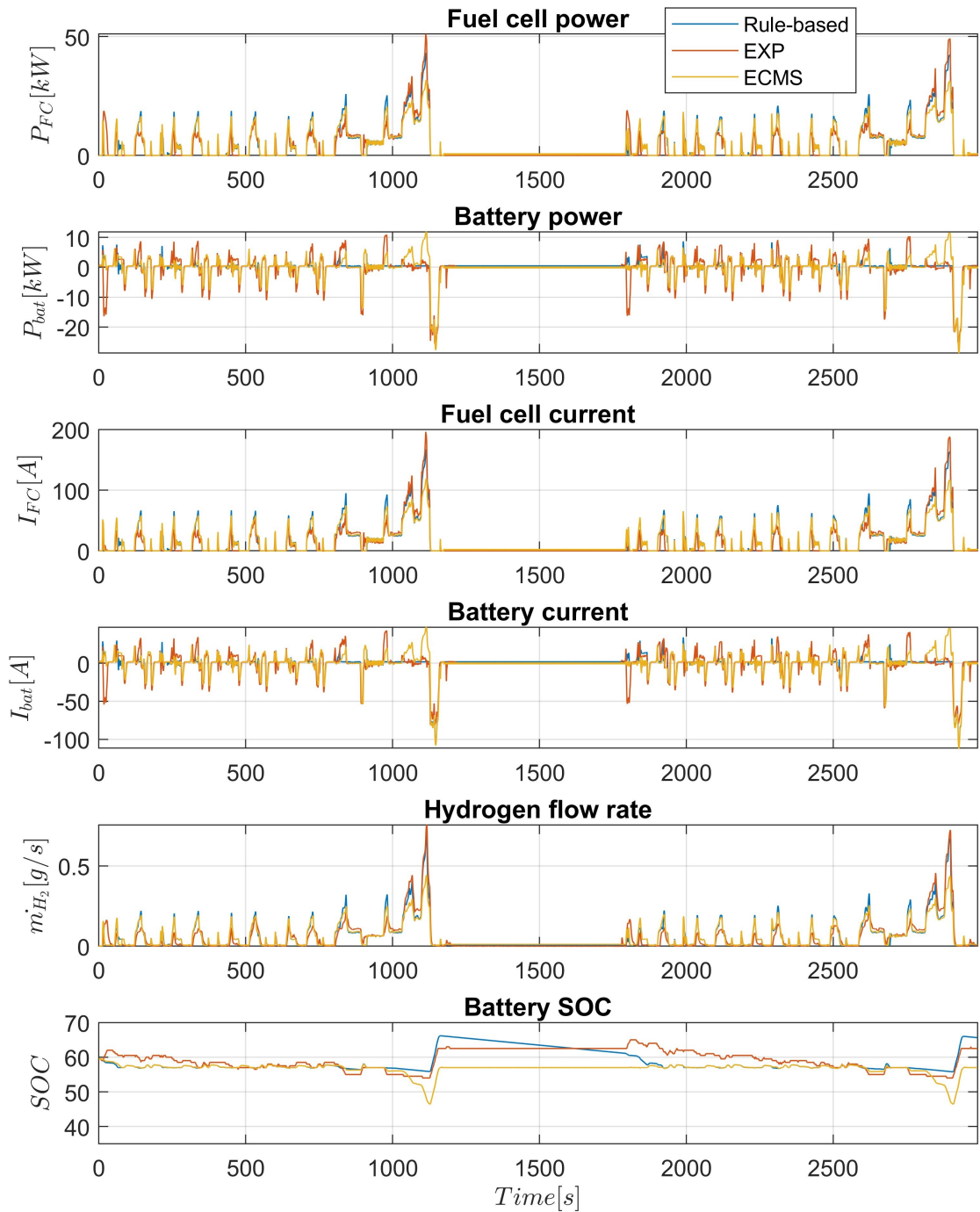


Figure 5.4: Simulation results over NEDCx2 driving cycle with ECMS controller

5.4.3 Results on UDDS driving cycle

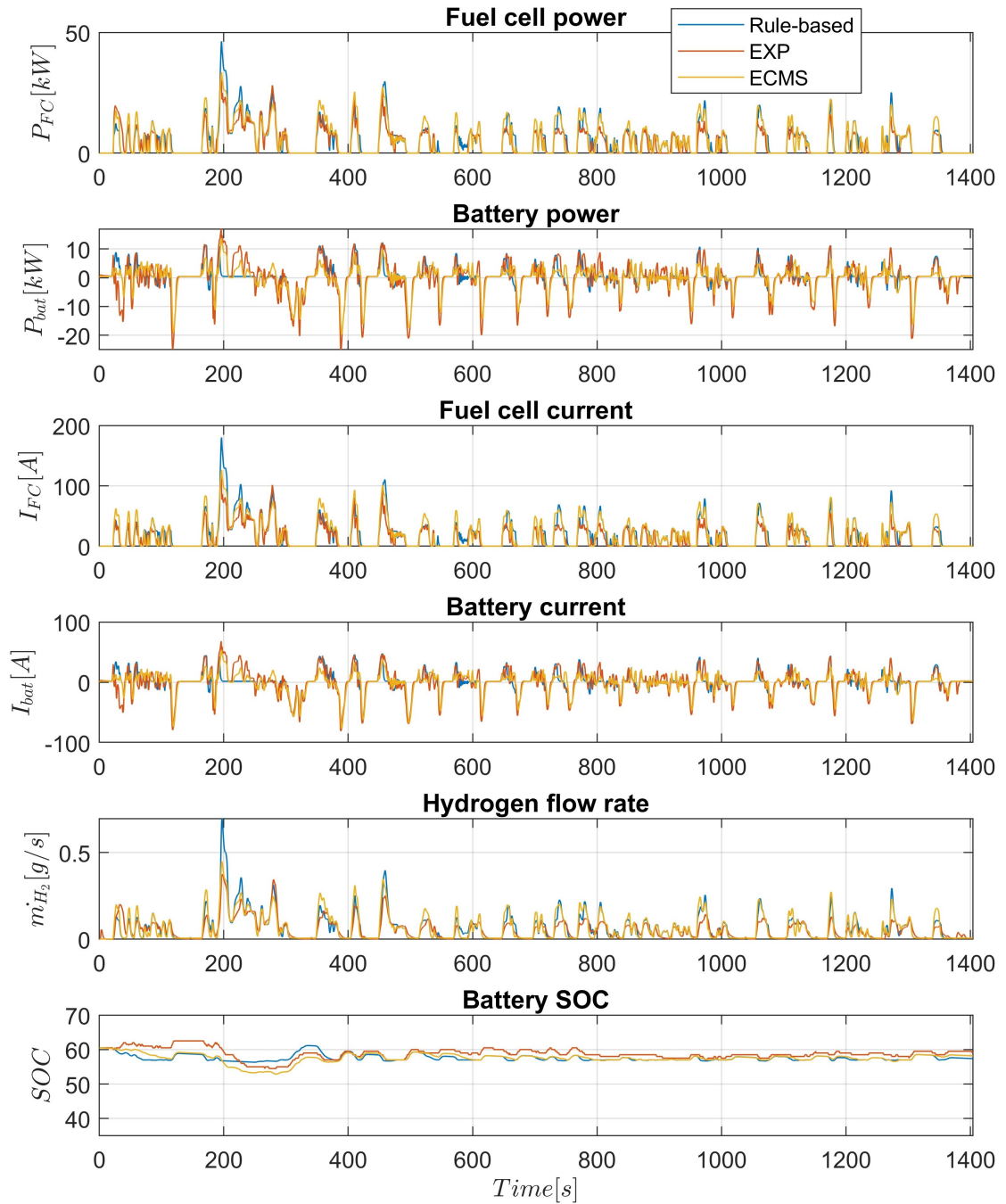


Figure 5.5: Simulation results over UDDS driving cycle with ECMS controller

5.4.4 Results on JC08 driving cycle

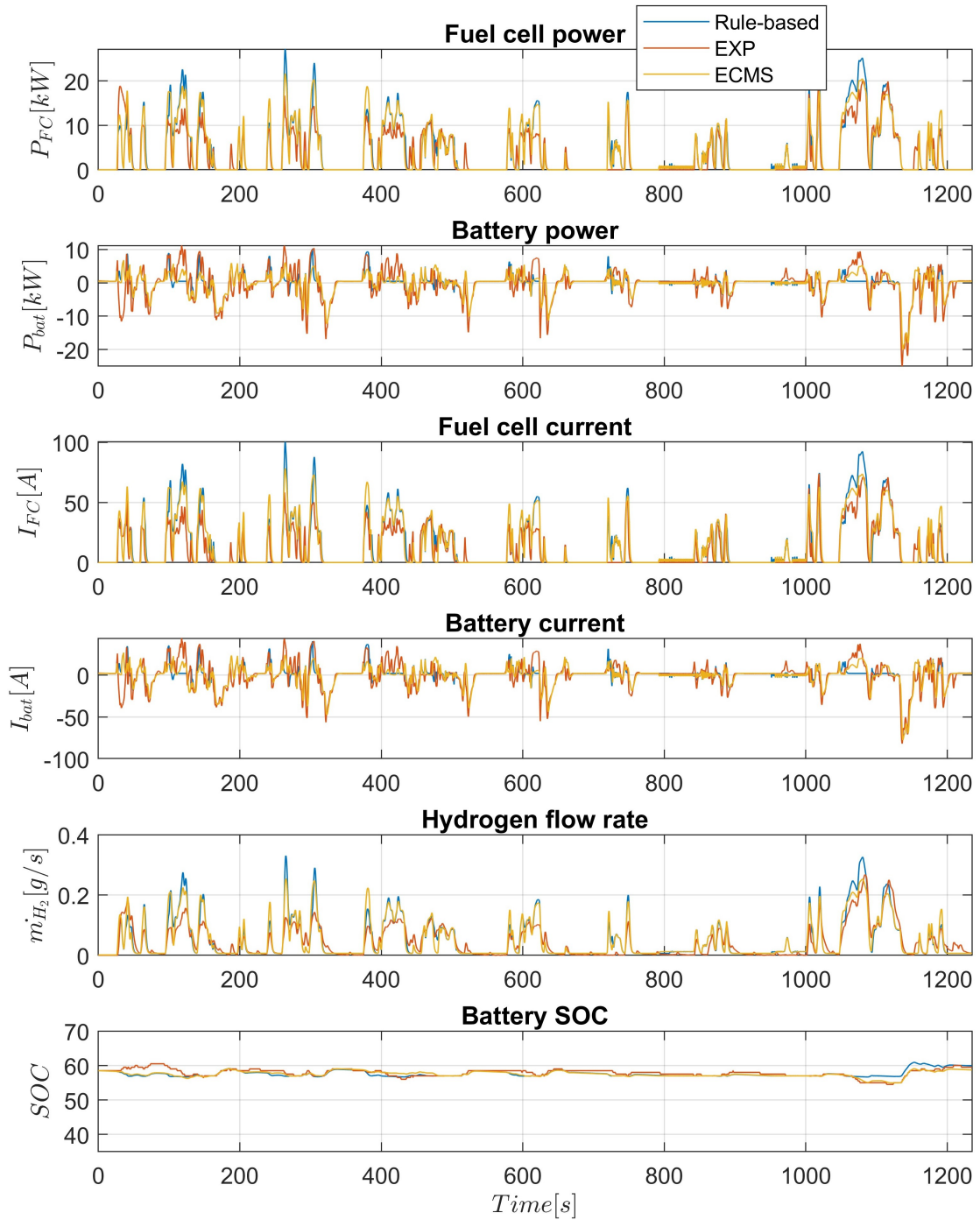


Figure 5.6: Simulation results over JC08 driving cycle with ECMS controller

5.4.5 Results on US06 driving cycle

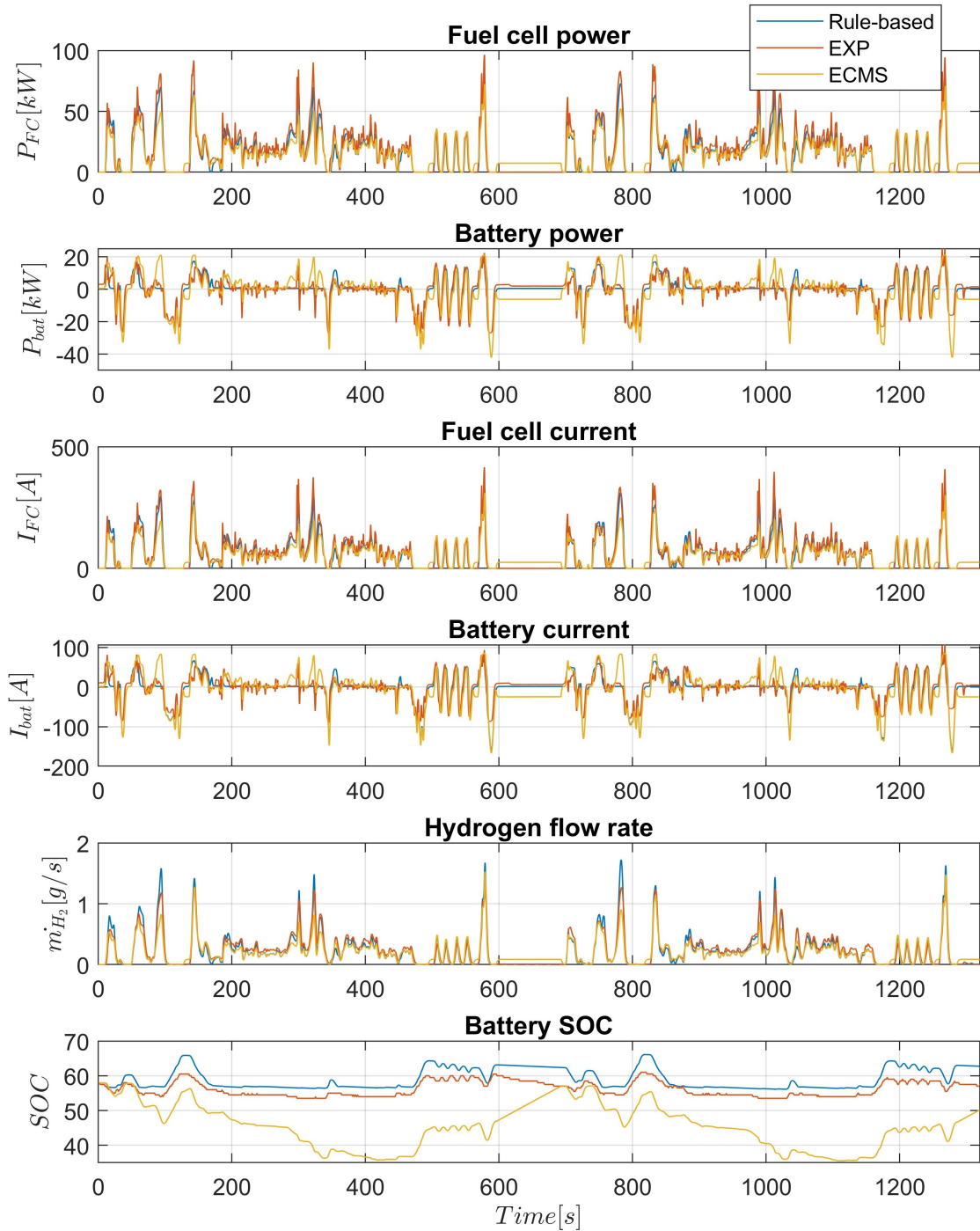


Figure 5.7: Simulation results over US06x2 driving cycle with ECMS controller

5.4.6 Results on HWY driving cycle

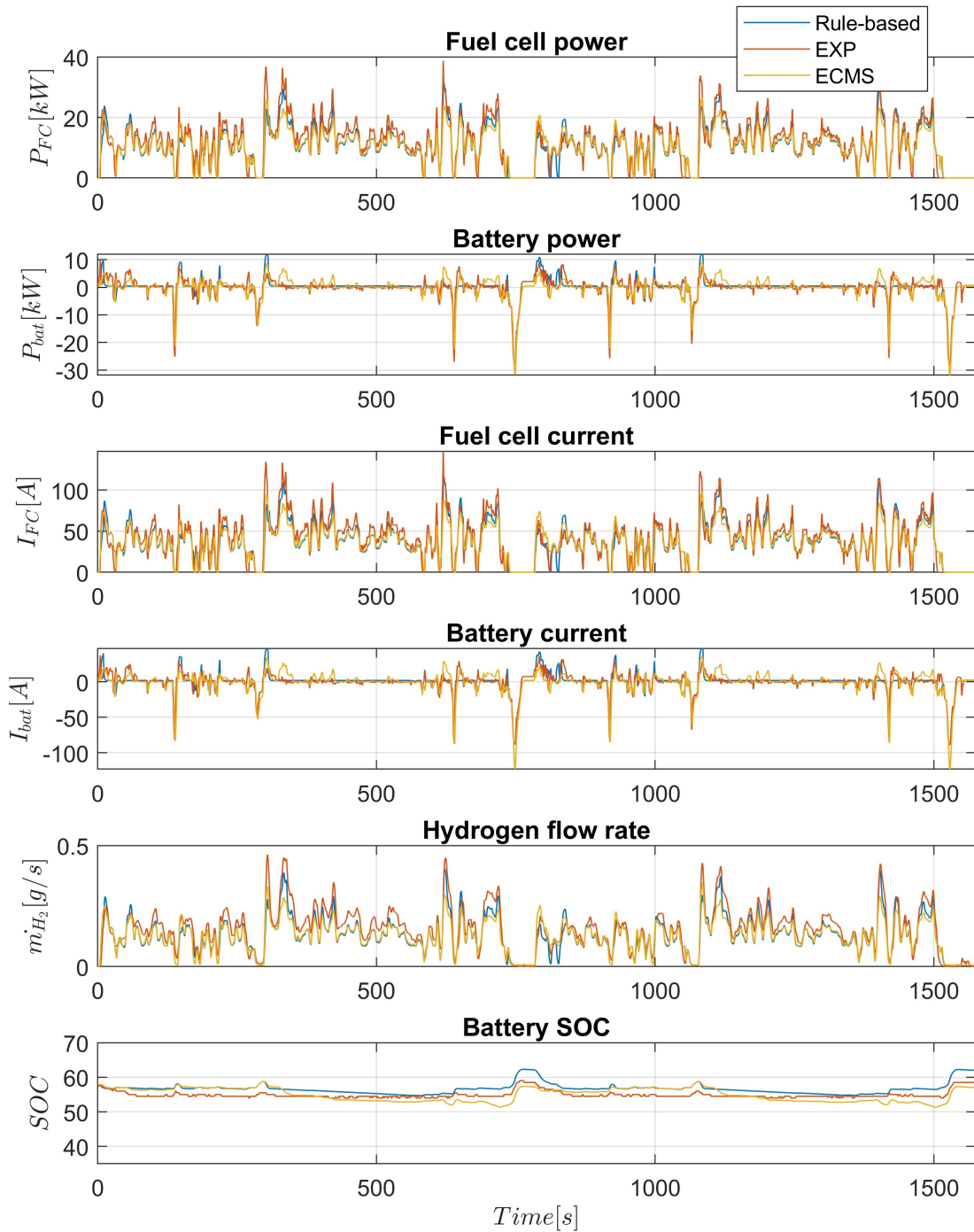


Figure 5.8: Simulation results over HWYx2 driving cycle with ECMS controller

Driving cycle	Hydrogen consumption [g]						
	SIM (ECMS)	SOC comp.	Total	Rule-based	EXP.	DIFF. (ECMS and rule-based)	DIFF. (ECMS and EXP)
WLTC	180.4	-13.4	166.8	197.7	196.8	-15.6 %	-15.2 %
NEDC	167.5	-5	162.6	177.8	160.3	-8.6 %	+1.4 %
UDDS	90.36	-0.7	89.6	89.9	76.18	-0.4 %	+17.6 %
JC08	61.27	-0.7	60.6	62.8	53.3	-3.6 %	+13.6 %
US06	272.6	-6.2	266.4	301.2	323	-11.5 %	-17.5 %
HWY	197.4	-1.3	196.1	204.7	243.9	-4.2 %	-19.6 %

Table 5.2: Simulation results for hydrogen consumption with ECMS controller

SOC [%]			
Driving cycle	SIM. (Rule-based)	EXP.	SIM.(ECMS)
WLTC	63.29	62.5	47.39
NEDC	65.62	62.5	57
UDDS	57.37	59	58.17
JC08	53.31	59.5	58.72
US06	62.74	57	50.15
HWY	61.99	58.5	57.02

Table 5.3: Simulation results for battery SOC with ECMS controller

5.5 ECMS simulation results analysis and discussion

Figures 5.3-5.8 present the graphical representation of FC power, battery power, FC current, battery current, hydrogen flow rate and battery SOC for six different driving cycles and three different control strategies. Fuzzy logic (experimental), rule based (reconstructed experimental) and ECMS control strategies has been tested in 1st generation Toyota Mirai FCHEV over WLTC, NEDC, UDDS, JC08, HWY and US06 driving cycles and implemented in MATLAB/Simulink environment. Red line represent experimental data, while blue and yellow illustrate modeled and optimized data.

Table 5.3 provide information about the final values of battery SOC for three different controllers over six various driving cycles. This data is necessary to calculate the corresponding hydrogen compensation for the objective comparison of fuel consumption. As it is noted before, that the energy content in one percent of battery SOC corresponds to 0.9 grams of hydrogen. Generally, final values of battery SOC for ECMS controller deviates much with respect to modeled and experimental one, since the SOC lower boundary constraint was set to 45 % (Table 5.1).

Table 5.2 shows the numerical values of hydrogen consumption in grams for three different control strategies over six various driving cycles. Specifically, hydrogen consumption for rule based, experimental fuzzy logic and optimized ECMS control strategies over WLTC, NEDC, UDDS, JC08, US06 and HWY driving cycles is provided. Moreover, the difference in percentage of hydrogen consumption between ECMS and rule-based as well as ECMS and experimental fuzzy logic controllers is presented too.

It is clear from obtained data that by implementing ECMS, the maximum

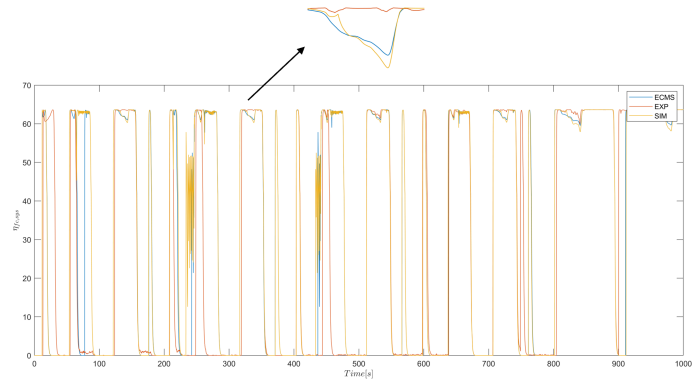


Figure 5.9: Fuel cell system efficiency for NEDC driving cycle

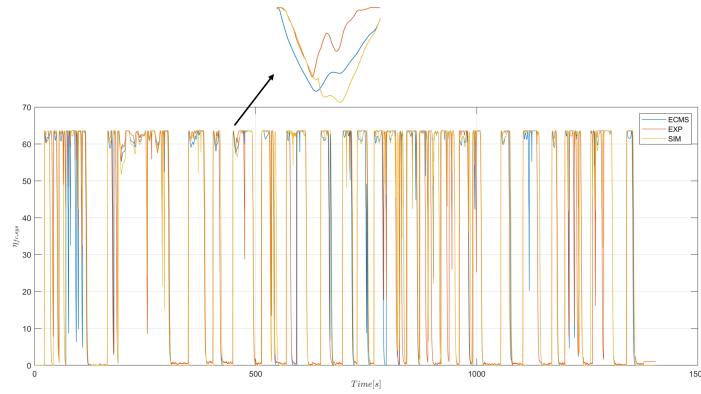


Figure 5.10: Fuel cell system efficiency for UDDS driving cycle

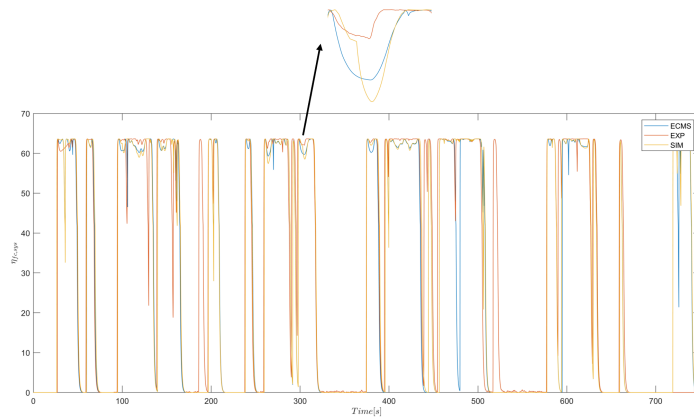


Figure 5.11: Fuel cell system efficiency for JC08 driving cycle

hydrogen consumption reduction of more than 15 % is obtained for WLTC, US06 and HWY driving cycle, comparing with rule based and experimental fuzzy logic control strategies. For WLTC, almost the same consumption reduction of about 15 % is observed while comparing with rule-based and fuzzy logic strategies, whereas only 11.5% with respect to rule-based and 17.5 % with respect to fuzzy logic strategies is estimated for US06 cycle. Concerning HWY cycle, the maximum advantage from ECMS controller of approximately 20 % can be taken with respect to experimental fuzzy logic strategy, while just 4.2 % regarding rule based one. ECMS turns out to performs better than rule based strategies for any driving cycles with a minimum advantage of 0.4 % for UDDS and maximum of 15.6 % for WLTC. With regard to NEDC, UDDS and JC08 driving cycles, ECMS turns out to perform worse than fuzzy logic controllers, with a contrary effect of fuel economy increase up to 17.6 % for UDDS and 13.6 % for JC08 and 1.4 % for NEDC cycles respectively. This is explained due to the fact the fuel cell system operates in a more efficient zones and the time average of FC system efficiency with fuzzy-logic controller over UDDS, NEDC and JC08 is higher than with ECMS controller. This fact is graphically illustrated in Figures 5.9, 5.10, 5.11, where the time history of FC system efficiency over these three driving cycles are presented for three different EMS. These results confirms the results obtained in Table 5.2. In all three plots, red line, which stands for experimental fuzzy-logic controller, is located above the blue and yellow line, which stand for rule-based and ECMS controllers. Moreover, blue and yellow lines are almost overlapped, which also confirms the nearly the same value of experimental and simulated hydrogen consumption for UDDS and JC08 cycles.

Chapter 6

Conclusion

In this thesis work, a complete MATLAB/Simulink model of FCHEV, which simulates all the vehicle subsystems in various driving cycles, has been designed and created. This model is observed to be quick and provide reliable and stable result. In addition, and ECMS control strategy has been designed for fuel cell vehicles and tested in Toyota Mirai FCHEV to find the optimal power split between fuel cell and battery.

In first part, a fuel cell hybrid electric vehicle mathematical model has been defined and created in MATLAB/Simulink environment. Backward simulation approach has been used, which provides stable and fast results. The whole FCHEV system consists of eight subsystems: Drive cycle, vehicle longitudinal dynamics, transmission system, electric machine, fuel cell system, battery, boost converter and EMS subsystems. Analysis has been done by taking into account both traction and regeneration modes of operation. This model requires as an input a predefined driving cycle and vehicle parameters while resulting in hydrogen consumption and SOC variation. EM model has been created by using efficiency map of YASA P400R SERIES AC synchronous machine and rescaling it to fit the parameters of Toyota Mirai's EM. FC system model has been created by following reverse engineering approach and using the ANL experimental data. Efficiency map, hydrogen consumption, air flow rate and polarization curve data has been processed and approximated with polynomials. Battery has been modeled through Thevenin equivalent circuit, that includes ideal voltage source, charging and discharging resistances. Although this model doesn't adequately captures the dynamic behaviour of the battery, it is simple, accurately describes the energy consumption and has an acceptable accuracy range. In addition, the effect of discharging current on the variation of battery capacity is taken into account with Peukert coefficient. FCHEV energy management system has been designed by reconstructing the experimental EMS by means of linear regression procedure and approximating it with rules-based

EMS, which consist of six different modes of operation. This model has been simulated over WLTC, NEDC, UDDS, JC08, US06 and HWY driving cycles. Results are observed to be similar with experimental data and the general shape of fuel cell and battery parameters to be well reproduced. For the objectiveness of the results comparison, a compensation in terms of hydrogen consumption was taken into account due to different battery SOC end values. The perfect match of modeled and experimental data with a difference of just 0.5 % was obtained to be for WLTC cycle while the maximum difference at about 18 % and 16 % for UDDS and HWY driving cycles. In conclusion, this model performs well, with an error of less than or approximately equal to 10 %, for low load driving cycles, such as WLTC, NEDC, JC08 and US06. These differences are present due to several reasons, which are EMS perfect mismatching, quasi-static simulation, effect of backward modeling, effect of reverse engineering for fuel cell mode, effect of different EM efficiency map, effect of Peukert coefficient and lack of data for some FC and battery parameters.

In part two, ECMS control strategy has been simulated in Toyota Mirai FCHEV to optimize the power split between the FC and battery. Instantaneous fuel cell and equivalent battery hydrogen consumption have been calculated from approximated hydrogen consumption polynomial. The objective function was defined by considering the penalty function that takes into account battery SOC. This function was minimized by using proper function in Matlab and the results was provided in both graphical and tabular form. It was observed that ECMS controller performs better than rule based strategies for all driving cycles with a minimum of fuel consumption reduction of 0.4 % for UDDS and maximum of 15.6 % for WLTC. On the other side, for NEDC, UDDS and JC08 cycles, ECMS controller turns out to perform worse than experimental fuzzy-logic controller, with a contrary effect of fuel economy increase up to 17.6 % for UDDS and 13.6 % for JC08 and 1.4 % for NEDC cycles, while for WLTC, US06 and HWY driving cycles, the fuel economy reduction was observed to be 15.2 %, 17.5 % and 19.6 % respectively.

Appendix A

Simulation model and its subsystems

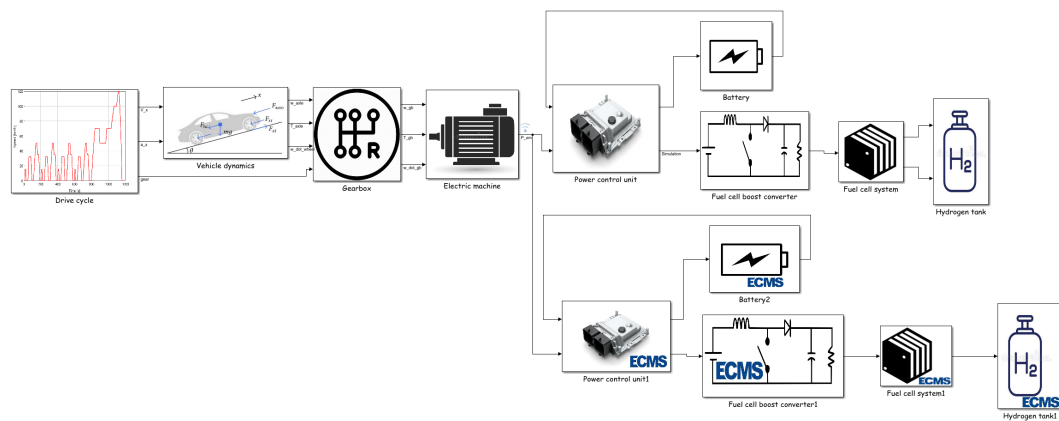


Figure A.1: Block diagram in MATLAB/Simulink environment

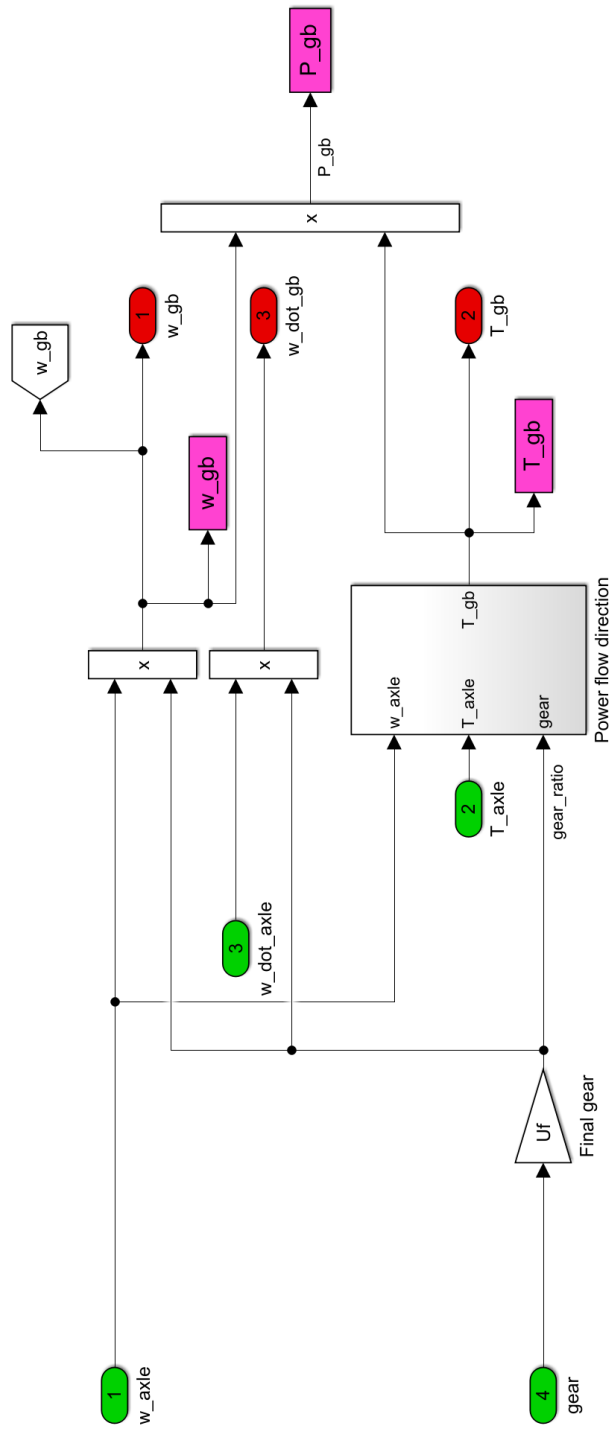


Figure A.4: Gearbox (Transmission system) subsystem

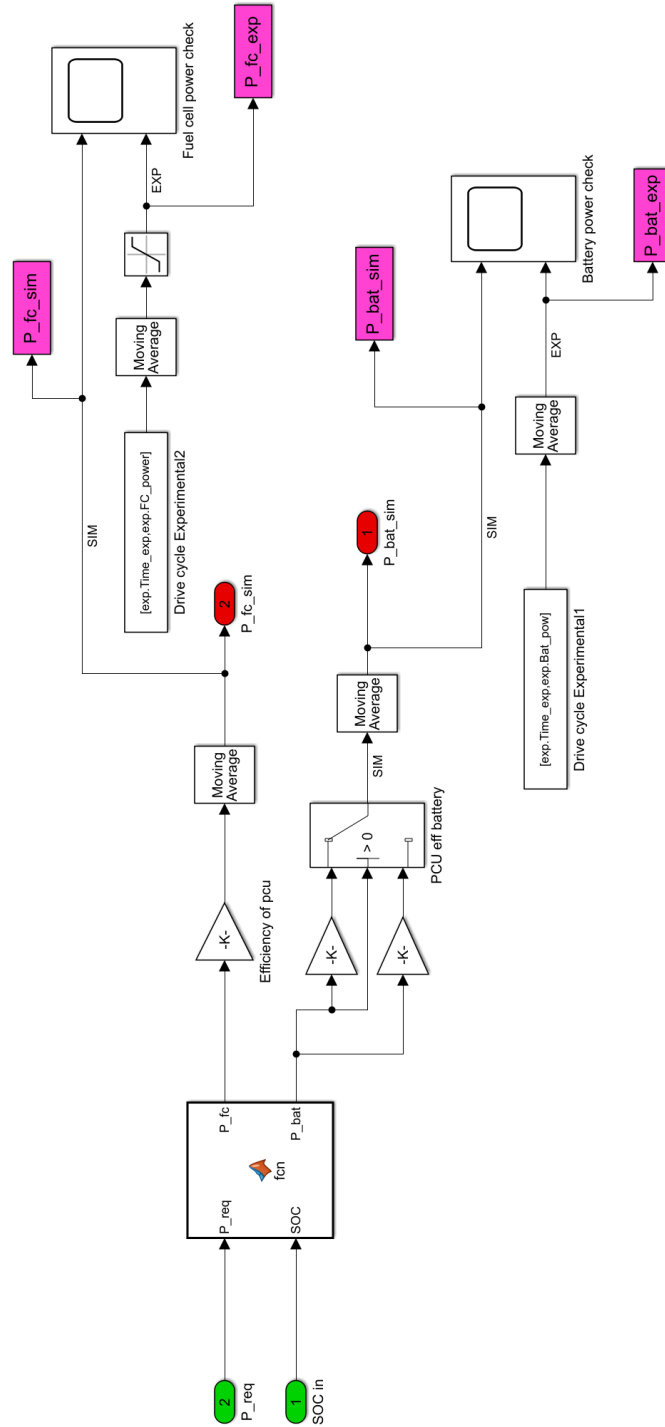


Figure A.6: Energy management system subsystem

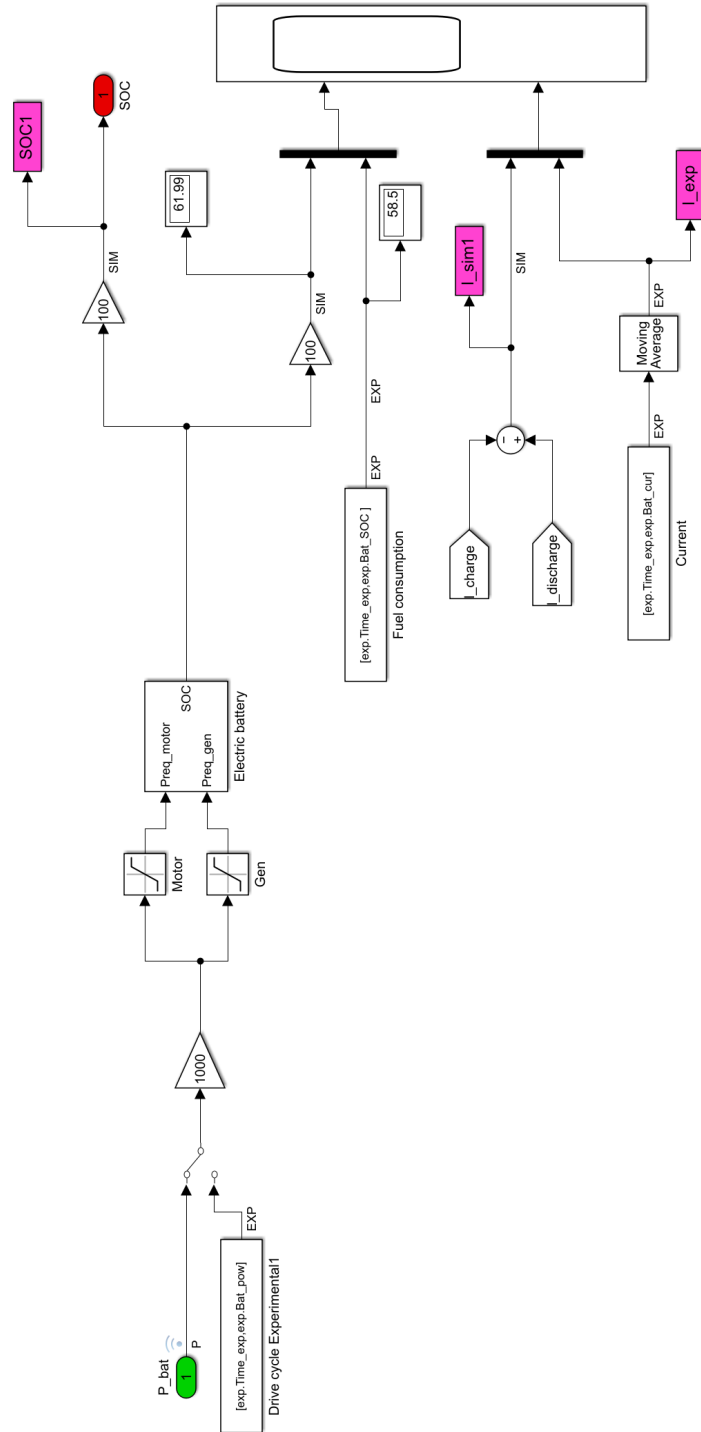


Figure A.7: Battery subsystem (Part 1)

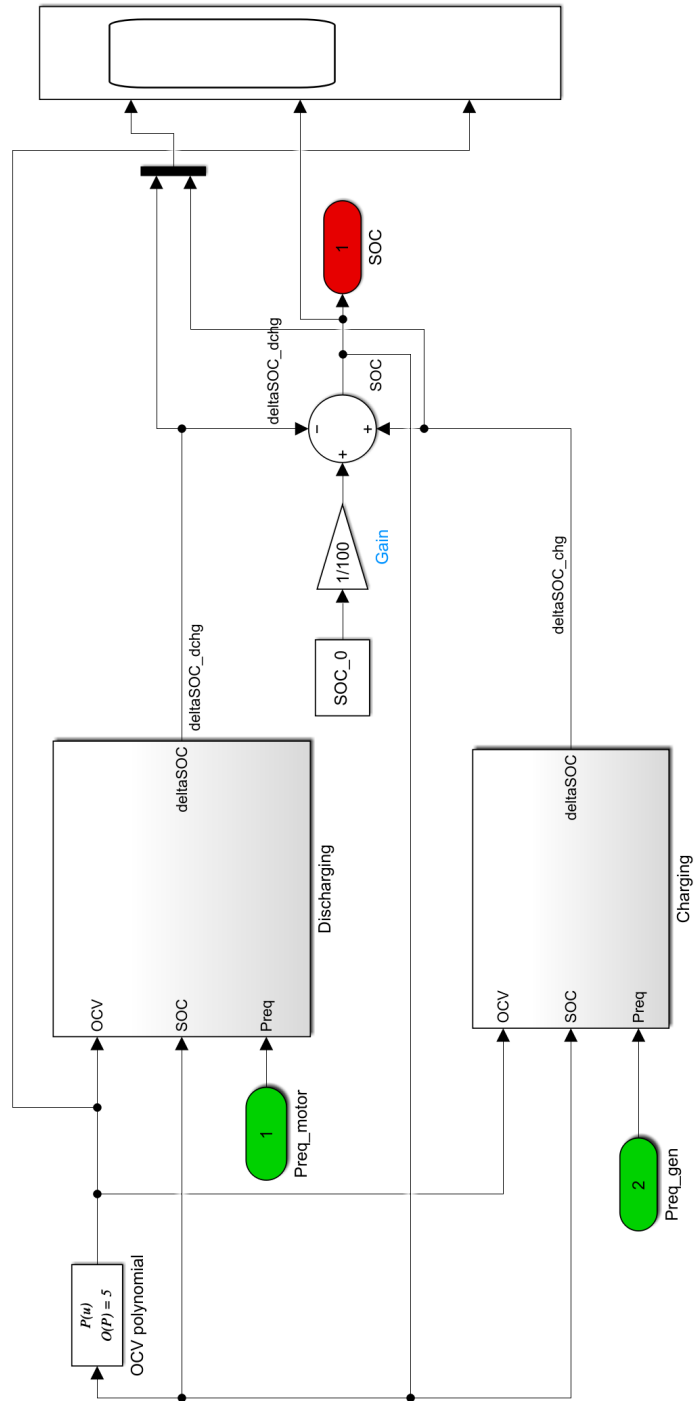


Figure A.8: Battery subsystem (Part 2)

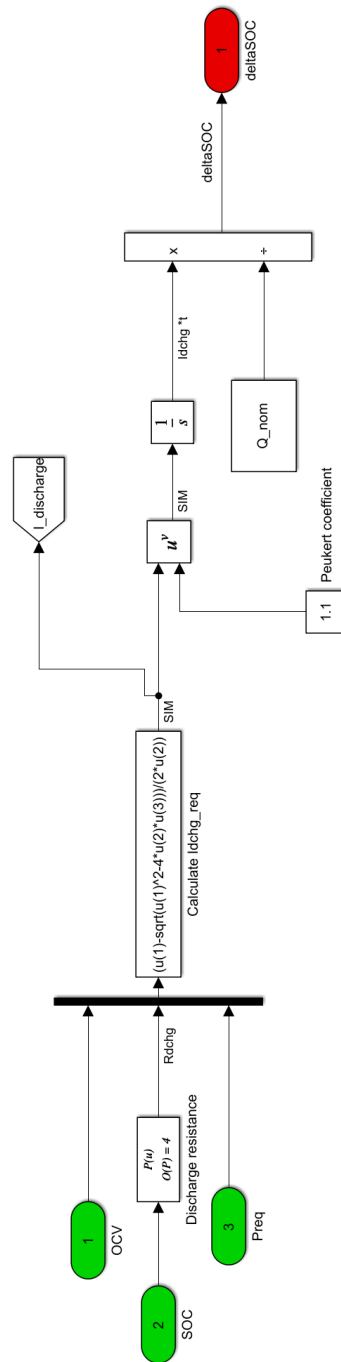


Figure A.9: Battery subsystem (Part 3)

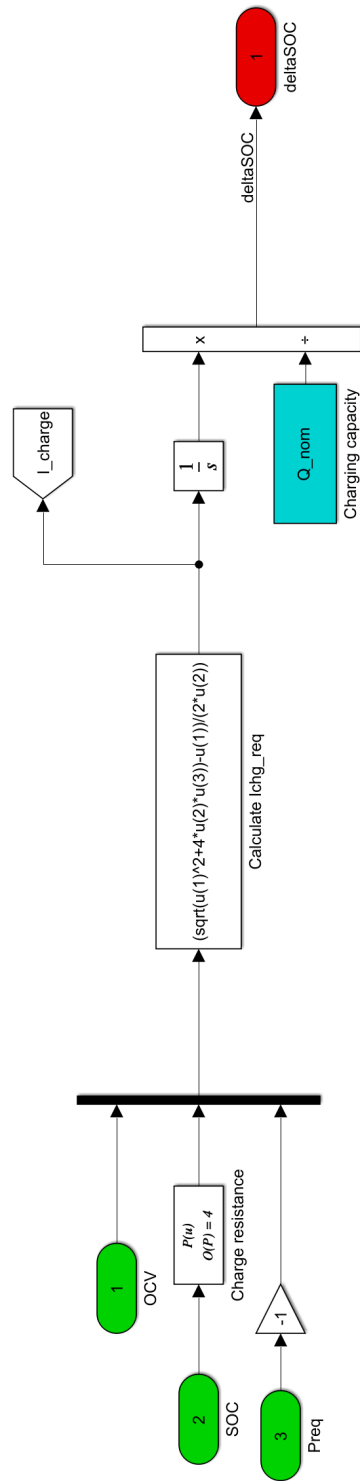


Figure A.10: Battery subsystem (Part 4)

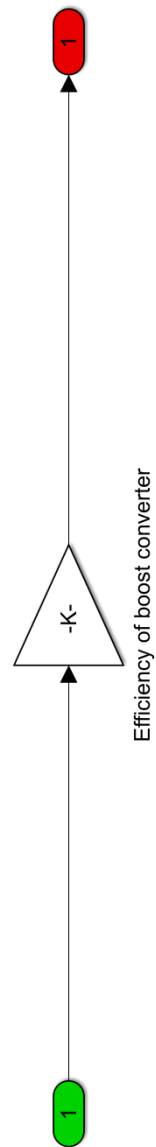


Figure A.11: Fuel cell boost converter subsystem

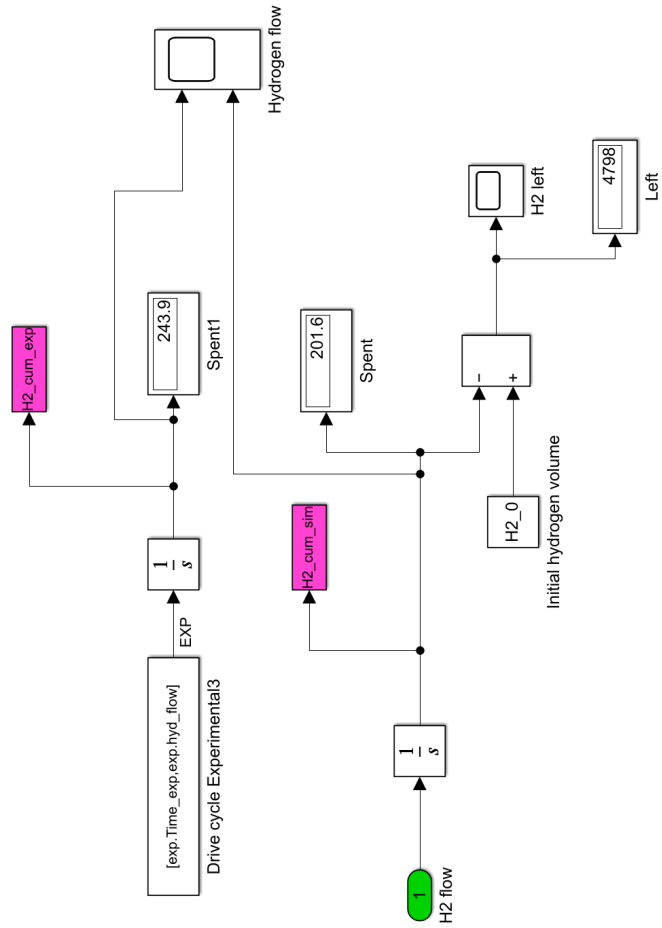


Figure A.13: Hydrogen tank subsystem

Bibliography

- [1] *Sources of greenhouse gas emissions*. <https://www.epa.gov/ghgemissions/sources-greenhouse-gas-emissions>. [EPA United States Environmental Protection agency report]. 2019 (cit. on p. 1).
- [2] Tristan Agaesse. «PhD manuscript - draft - Simulations of one and two-phase flows in porous microstructures, from tomographic images of gas diffusion layers of proton exchange membrane fuel cells.» PhD thesis. Nov. 2016 (cit. on p. 6).
- [3] Abdulrazzak Akroot, Özgür Ekici, and Murat Köksal. «Process modeling of an automotive pem fuel cell system». In: *International Journal of Green Energy* 16 (July 2019), pp. 1–11. DOI: 10.1080/15435075.2019.1641105 (cit. on p. 7).
- [4] Uktam Salomov. «PhD manuscript - 3D pore-scale simulation of the fluid flow through the electrodes of High Temperature Polymeric Electrolyte Fuel Cell». PhD thesis. Apr. 2014 (cit. on p. 8).
- [5] M.S.Wilson, F.H.Garzon, K.E.Sickafus, and S.Gottesfeld. «Surface Area Loss of Supported Platinum in Polymer Electrolyte Fuel Cells». In: *Journal of Electrochem. Soc.* 140 (1993), pp. 2872–2877 (cit. on p. 9).
- [6] H. Uchida, J.M. Song, S. Suzuki, E. Nakazawa, N. Baba, and M. Watanabe. «Electron Tomography of Nafion Ionomer Coated on Pt/Carbon Black in High Utilization Electrode for PEFCs». In: *Journal of Physical Chemistry B* 110 (2006), pp. 13319–13321 (cit. on p. 9).
- [7] D.A. Stevens and J.R. Dahn. «Thermal degradation of the support in carbon-supported platinum electrocatalysts for PEM fuel cells». In: *Carbon* 43 (Dec. 2005), pp. 179–188. DOI: 10.1016/j.carbon.2004.09.004 (cit. on p. 9).
- [8] T.J.Schmidt. «Durability and degradation in high-temperature polymer electrolyte fuel cells». In: *ECS Transactions* 1(8) (2006), pp. 19–31 (cit. on p. 9).

- [9] Chris Yang, S. Srinivasan, A.B. Bocarsly, S. Tulyani, and J.B. Benziger. «A comparison of physical properties and fuel cell performance of Nafion and zirconium phosphate/Nafion composite membranes». In: *Journal of Membrane Science* 237.1 (2004), pp. 145–161. ISSN: 0376-7388. DOI: <https://doi.org/10.1016/j.memsci.2004.03.009>. URL: <https://www.sciencedirect.com/science/article/pii/S0376738804001863> (cit. on p. 9).
- [10] Yu Kim, Feng Wang, Michael Hickner, Thomas Zawodzinski, and James Mcgrath. «Fabrication and characterization of heteropolyacid (H 3PW 12O 40)/directly polymerized sulfonated poly(arylene ether sulfone) copolymer composite membranes for higher temperature fuel cell applications». In: *Journal of Membrane Science - J MEMBRANE SCI* 212 (Feb. 2003), pp. 263–282. DOI: 10.1016/S0376-7388(02)00507-0 (cit. on p. 9).
- [11] Felix N. Büchi, Bhuvanesh Gupta, Otto Haas, and Günther G. Scherer. «Study of radiation-grafted FEP-G-polystyrene membranes as polymer electrolytes in fuel cells». In: *Electrochimica Acta* 40.3 (1995). Polymer electrolyte fuel cells, pp. 345–353. ISSN: 0013-4686. DOI: [https://doi.org/10.1016/0013-4686\(94\)00274-5](https://doi.org/10.1016/0013-4686(94)00274-5). URL: <https://www.sciencedirect.com/science/article/pii/0013468694002745> (cit. on p. 9).
- [12] Yuka Oono, Atsuo Sounai, and Michio Hori. «Long-term cell degradation mechanism in high-temperature proton exchange membrane fuel cells». In: *Journal of Power Sources* 210 (2012), pp. 366–373. ISSN: 0378-7753. DOI: <https://doi.org/10.1016/j.jpowsour.2012.02.098>. URL: <https://www.sciencedirect.com/science/article/pii/S0378775312005204> (cit. on p. 9).
- [13] Thamo Sutharssan, Diogo Montalvão, Y. Chen, Wen-Chung Wang, Claudia Pisac, and Hakim Elemara. «A review on prognostics and health monitoring of proton exchange membrane fuel cell». In: *Renewable and Sustainable Energy Reviews* 75 (Nov. 2016). DOI: 10.1016/j.rser.2016.11.009 (cit. on p. 14).
- [14] Felix Büchi, Mathias Reum, Stefan Freunberger, and Antonio delfino. «On the Efficiency of Automotive H₂/O₂ PE Fuel Cell Systems». In: (Jan. 2005) (cit. on p. 15).
- [15] *Toyota Industries Develops New FC Air Compressor and Hydrogen Circulation Pump, Now Installed in the New Toyota Mirai FCEV*. <https://www.toyota-industries.com/news/2020/12/10/005056/>. [Toyota Industries Corporation]. 2020 (cit. on pp. 17, 18).
- [16] Tiancai Ma, Weikang Lin, Yanbo Yang, Ming Cong, Zhuoping Yu, and Qiongqiong Zhou. «Research on Control Algorithm of Proton Exchange

- Membrane Fuel Cell Cooling System». In: *Energies* 12.19 (2019). ISSN: 1996-1073. DOI: 10.3390/en12193692. URL: <https://www.mdpi.com/1996-1073/12/19/3692> (cit. on p. 18).
- [17] Ravello V. *Electric and Hybrid propulsion system course lecture notes*. [Politecnico di Torino]. 2020/2021 (cit. on p. 21).
- [18] *Hydrogen and fuel cell technologies office*. <https://www.energy.gov/eere/fuelcells/hydrogen-resources>. [Hydrogen resources] (cit. on p. 22).
- [19] Marco Bonci. «Master’s Thesis - Fuel Cell Vehicle simulation: an approach based on Toyota Mirai». PhD thesis. 2021 (cit. on pp. 23, 28–30).
- [20] Xiao-Hong Yuan, Guo-Dong Yan, Hong-Tao Li, Xun Liu, Chu-Qi Su, and Yi-Ping Wang. «Research on energy management strategy of fuel cell–battery–supercapacitor passenger vehicle». In: *Energy Reports* 8 (2022). 2021 The 8th International Conference on Power and Energy Systems Engineering, pp. 1339–1349. ISSN: 2352-4847. DOI: <https://doi.org/10.1016/j.egy.2021.11.244> (cit. on p. 24).
- [21] Liu W. *Introduction to Hybrid Vehicle System Modeling and Control*. John Wiley Sons, Inc, 2013 (cit. on p. 25).
- [22] Yanjun Huang, Hong Wang, Amir Khajepour Amir, Bin Li, Jie Ji, Kegang Zhao, and Chuan Hu. «A review of power management strategies and component sizing methods for hybrid vehicles». In: *Renewable and Sustainable Energy Reviews* 96 (Nov. 2018), pp. 132–144. DOI: 10.1016/j.rser.2018.07.020 (cit. on p. 25).
- [23] Aishwarya Panday and Hari Bansal. «A Review of Optimal Energy Management Strategies for Hybrid Electric Vehicle». In: (Dec. 2014) (cit. on pp. 26, 28, 30, 31, 34, 38, 39).
- [24] M. Sabri, Kumeresan A. Danapalasingam, and Mohd Rahmat. «A review on hybrid electric vehicles architecture and energy management strategies». In: *Renewable and Sustainable Energy Reviews* 53 (Jan. 2016), pp. 1433–1442. DOI: 10.1016/j.rser.2015.09.036 (cit. on p. 28).
- [25] Siang Tie and Chee Wei Tan. «A review of energy sources and energy management system in electric vehicles». In: *Renewable and Sustainable Energy Reviews* 20 (Apr. 2013), pp. 82–102. DOI: 10.1016/j.rser.2012.11.077 (cit. on pp. 28, 32).
- [26] Sara Luciani and Andrea Tonoli. «Control Strategy Assessment for Improving PEM Fuel Cell System Efficiency in Fuel Cell Hybrid Vehicles». In: *Energies* 15 (Mar. 2022), p. 2004. DOI: 10.3390/en15062004 (cit. on pp. 29, 30).

- [27] G. Paganelli, Sebastien Delprat, Thierry-Marie Guerra, J. Rimaux, and Jean-Jacques Santin. «Equivalent consumption minimization strategy for parallel hybrid powertrains». In: vol. 4. Feb. 2002, 2076–2081 vol.4. ISBN: 0-7803-7484-3. DOI: 10.1109/VTC.2002.1002989 (cit. on pp. 32, 81).
- [28] *What is a neural network*. <https://www.tibco.com/reference-center/what-is-a-neural-network> (cit. on p. 34).
- [29] D.E Kirk. *Optimal control theory: an introduction*. [Courier Corporation]. 2012 (cit. on p. 35).
- [30] Sukanta Nayak. «Chapter seven - Dynamic programming». In: *Fundamentals of Optimization Techniques with Algorithms*. Ed. by Sukanta Nayak. Academic Press, 2020, pp. 191–221. ISBN: 978-0-12-821126-7. DOI: <https://doi.org/10.1016/B978-0-12-821126-7.00007-3>. URL: <https://www.sciencedirect.com/science/article/pii/B9780128211267000073> (cit. on p. 37).
- [31] I. Ross and R. Proulx. «Further Results on Fast Birkhoff Pseudospectral Optimal Control Programming». In: *Journal of Guidance, Control, and Dynamics* 42 (Apr. 2019), pp. 1–7. DOI: 10.2514/1.G004297 (cit. on p. 37).
- [32] I. Ross and Mark Karpenko. «A review of pseudospectral optimal control: From theory to flight». In: *Annual Reviews in Control* 36 (Dec. 2012), pp. 182–197. DOI: 10.1016/j.arcontrol.2012.09.002 (cit. on p. 37).
- [33] Fariba Fahroo and I Ross. «Advances in Pseudospectral Methods for Optimal Control». In: *AIAA Guidance, Navigation and Control Conference and Exhibit* (Aug. 2008). DOI: 10.2514/6.2008-7309 (cit. on p. 37).
- [34] Iliass Ouachani, Abdelhamid Rabhi, Imene Yahyaoui, B.Tidhaf, and Fernando Tadeo. «Renewable Energy Management Algorithm for a Water Pumping System». In: vol. 111. Sept. 2016. DOI: 10.1016/j.egypro.2017.03.266 (cit. on p. 39).
- [35] *Outline of the Mirai*. <https://www.toyota-europe.com>. accessed 14.03.2017 (cit. on p. 41).
- [36] P. Pettersson, B. Jacobson, F. Bruzelius, P. Johannesson, and L. Fast. «Intrinsic differences between backward and forward vehicle simulation models». In: *IFAC-PapersOnLine* 53.2 (2020). 21st IFAC World Congress, pp. 14292–14299. ISSN: 2405-8963. DOI: <https://doi.org/10.1016/j.ifacol.2020.12.1368>. URL: <https://www.sciencedirect.com/science/article/pii/S2405896320317754> (cit. on pp. 43, 44).
- [37] Ganesh Mohan, Francis Assadian, and Stefano Longo. «Comparative analysis of forward-facing models vs backward-facing models in powertrain component sizing». In: vol. 2013. Jan. 2013. DOI: 10.1049/cp.2013.1920 (cit. on p. 44).

- [38] *YASA P400R SERIES electric machine datasheet*. <https://www.yasa.com/products/yasa-p400/> (cit. on p. 50).
- [39] Guoliang Wu, Rengui Lu, Chunbo Zhu, and C. Chan. «Apply a Piece-wise Peukert's Equation with Temperature Correction Factor to NiMH Battery State of Charge Estimation». In: *Journal of Asian Electric Vehicles* 8 (Jan. 2010), pp. 1419–1423. DOI: 10.4130/jaev.8.1419 (cit. on pp. 59, 79).
- [40] *D3 2016 Toyota Mirai*. <https://www.anl.gov/taps/d3-2016-toyota-mirai>. Toyota Mirai Argonne National Laboratory testing results (cit. on p. 59).
- [41] M. Fleuren, T.C.J. Romijn, and M.C.F. Donkers. «An Equivalent Consumption Minimisation Strategy based on 1-Step Look-Ahead Stochastic Dynamic Programming This work has received financial support from the FP7 of the European Commission under the grant CONVENIENT (312314).» In: *IFAC-PapersOnLine* 48.15 (2015). 4th IFAC Workshop on Engine and Powertrain Control, Simulation and Modeling E-COSM 2015, pp. 72–77. ISSN: 2405-8963. DOI: <https://doi.org/10.1016/j.ifacol.2015.10.011>. URL: <https://www.sciencedirect.com/science/article/pii/S240589631501887X> (cit. on p. 81).
- [42] Yongfei Liu, Longlong Zhu, Fazhan Tao, and Zhumu Fu. «Energy Management Strategy of FCHEV Based on ECMS Method». In: Dec. 2019, pp. 197–201. DOI: 10.1145/3375998.3376019 (cit. on pp. 81, 82).
- [43] Gino Paganelli, Yann Guezennec, and Giorgio Rizzoni. «Optimizing Control Strategy for Hybrid Fuel Cell Vehicle». In: *SAE Transactions* 111 (2002), pp. 398–406. ISSN: 0096736X, 25771531. URL: <http://www.jstor.org/stable/44743070> (visited on 07/10/2022) (cit. on p. 81).
- [44] Jihun Han, Youngjin Park, and Dongsuk Kum. «Optimal adaptation of equivalent factor of equivalent consumption minimization strategy for fuel cell hybrid electric vehicles under active state inequality constraints». In: *Journal of Power Sources* 267 (2014), pp. 491–502. ISSN: 0378-7753. DOI: <https://doi.org/10.1016/j.jpowsour.2014.05.067>. URL: <https://www.sciencedirect.com/science/article/pii/S0378775314007502> (cit. on p. 81).
- [45] Ameen Bassam, Alexander Phillips, Stephen Turnock, and Philip Wilson. «An improved energy management strategy for a hybrid fuel cell/battery passenger vessel». In: *International Journal of Hydrogen Energy* 41 (Aug. 2016). DOI: 10.1016/j.ijhydene.2016.08.049 (cit. on p. 82).

- [46] Huan Li, Alexandre Ravey, A. N'diaye, and A. Djerdir. «Equivalent consumption minimization strategy for fuel cell hybrid electric vehicle considering fuel cell degradation». In: June 2017, pp. 540–544. DOI: 10.1109/ITEC.2017.7993328 (cit. on p. 82).
- [47] Elkhatib Kamal and Lounis Adouane. «Optimized EMS and a Comparative Study of Hybrid Hydrogen Fuel Cell/Battery Vehicles». In: *Energies* 15 (Jan. 2022), p. 738. DOI: 10.3390/en15030738 (cit. on p. 82).
- [48] S. Onori, L. Serrao, and Giorgio Rizzoni. *Hybrid Electric Vehicles: Energy management strategies*. London: Springer, 2016 (cit. on p. 82).
- [49] Xixue Liu, Datong Qin, and Shaoqian Wang. «Minimum Energy Management Strategy of Equivalent Fuel Consumption of Hybrid Electric Vehicle Based on Improved Global Optimization Equivalent Factor». In: *Energies* 12 (May 2019), p. 2076. DOI: 10.3390/en12112076 (cit. on p. 84).
- [50] Bin Zhou, Amir Rezaei, and Jeffrey Burl. «Effect of Battery Temperature on Fuel Economy and Battery Aging When Using the Equivalent Consumption Minimization Strategy for Hybrid Electric Vehicles». In: Apr. 2020. DOI: 10.4271/2020-01-1188 (cit. on p. 84).